Analysis of Transvascular Transport Phenomena in the glomerular and peritoneal microcirculation

ÖBERG, CARL

2016

Document Version:
Publisher's PDF, also known as Version of record

Analysis of Transvascular Transport Phenomena

in the glomerular and peritoneal microcirculation

CARL M. ÖBERG | FACULTY OF MEDICINE | LUND UNIVERSITY

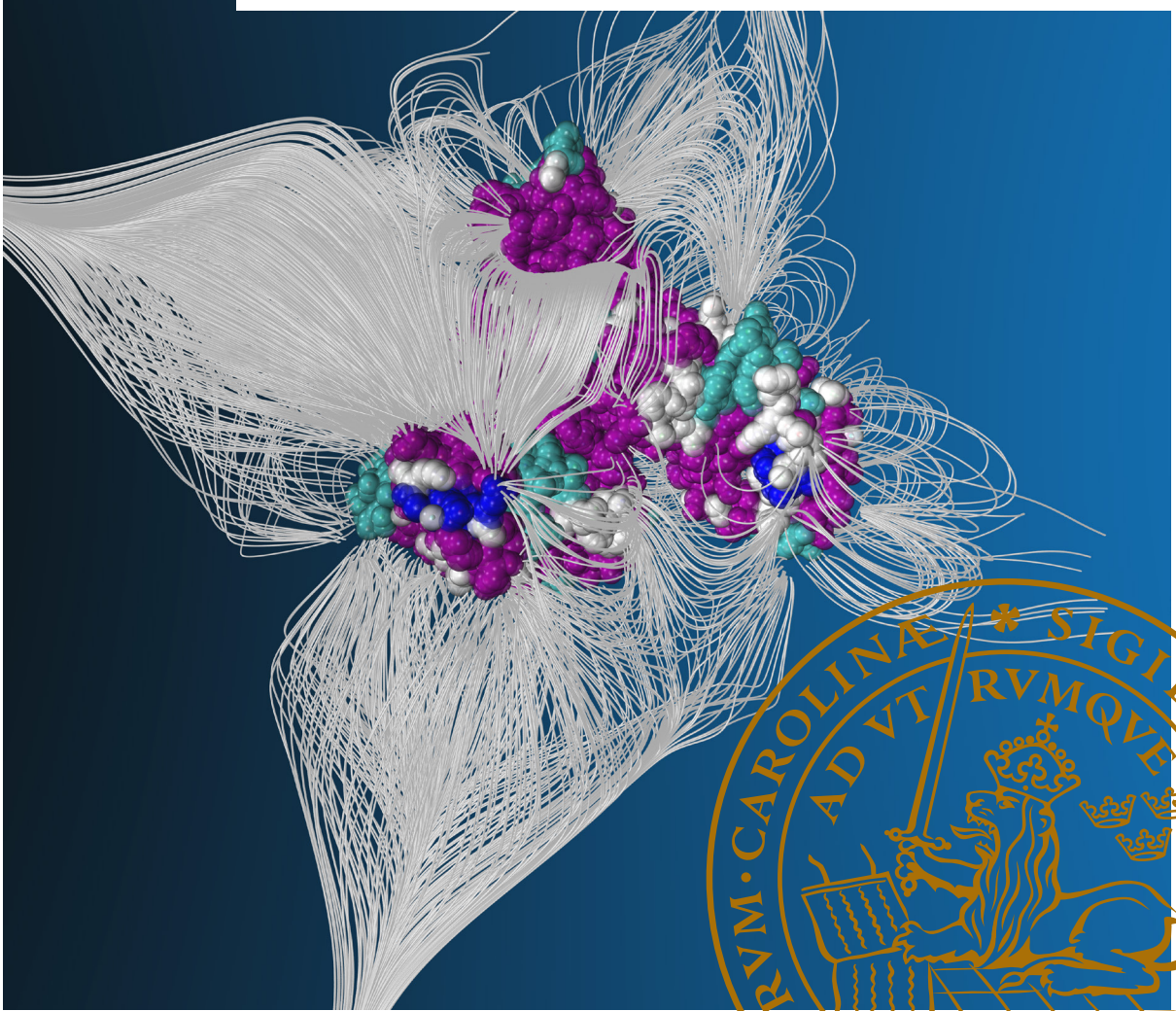

Analysis of Transvascular Transport Phenomena

Analysis of Transvascular Transport Phenomena

in the glomerular and peritoneal microcirculation

by Carl M. Öberg

LUND
UNIVERSITY

Thesis for the degree of Doctor of Philosophy
Thesis advisors: Prof. Bengt Rippe, Dr. Josefin Axelsson
Faculty opponent: Assoc. Prof. John Kenneth Leypoldt

To be presented, with the permission of the Faculty of Medicine of Lund University, for public criticism in the Segerfalk lecture hall (Wallenberg Neurocentrum, BMC) at the Department of Clinical Sciences, Lund on Friday, the 9th of December 2016 at 13:00.

Organization	Document name
LUND UNIVERSITY Department of Clinical Sciences, Lund Box 188 SE–221 00 LUND Sweden	**DOCTORAL DISSERTATION** Date of disputation 2016-12-09 Sponsoring organization
Author(s) Carl M. Öberg	

Title and subtitle

Analysis of Transvascular Transport Phenomena in the glomerular and peritoneal microcirculation

Abstract

The current work is devoted entirely to the study of passive transport phenomena, or more specifically, the more simple diffusion, electric migration and filtration of solute matter and water over glomerular and peritoneal capillary walls. The driving forces behind such trans-capillary transport phenomena have long been assumed to be simple gradients of concentration, hydrostatic pressure and electric potential. Despite decades of research, the relative importance of these different transport mechanisms remains a highly controversial subject.

In Study I we explore the subject of charge selectivity in the glomerular filtration barrier (GFB). The results of this study indicate that electrical charge may be of less importance in the hindrance of charged molecules in the GFB than previously thought.

In Study II, we construct a distributed two-pore model and use it to analyze experimental data (θ vs. SE-radius). The results indicate that the wide distribution obtained in the data analysis may be due to a variation in solute size rather than a true variation in pore size. In addition, several theoretical results are presented such as Poiseuille's law for a distributed pore population.

One of the many unresolved questions regarding the GFB is the reason behind the marked difference in permeability between albumin and Ficoll. In Study III the distributed two-pore model is extended by introducing size distributions on the solute molecules. Experimental data from the rat glomerulus and from precision-made nanopore membranes are analyzed. We show that a variation of only 16% in the size of the solute molecule is sufficient to explain the difference in permeability between albumin and Ficoll.

Study IV: The three-pore model is a widely applied model of peritoneal dialysis. Here an extended version of the classical model is used to optimize automated peritoneal dialysis for a wide range of different scenarios. The results show that large reductions (>20%) in glucose absorption are possible by using optimized (bi-modal) regimes.

Key words

dialysis, CAPD, APD, two-pore model, three-pore model, glomerular filtration

Classification system and/or index terms (if any)

Supplementary bibliographical information	Language
	English
ISSN and key title ISSN 1652-8220 Lund University, Faculty of Medicine Doctoral Dissertation Series 2016:145	ISBN 978-91-7619-372-3 (print) 978-91-7619-377-8 (pdf)
Recipient's notes	Number of pages 179 / Price
	Security classification

Analysis of Transvascular Transport Phenomena

in the glomerular and peritoneal microcirculation

by Carl M. Öberg

LUND
UNIVERSITY

A doctoral thesis at a university in Sweden takes either the form of a single, cohesive research study (monograph) or a summary of research papers (compilation thesis), which the doctoral student has written alone or together with one or several other author(s).

In the latter case the thesis consists of two parts. An introductory text puts the research work into context and summarizes the main points of the papers. Then, the research publications themselves are reproduced, together with a description of the individual contributions of the authors. The research papers may either have been already published or are manuscripts at various stages (in press, submitted, or in draft).

Cover illustration front: Electrical field lines of Human Serum Albumin. Computations were performed with APBS version 1.3 (http://www.poissonboltzmann.org/).

Funding information: This work was financially supported by Swedish Research Council Grant 08285, the Swedish Heart and Lung Foundation (Hjärt-Lungfonden), and the Medical Faculty at Lund University (ALF Grant).

Faculty of Medicine, Department of Clinical Sciences, Lund

ISBN: 978-91-7619-372-3 (print)
ISBN: 978-91-7619-377-8 (pdf)
ISSN: 1652-8220

Lund University, Faculty of Medicine Doctoral Dissertation Series 2016:145

Printed in Sweden by Media-Tryck, Lund University, Lund 2016

To science
enlightening us

Contents

List of publications

This thesis is based on the following publications, referred to by their Roman numerals:

I **Quantification of the electrostatic properties of the glomerular filtration barrier modeled as a charged fiber matrix separating anionic from neutral Ficoll**

Öberg CM, Rippe B.
American Journal of Physiology Renal Physiology 304: F781-F787, 2013

II **A distributed two-pore model: Theoretical implications and practical application to the glomerular sieving of Ficoll**

Öberg CM, Rippe B.
American Journal of Physiology Renal Physiology 306: F844-F854, 2014

III **A distributed solute model: an extended two-pore model with application to the glomerular sieving of Ficoll**

Öberg CM, Groszek JJ, Roy S, Fissell WH, Rippe B.
Draft, 2016

IV **Optimizing automated peritoneal dialysis (APD) using an extended three-pore model**

Öberg CM, Rippe B.
Draft, 2016

Acknowledgements

First and foremost I would like to express my deepest gratitude to **Bengt Rippe**, my teacher in research. Thank you for letting me be a part of your fantastic research group and for your excellent supervision during my graduate and doctoral studies. You never ceased to inspire and impress us all with your vast knowledge within physiology, medicine and mathematical modeling. Thank you!

Anna Rippe, my mentor in the laboratory, thank you for teaching me almost everything I know about laboratory work.

Dr. Josefin Axelsson, my co-supervisor for fantastic support, co-operation, sharing of ideas and fruitful discussions.

Jürgen Kuhn, manager at the mass spectrometry lab at the Department of Biology. Your expert assistance has been worth its weight in gold.

Per-Olof Grände, **Peter Bentzer**, **Helene Axelberg**, **Bert-Inge Rosengren**, **Cornelia Lundblad** and **Daniel Asgeirsson** at the physiology lab. Thank you for coffee talks and fruitful discussions about physiology and life in general.

The excellent people at Gambro-Lundia AB, especially **Ola Carlsson**, **Anders Wieslander**, **Gunilla Grundström** and **Anneli Jönsson** for fruitful collaboration and money for doing more research!

The **Department of Nephrology in Malmö and Lund**, **Dr. Kirsten Vang Hendriksen**, **Dr. Ann-Cathrine Johansson**, **Dr. Anders Christensson**, **Dr. Julia Dolinina**, **Dr. Kerstin Westman**, **Dr. Marinka Petkovic** and many more.

Zisis Bimpisidis and prof. **Angela Cenci-Nilsson**, for introducing me to the fascinating world of neuroscience and the physiology of cerebral blood flow and metabolism.

Kerstin Wihlborg for expert secretarial assistance.

And last but not least, my sister **Karin Gunnarsson Nomura** and her family.

Popular summary in English

Most of us go through life without giving much thought to the smallest blood vessels in the body - the capillaries. It is in these, extremely thin, only about 5-7 thousandths of a millimeter thick, blood vessels that the exchange of important nutrients and water occur between the blood circulation and the tissues and different organs in the human body. Among the most important substances that are transported to the tissue are, for example, oxygen and glucose without which the cells in the body cannot survive for very long. Similarly, the end-products of the metabolic activity that occurs throughout the different tissues in the body, such as carbon dioxide and water, are transported away from the tissue. The aim of this thesis is to understand the basic mechanisms behind the transport of various substances that occur over the walls of capillaries - the smallest blood vessels in the body. In general terms, this is accomplished by constructing mathematical models which are then used to analyze experimental data from such transport phenomena. The main focus will, in this thesis, be on the capillaries in the kidney and in the peritoneum - two very different kinds of blood vessels.

The capillaries in the kidney are highly specialized blood vessels that form tiny tufts called glomeruli (singular glomerulus). This capillary tuft is enclosed by a capsule, Bowman's capsule, in which the so-called primary urine is formed by allowing blood to be filtered over the walls of the blood vessels in the tuft. In a pair of human kidneys there are about two million such small vascular bundles through which about one liter of blood per minute flows in a normal-sized adult human. About a fifth of this blood is filtered through the vascular walls of the glomerular capillaries which accommodate the so-called glomerular filtration barrier (GFB). The fluid that is filtered out on the other side of the barrier is called primary urine and contains almost no blood cells or proteins (albumin) at all. The small amounts of protein that do end up in the primary urine is almost completely absorbed and broken down and secreted into the bloodstream as amino acids (the building blocks of proteins) and only a tiny portion of the filtered proteins are normally excreted in urine. The rate with which the primary urine is formed - the so-called glomerular filtration rate (GFR, glomerular filtration rate) - is normally about 180 liters per day (125 ml/min). GFR is commonly used by doctors and other healthcare professionals to measure kidney function. In kidney disease, the GFR is often decreased, reflecting temporary or permanent kidney injury (=meaning that parts of the glomeruli either do not work or filter less blood). This will usually also mean that less urine is produced. There is often also an increased amount of proteins in the urine, called proteinuria, which can be caused by damages in the glomerular capillary wall and, also, a decreased absorption of filtered proteins. In some cases there may also be leakage of blood into the urine which is often a sign of severe damage to the glomeruli.

As Goethe wrote in his famous play Faust, blood is "a rather peculiar fluid" which, in addition to blood cells, contains many important nutrients which the body needs. These include the protein albumin of which there is normally about 40 g per liter of blood (plasma). Since the body normally only produces about 12 grams of albumin per day, any degradation or loss of albumin should not be greater than that. Almost all degradation of albumin occurs in the cells lining the blood vessels of the body, the endothelial cells, while only about 10% (1.2 g / day) is degraded in the kidney. Since 180 L (amount of primary urine per day) multiplied by 40 g/L (7.2 kg!) of albumin is filtered by the kidney barrier every day, this means that only about 0.02% (1.2 g) of albumin can be allowed to "leak" through the kidney filter to prevent the body of being depleted of this important protein. The so-called sieving coefficient (the ratio between the concentration in the water portion of the blood and the primary urine) of albumin is thus in the order of $1 - 2 \cdot 10^{-4}$. The albumin concentration in the primary urine is thus normally only about 4 mg/L. This amazing ability of the kidney to "clean the blood" without leaking important proteins that the body needs is unique to the capillaries in the kidney. The exact mechanisms behind this impressive selectivity towards proteins are, despite years of research, a highly controversial subject.

Study I

Both the GFB and many blood proteins, such as albumin, are negatively charged. A widely accepted explanation for the selectivity of the GFB towards large proteins (like albumin) is that of charge selectivity. The concept of charge selectivity is based on the fact that a negatively charged filter (like the GFB) will repel molecules having a negative charge (anions) to a higher degree than uncharged or positively charged molecules. It is the very same forces that act when a hairbrush gets electrically charged, so-called electrostatic forces. The current view is that the kidney's filter is highly charge selective. This view was, among others, introduced by the British nephrologist and researcher Barry M. Brenner whom made a number of widely publicized experiments in the 1970s. His results are still presented in many textbooks of physiology. Brenner studied the urinary excretion of large synthetic sugar molecules (Dextran) that were either uncharged or negatively or positively charged. He found very large differences in sieving coefficients (the ratio between the measured water concentration in the blood and that in the primary urine) between charged and uncharged molecules. However it was later found that there was binding of the negatively charged sugar molecules to proteins in the blood which resulted in a falsely low sieving coefficient. When the classic experiments were repeated in the 1990ies with a different type of negatively charged sugar molecule (CM-dextran), the differences in transport between charged and uncharged molecules disappeared completely. In Study I, the controversial effects of electric charge on the selectivity in the GFB is explored anew. Here we study a different negatively charged probe molecule (CM-Ficoll) than Dextran. In a previous experiment with CM-Ficoll it was shown that its transport through the GFB was slightly reduced compared to

neutral Ficoll molecules of the same size. Thus, it would appear that their negative charge somehow reduced their transport through the renal filter. In this study, data from the previous experiment were analyzed using a sophisticated mathematical model where the renal filter is modeled as a negatively charged fiber network (a so called fiber matrix). The surface charge of the fiber network can be varied arbitrarily in the mathematical model and we found that a surface charge between 5-20 mC/m^2 (albumin has a surface charge of 22 mC/m^2) was sufficient to explain the reduced transport that the negatively charged Ficoll exhibited in the earlier experiments. In summary, the results from study I indicate that electric charge is of less importance for the transport of charged molecules in GFB than was previously thought. Furthermore it was found that the amount of charge (the surface charge density) on the GFB is similar to that found on many proteins in the body such as albumin.

Study II

By assuming that the capillary walls of the renal vascular bundles (the glomeruli) behave like a porous membrane - as a synthetic filter - one can use already established scientific models to describe and simulate the transport. One such scientific model, that is particularly well developed, is the pore model. It is a model of an ideal spherical molecule in a water solution that is transported through a small cylindrical channel (pore). The entire membrane is simulated by assuming that several such pores are "coupled in parallel". In both the kidney as well as in other capillary walls, there seems to be two different kinds of pathways through which dissolved substances in the blood can be transported. In this study, an extended version of the so-called two-pore model is presented that simulates the transport pathways in the kidney filter by using small and large pores. A prominent feature in the renal filter is that there are far more small pores than there are large pores. Indeed, we might as well just use a small pore if we were only interested in the transport of small molecules since the contribution of the large pores in the transport of small molecules is, for all practical purposes, negligible. In addition to the assumption that there are two porous transport routes through the capillary wall, we assume that the sizes (expressed as the radius of the pore in angstroms, 10^{-10} m) of these porous microchannels are not fixed but can be described by a (log-)normal distribution of different pore sizes. Thus, instead of using fixed pore sizes as in the classic two-pore model, the effective size of the pores are, in this Study, described by average small- and large pore radii with associated standard deviations (which are a measure of the spread/width of the pore size distributions). Just as in the Study I, we analyzed experimental data of the transport of Ficoll through the GFB, but this time only data for uncharged Ficoll were analyzed. We found, among other things, that the average radius of the small pores were about 36 angstroms (1 angstrom = one tenth of a millionth of a millimeter). This can be compared to the effective radius of the albumin molecule which is about 35.5 angstroms. The "spread" of the small pore distribution was

found to be approximately +/- 5 angstroms. If the kidney filter is slightly charge selective - which the results in Study I indicate - that means that albumin could be entirely blocked from entering the small pores in the GFB. However, that would require a smaller spread of the pore-size distribution than what we found in this study (which we will return to in Study III). Study II in combination with the Study I indicate that electric charge may play an important role in the transport of the albumin in the kidney - but only as a 'threshold phenomenon'.

Study III

Already in the 1970s it was realized, by means of studying the urinary excretion of large synthetic sugar molecules (polysaccharides), that polysaccharides, particularly Dextran, seemed to pass through the kidney filter a lot easier than proteins of the same size. This has been interpreted to be due to the negative charge of the proteins, i.e. due to charge selectivity, since the polysaccharides are essentially uncharged. From the results of Study I and II arise, however, an inescapable paradox: how can one explain the difference in transport between sugar molecules (such as Ficoll) and proteins (such as albumin) if molecular charge does not play such a major role as was previously thought? In this work we explore the hypothesis that the sugar molecules are "softer" or "more flexible" than the often more rigid molecular structures of proteins. Here we again use the two-pore model but instead of assuming that the pore sizes are normally distributed (as in Study II), we let the radius of the molecule be normally distributed instead. The molecule thus becomes "soft" and its size is no longer fixed but is described by a statistical distribution. So how soft does a Ficoll molecule have to be to explain its increased transport through the kidney's filter compared to proteins? The answer in this study is that it is enough with only about 16% variation in the size (radius) of the Ficoll molecule. The so-called geometric standard deviation of the molecular radius was thus estimated to approximately 1.16. By contrast, if charge selectivity would be the cause of the difference in transport between polysaccharides and proteins, it can be estimated, by using the model in Study I, that the GFB would have to be super-charged, having a surface charge density roughly 10 times higher than that found on the albumin molecule.

Summary of Study I-III

From Study I-III, it would appear that a molecule's size and structure are of far greater importance than its electrical charge to whether it will leak through the kidney filters or stay in the blood circulation. This result is markedly different from that which is often presented in physiology textbooks where the importance of electric charge is often highlighted. Thus, the question of how the kidney's filter actually works remains unresolved and is still a highly contentious subject.

Study IV

Background

Peritoneal dialysis (PD) is a form of dialysis treatment for patients with severe kidney disease. The dialysis is performed by means of the patients own peritoneum acting as a dialysis membrane. A sugar water solution (usually dextrose and saline) is instilled into the abdominal cavity through a small plastic tube. The dialysis fluid then stays in the peritoneal cavity and absorbs water and solutes from the blood and is discarded after a predetermined dwell time. Unfortunately, dextrose in the dialysis fluid is absorbed into the bloodstream of the patient which can have undesirable effects, especially for diabetic patients. In fact, many patients with kidney failure are diabetics and, in many countries, diabetes has become the leading cause of chronic kidney disease (called diabetic nephropathy). Reducing the ”sugar burden” - the so-called metabolic cost of treatment - has therefore become increasingly important. More and more patients have a machine that automatically pumps dialysis fluid in and out of the peritoneal cavity, so-called automated peritoneal dialysis (APD). This allows treatment at night and often also the use of larger volumes of dialysis fluid, which, in general, increases the efficacy of the treatment. In simplified terms, one can say that the capillaries of the peritoneum are used as a surrogate for the kidney filter in the glomerular capillaries. One of the big differences between peritoneal and renal capillaries is however that the former has a much smaller effective surface area available for transport (at least a factor of 20). This means that the removal of toxins and other waste products from the blood into the dialysis fluid becomes less effective. In addition, the capillaries of the peritoneum lack the great selectivity for large molecules (such as albumin) which is characteristic of kidney capillaries. Thus, patients treated with PD have increased albumin losses (on the order of a few grams per day). Most patients, however, manage to compensate this loss by an increased production in the liver. Nevertheless, the transport of blood solutes across the peritoneal capillary walls can be modeled with two pore systems - just like in the kidney. However, there are more large pores in capillary walls than in the peritoneum. Furthermore, there are water channels in the peritoneum, called aquaporins, through which only water can be transported. So you need three different transport routes through the peritoneum membrane if you want to make a model of the transport that occurs during peritoneal dialysis resulting in the so-called three-pore model. This model is currently the most applied model of PD and is used in many commercial computer software packages to simulate PD, such as PD Adequest® and PDC®. Although the three-pore model is over 20 years old there are still many unresolved issues concerning the actual transport mechanisms involved during PD.

The simulation and optimization of automated peritoneal dialysis

In Paper IV an extended three-pore model is presented which has the unique property that it can also simulate the dialysis process while the dialysis liquid is pumped in and out of

the abdomen. This was not possible with the classic three-pore model. During APD a considerable part of the total dwell time is spent either draining or filling the abdomen with dialysis fluid. This means that the new model is particularly well suited to simulate and optimize the treatment with APD. In particular, the new model is used to find strategies to reduce the absorption of dextrose that inevitably occurs when using dextrose solutions. It is shown that, by using sugar-free solution for longer dwells interspersed with sugar containing solution during shorter dwells, the total glucose absorption can be reduced by 20-30% while providing the same or better effect of the treatment. In addition, it is possible to shorten the total treatment which is desirable in many patients since treatments are often longer than 8 hours - which typically means that the patient must stay in bed and wait for the end of treatment.

Final reflection

The physiological models that are presented and developed in this PhD project attempt, as far as possible, to describe the transport mechanisms that occur in the actual tissue - in the simplest possible way. Although there are clear limitations in the use of simplified models it is often possible to use such models to discern the dominant physiological mechanisms involved in particular phenomena. Perhaps the main advantage of simple scientific models is that they can be invalidated, that is, proven - by direct measurement or calculation - to be incorrect. If this occurs, it may happen that the entire model is rejected or, more commonly, that the model is adjusted based on the new results. The possibility to invalidate a theory is what makes it valuable from a scientific standpoint - and vice-versa.

Populärvetenskaplig sammanfattning på svenska

De flesta av oss går genom livet utan att ägna minsta tanke åt de allra minsta blodkärlen i kroppen – de fina hårrörskärlen – eller kapillärerna som de också kallas. Det är i dessa ytterst tunna, endast cirka 5-7 tusendelar av en millimeter tjocka, blodkärl som utbytet av viktiga näringsämnen och vatten sker mellan blodomloppet och kroppens olika vävnader. Några av de viktigaste ämnena som transporteras till vävnaden är till exempel syrgas och glukos utan vilka vävnaden inte kan överleva särskilt länge. Restprodukterna av den näringsomsättning som sker i vävnaden, bland annat koldioxid och vatten, transporteras i sin tur bort från vävnaden. Syftet med denna avhandling är att förstå mekanismerna bakom den transport av olika ämnen som sker över väggarna i kroppens allra tunnaste blodkärl. I korthet kommer ett antal matematiska modeller att konstrueras med vilka man kan simulera dessa transportfenomen. Modellerna används sedan för att analysera data från experiment i totalt fyra olika delarbeten som redovisas i korthet nedan. Fokus kommer att ligga på njurens och bukhinnans kapillärer - två mycket olika sorters blodkärl.

Njurens kapillärer är specialiserade blodkärl som bildar små nystan som kallas för glomeruli (singularis glomerulus). Nystanet omsluts av en kapsel i vilken den så kallade primärurinen bildas genom att blod filtreras över kapillärväggarna i kärlnystanet. I de mänskliga njurarna finns cirka två miljoner sådana små kärlnystan genom vilka cirka 1 liter blod per minut flödar hos en normalstor vuxen människa. Cirka en femtedel av detta blod filtreras genom kärlväggarna i de glomerulära kapillärerna som rymmer den så kallade glomerulära filtrationsbarriären (GFB). Det som filtreras ut på andra sidan barriären kallas för primärurin och innehåller nästan inga blodkroppar eller proteiner (äggviteämnen) överhuvudtaget. De små mängder äggviteämnen som ändå tar sig över från blodet till primärurinen bryts till största delen ner och utsöndras i blodbanan som aminosyror (proteinernas byggstenar) medan endast en mycket liten del proteiner utsöndras i urinen. Den hastighet med vilken primärurinen bildas – den s.k. glomerulära filtrationshastigheten (GFR; glomerular filtration rate) - brukar läkare och annan sjukvårdspersonal använda för att mäta njurfunktionen och uppgår normalt till hela 180 L per dag (125 mL/min). Vid njursjukdom, är GFR ofta minskad, vilket tyder på en tillfällig eller permanent njurskada (= vilket innebär att delar av glomeruli inte fungerar eller filtrerar mindre blod). Detta kommer vanligtvis också att innebära att mindre urin produceras. Det finns ofta också en ökad mängd proteiner i urinen, vilket kallas proteinuri, vilket kan tyda både på skador i kapillärväggen och, också, en minskad absorption av filtrerade proteiner. I vissa fall kan det också finnas ett läckage av blod ut i urinen vilket, i detta sammanhang, ofta är ett tecken på svåra skador i glomerulus.

Precis som Goethe skrev i sin berömda pjäs Faust är blod ”en ganska egendomlig vätska” som, förutom blodkroppar, innehåller många viktiga ämnen som kroppen behöver. Bland dessa kan nämnas proteinet albumin av vilket det normalt finns cirka 40 g per liter blod (plasma). Eftersom kroppen endast tillverkar cirka 12 g albumin per dygn så bör nedbryt-

ningen eller förlusterna av albumin inte vara större än så. Nästan allt albumin bryts ner av de celler som sitter i kroppens blodkärlsväggar, av de så kallade endotelcellerna, medan bara ungefär 10% (1.2 g/dygn) bryts ner i njuren. Eftersom 180 L (mängden primärurin per dygn) multiplicerat med 40 g/L (7.2 kg!) albumin filtreras av njurens barriär varje dygn, så innebär detta att endast cirka 0.02% (1.2 g) av albuminet får ”läcka ut” genom njurens filter för att undvika att kroppen utarmas på detta för kroppen mycket viktiga protein. Den så kallade sievingkoefficienten (kvoten mellan vattenkoncentrationen i blodet och i primärurinen) för albumin är alltså i storleksordningen $1 - 2 \cdot 10^{-4}$. Koncentrationen av albumin i primärurinen är alltså normalt kring 4 mg/L. Denna fantastiska förmåga att rena blodet utan att det läcker ut viktiga ämnen som kroppen behöver är unik för njurens kapillärer och det är just denna selektivitet som, trots många års forskning, fortfarande är högst kontroversiell.

Arbete I

Både njurens filter och många proteiner i blodet såsom albumin är negativt elektriskt laddade. En sedan länge accepterad förklaring på den otroliga selektivitet som njurens filter har gentemot stora proteiner som albumin är det som kallas för laddningsselektivitet (eng. charge selectivity) och går ut på att ett negativt elektriskt laddat filter (som njurens filter) kommer att repellera molekyler med negativ laddning till en högre grad än oladdade eller positivt laddade molekyler. Det är precis samma krafter som verkar som när en hårborste blir laddad, så kallade elektrostatiska krafter. Denna syn på njurens filter som varandes otroligt laddningsselektivt härstammar, bland andra, från den engelske njurmedicinaren och forskaren Barry M. Brenner som gjorde ett antal mycket uppmärksammade studier på 70-talet som citeras flitigt i många läroböcker i fysiologi. Brenner studerade utsöndringen i urinen av stora syntetiska sockermolekyler (Dextran) som antingen var elektriskt neutrala eller hade en negativ eller positiv laddning och fann mycket stora skillnader i sievingkoefficienterna (kvoten mellan koncentrationen i blodet och i primärurinen) mellan dessa olika laddade molekyler. Dock har man i efterhand funnit att de negativt laddade sockermolekylerna binder till äggviteämnen (så kallade plasmaproteiner) i blodet vilket åstadkommit en skenbart låg sievingkoefficient för dessa. När man gjort om de klassiska försöken med en annan typ av negativt laddade sockermolekyler (CM-Dextran) så har laddningseffekterna försvunnit helt. Arbete I utforskar på nytt de kontroversiella effekterna av elektrisk laddning för selektiviteten i njurens filter. Här använder vi en annan negativt laddad probmolekyl (CM-Ficoll) än Dextran. Tidigare försök med CM-Ficoll visade att dess transport genom njurens filter var något minskad jämfört med neutrala molekyler av samma sort. Alltså verkar det som om att deras negativa laddning minskade deras transport. Här analyseras data från det tidigare försöket med hjälp av en avancerad matematisk modell där njurens filter modelleras som ett negativt elektriskt laddat fibernätverk. Ytladdningen på fibernätverket kan varieras helt godtyckligt i den matematiska modellen och vi fann att en ytladdning mel-

lan 5-20 mC/m² (proteinet albumin har en ytladdning på 22 mC/m²) kunde förklara den minskade transport som de negativt laddade molekylerna uppvisade. Sammanfattningsvis visar resultaten från denna studie att elektrisk laddning kan vara av mindre betydelse för transporten av laddade molekyler i GFB än man tidigare trott och att den laddning som finns på njurens barriär liknar den hos många proteiner i blodet som till exempel albumin.

Arbete II

Genom att anta att kapillärväggen i njurens kärlnystan beter sig som ett poröst membran - som ett syntetiskt filter - kan man använda redan etablerade vetenskapliga modeller och koncept för att beskriva transporten. En sådan vetenskaplig modell som är särskilt välutvecklad är pormodellen. Den beskriver en idealisk rund molekyl i vattenlösning som transporteras genom en cylindrisk liten kanal (por). Ett helt membran simuleras sedan genom att anta att flera sådana porer är ”parallellkopplade”. I såväl njurens som andra kapillärers väggar verkar det finnas två olika porsystem genom vilka ämnen i blodet kan transporteras. I detta delarbete presenteras en utökad variant av den så kallade två-porsmodellen som delar upp njurens filter i små och stora porer. En framträdande egenskap i njurens filter är att det finns långt mycket fler små porer än stora porer. Faktiskt hade det gått lika bra att bara använda en småpor om vi bara var intresserade av transporten av mindre molekyler. Förutom antagandet att det finns två transportvägar genom kapillärväggen antar vi att storlekarna (uttryckt som radie i ångström, $10^{-10}m$) på dessa mikrokanaler inte är fasta utan kan beskrivas av en normalfördelning (distribution) av olika porstorlekar. Medelvärdet på denna normalfördelning av porstorlekar är den så kallade medelporradien. Alltså finns i den nya modellen en småporsmedelradie och en storporsmedelradie med tillhörande spridningsmått eller standardavvikelse som är ett mått på hur stor spridningen är i de olika fördelningarna. Precis som i Arbete I, analyserades experimentell data av transporten av Ficoll över njurens filter, fast denna gång bara elektriskt oladdat Ficoll. Vi fann bland annat att medelradien för de små porerna var cirka 36 ångström (en ångström = en tiondels miljondel av en millimeter!). Detta kan jämföras med den effektiva radien av albuminmolekylen som är cirka 35.5 ångström. Spridningen för de små porerna fann vi vara cirka +/- 5 ångström. Om njurens filter är lätt laddningsselektivt – vilket resultaten i Studie I pekar på – så innebär det att albumin i stort sett inte alls passerar genom de små porerna i njurens membran. Detta förutsätter dock en mindre spridning än vad vi fann i denna studie (vilket vi återkommer till i Arbete III). Arbete II i kombination med Arbete I tyder alltså på att elektrisk laddning - trots allt - kan spela en viktig roll för transporten av det albumin i njurens membran - men som ett *tröskelfenomen*.

Arbete III

Redan på 70-talet hade man med hjälp av att studera utsöndringen i urinen av stora syntetiska sockermolekyler (polysackarider) kommit fram till att sockermolekyler, framförallt Dextran, verkade passera njurens filter mycket lättare än proteiner av samma storlek. Detta har tolkats bero på att den negativa laddningen hos proteinerna gör att de passerar i mycket mindre utsträckning än de oladdade sockermolekylerna. Från resultatet från Arbete I och II uppstår dock en ofrånkomlig paradox: hur kan man förklara skillnaden i transport mellan sockermolekyler såsom Ficoll och proteiner om nu laddning inte spelade så stor roll? I detta arbete utforskar vi hypotesen att sockermolekylerna är ”mjukare” eller ”mer flexibla” än de ofta mer rigida molekylstrukturerna hos proteiner. Här tar vi återigen användning av tvåporsmodellen men i stället för att anta att porstorlekarna är normalfördelade så låter vi själva radien på molekylen vara normalfördelad. Molekylen blir därmed ”mjuk” och dess storlek är inte längre fast utan beskrivs av en statistisk distribution. Så hur mjuk måste en Ficoll-molekyl vara för att förklara dess ökade transport genom njurens filter? Svaret i denna studie är att det räcker med endast cirka 16% variation i storleken (radien). Den så kallade geometriska standardavvikelsen för molekylradien uppskattades därmed till cirka 1.16. Om vi leker med tanken att det skulle vara laddningsselektivitet som orsakade skillnaden i transport mellan polysackarider och proteiner, så kan man räkna ut, med hjälp av modellen i Arbete I, att det skulle krävas en ”super-laddad” barriär i njuren med ungefär 10 gånger högre laddningstäthet än den som finns på albuminmolekylen.

Sammanfattning av Arbete I-III

Utifrån Arbete I-III verkar det som om att en molekyls storlek och struktur är av betydligt större betydelse än elektrisk laddning för huruvida ett ämne kommer att läcka igenom njurens filter. Detta resultat skiljer sig markant från den som ofta återges i läroböcker där betydelsen av elektrisk laddning ofta lyfts fram. Således är frågan om hur njurens filter ”sorterar molekyler” fortfarande olöst och högst kontroversiell.

Arbete IV

Bakgrund

Peritonealdialys (PD) är en form av dialysbehandling för patienter med svår njursvikt. Dialysen sker med hjälp av den egna bukhinnan som dialysmembran genom att en sockerlösning (vanligen glukos och salter) tappas in i bukhålan via en liten plastslang. Dialysvätskan drar sedan till sig vatten och i blodet lösta ämnen och tappas ut efter en förutbestämd tid. Den glukos som finns i dialysvätskan tas upp i blodet hos patienten vilket kan ha icke-önskvärda effekter, särskilt för patienter som har diabetes. Faktum är att många patienter

med njursvikt har diabetes och i många länder har diabetes blivit den ledande orsaken till kronisk njursvikt (så kallad diabetesnefropati). Att minska "sockerbördan" – den så kallade *metabola kostnaden* för behandlingen – har därför blivit allt viktigare. Allt fler patienter har en maskin som hjälper till att tappa in och ut dialysvätska, så kallad automatiserad peritonealdialys (APD). Detta möjliggör behandling nattetid och dessutom ofta användande av större volymer dialysvätska vilket, generellt sett, ökar effekten av behandlingen. Förenklat kan man alltså säga att kapillärerna i bukhinnan (peritoneum) används som surrogat för njurens kapillärnystan (glomeruli). Den stora skillnaden mellan bukhinnans och njurens kapillärer är dock att de förra har en mycket mindre effektiv yta tillgänglig för transport (cirka en faktor 10-20) vilket innebär att transporten av toxiner och andra restprodukter till dialysvätskan blir mindre effektiv. Dessutom saknar kapillärerna i bukhinnan den stora selektivitet för stora molekyler som t ex albumin som är kännetecknande för njurens kapillärer och patienter som behandlas med PD har alltså större albuminförluster (några gram per dygn) – de flesta patienter lyckas dock kompensera genom en ökad produktion i levern. Icke desto mindre kan transporten av lösta ämnen över bukhinnans kapillärväggar modelleras med två porsystem – precis som i njuren! Dock finns det alltså fler stora porer i bukhinnans kapillärväggar. Därutöver finns det i bukhinnan vattenkanaler, så kallade aquaporiner, genom vilka endast vatten kan transporteras. Alltså behöver man tre olika transportvägar genom bukhinnans membran om man vill göra en modell över den transport som sker vid peritonealdialys vilket resulterat i den så kallade tre-porsmodellen. Denna modell är idag den mest tillämpade och används i flera kommersiella programvaror för att simulera PD, exempelvis PD Adequest® och PDC®. Trots att tre-porsmodellen är över 20 år gammal finns fortfarande många olösta frågor kring de faktiska transportmekanismerna.

Att simulera och optimera automatiserad peritonealdialys

I Arbete IV presenteras en utökad treporsmodell som har egenskapen att den också kan modellera dialysprocessen under det att dialysvätska tappas in och ut ur buken. Detta var inte i detalj möjligt med den klassiska tre-porsmodellen. Vid APD spenderas ofta en avsevärd del av den totala dialystiden åt att antingen tappa ur eller fylla buken med dialysvätska vilket gör att den nya modellen lämpar sig särskilt väl till att simulera och – inte minst – optimera behandlingen med APD. I synnerhet ägnas en del av detta arbete åt att försöka hitta strategier för att minska det upptag av socker som ofrånkomligen sker när man använder sockerlösningar. Det visade sig att man, genom att använda sig av sockerfri lösning under långa perioder varvat med sockerlösning under kortare perioder, kan minska den totala sockerabsorptionen med 20-30% samtidigt som man får samma eller bättre behandlingseffekt. Detta kan motsvara 40-60 g minskat glukosupptag per dygn för en typisk behandling. Samtidigt är det möjligt att korta ner den totala behandlingstiden vilket är önskvärt hos många patienter då behandlingarna i nuläget ofta sträcker sig över 8 timmar - vilket innebär att patienten måste ligga kvar i sängen och vänta på att behandlingen avslutats.

Avslutande reflektion

De fysiologiska modeller som används och utvecklas i detta doktorandprojekt försöker så långt som möjligt efterlikna de transportmekanismer som förekommer i den verkliga biologiska vävnaden – på enklast möjliga sätt. Även om det finns klara begränsningar i att använda sig av förenklade modeller kan man – med deras hjälp - ofta urskilja de dominerande fysiologiska mekanismerna i ett fenomen eller skeende i kroppen. Den kanske största fördelen med sådana enkla naturvetenskapliga modeller är att de kan vederläggas, det vill säga motbevisas - genom direkt mätning eller uträkning. När så sker kan det hända att hela modellen förkastas eller, vilket är vanligare, att modellen korrigeras utifrån de nya resultaten.

Background

Everything should be made as simple as possible, but not simpler
— Albert Einstein

1 Introduction

The mechanisms of transport of water and solute matter between the different compartments in the human body are of the greatest importance for the normal function of the entire organism. Both nutrition and removal of waste products from the metabolic activity of living tissue is ultimately a matter of transport and even small perturbations in this transport may have severe effects. Thus the harmonious interplay between these transport mechanisms is a condition necessary for life.

Biological transport phenomena may occur both actively and passively. An example of active transport is the reabsorption of glucose in the kidney, where transport is facilitated via an energy consuming glucose transporter (SGLT1) in the proximal tubular cells. An example of passive transport is the rapid electrodiffusion of sodium ions into a cardiomyocyte in order to cause depolarization and subsequent contraction. While there are many examples of facilitated transport, most transport processes in the human body are of a passive nature. Thus, insight into the mechanisms behind this transport can be used to treat and improve conditions in which this transport is perturbed due to disease or - as is the case in Study IV - during dialysis treatment.

The current work is devoted entirely to understanding and modeling passive transport phenomena, or more specifically, the simple diffusion, electric migration and filtration of solute matter and water over glomerular and peritoneal capillary walls. The driving forces behind these passive transport processes have long been assumed to be simple gradients of concentration, hydrostatic pressure and electric potential. Despite decades of research, the relative importance of these different transport mechanisms remains a highly controversial subject.

2 Historical background

Already in the 1950ies it was noted by Pappenheimer et al [60] that the transport of solute matter and water over capillary walls was very similar to that occurring over artificial membranes. This observation gave birth to the theory that the entire circulation is in direct contact with the extravascular fluid via small microchannels that were large enough to allow the passage of water and small solutes but smaller than large plasma proteins [59]. To this day it is believed that the main pathway for transvascular transport of smaller lipid-insoluble molecules is via the intercellular gaps and junctions between endothelial cells [51]. The entire cardiovascular system is lined by a capillary endothelium which is a simple layer of flattened cells joined by such intercellular junctions. The endothelium is supported by an acellular basement membrane largely composed of collagenous fibers. Throughout the body, there are differences in the thickness of the endothelium, the presence of intercellular gaps (fenestrae), the type of intercellular junctions et cetera. Thus, the transport characteristics through different capillary beds can be expected to vary. Lipid-soluble molecules are able to pass through the cells and are not restricted to the same extent as lipid-insoluble solutes. A large body of evidence also existed early on for a second pathway of larger microchannels through which macromolecules can pass which would explain, among other things, the existence of large macromolecules in the extravascular fluid [65, 70, 71]. Concerning plasma to lymph transport, studies using polydisperse Dextran demonstrated the bi-selective nature of peripheral capillaries demonstrating a steep slope indicating small microchannels (pores) through the capillary wall of 35-40Å and "a tail" demonstrating the presence of large pores [20, 33]. A similar pattern of two different pathways for Dextran was found in the glomerular filtration barrier [97].

Since the pioneering studies of Pappenheimer and others, a large number of studies have confirmed the passive nature of the transport of both small solutes [51] and macromolecules [33]. For albumin and Cr-EDTA, the transport has been shown to be reduced when the viscosity of the filtrate was increased by lowering the temperature [68]. Furthermore, the transvascular transport of albumin is increased with increasing venous pressure and increasing oncotic pressure (during isovolumetric conditions) [73]. These findings all support the concept of "large pores" in the peripheral capillary wall as being the principal pathway for the passive transport of macromolecules like albumin. Thus, although passive transport mechanisms ("large pore transport") of macromolecules seem to dominate in both renal and peripheral capillaries, the relative contribution of transcytosis is a much debated issue [76]. In renal glomerular capillaries, there is some evidence for transcellular transport of albumin via podocytes comprising about 10% of the total transvascular albumin transport during normal conditions [17]. Interestingly, in peripheral capillaries, there seems to be a break-point in venous pressure at 40-60 mmHg where the trans-capillary albumin clearance is greatly enhanced, representing the so called "stretched pore phenomenon" [45, 72, 73, 87] which may reflect an actual stretching of the interendothelial gaps. Rippe and Har-

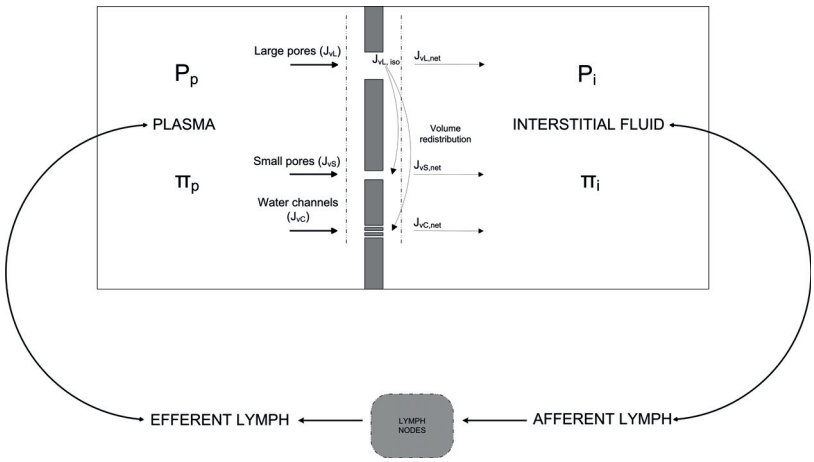

Figure 1: A systematic overview of the different trans-vascular transport pathways. Due to the difference in selectivity a volume recirculation occurs during isovolumetric conditions.

aldsson however observed that small solute diffusion only increased moderately (30-40%) whereas marked increases in hydraulic conductance were observed during marked elevations of venous pressure [72]. The reasons behind such an uncoupling is unclear but may, in terms of pore theory, represent a marked increase in large pore radius or the formation of very large gaps in the vascular wall in addition to an increased small-pore radius. Such alterations of a porous membrane would lead to large increases in LpS (power of 4) and smaller changes in PS (power of 2). As is discussed by Rippe et al, the likely site for the formation of such very large gaps is in the venular vascular walls [72].

Nearly 50 years ago, the presence of a trans-cellular water pathway was hypothesized by Yudilevich et al [104]. Decades later, advances in molecular biology made possible the discovery of the aquaporine family of water channels [3]. While a large portion of water passes through these channels, a significant amount will be transported via the inter-cellular pathway (the small pores). The relative contribution of the AQP-1 to water transport in the peritoneum has been quantified by using aquaporin knock-out mice and contributes to a few percent of the total hydraulic conductance [55]. Nevertheless, the aquaporins play an important role for the osmotic pressure of small solutes and contribute to about 40-50% of the osmotic reflection coefficient of glucose in the peritoneal barrier (i.e. almost half of the osmotic water transport at the beginning of the dwell in PD occurs via the aquaporins) [77].

3 The Kedem & Katchalsky Model

The simultaneous transport of a solute immersed in a solvent over a membrane into another compartment filled with the same solvent and solute is non-trivial to describe mathematically. More than 50 years ago, Kedem and Katchalsky (K & K) used basic principles of non-equilibrium thermodynamics to derive a single set of permeability coefficients that have been widely used to describe the steady-state transport of plasma solutes and water over the vascular wall [39-42] and other biological barriers. The equations were constructed in order to address shortcomings in the previous models in correctly describing observed transport phenomena. For example, the diffusion of heavy water (D_2O) in an isotonic Ringer solution into fish and frog eggs can be accurately described by Fick's equation

$$\frac{dN_i}{dt} = PA\left(\frac{N_i}{V_i} - c_o\right) \tag{1}$$

where $N_i(t)$ is the molar amount of D_2O in the inner compartment at time t with volume V_i, P is the permeability coefficient, A the surface area and c_o the amount of D_2O in the outer solution. Discrepancies from this equation were noted when the eggs were put in a non-equilibrated Ringer solution which was interpreted as being the result of the simultaneous diffusion and filtration of D_2O [42, 63]. The transport of D_2O was more rapid in hypotonic solutions and vice versa. The product PA (often written PS) is nowadays often called the *diffusion capacity* or *mass transfer area coefficient* (MTAC) of the solute and represents the maximal diffusive clearance of the solute (in mL/min) for a particular biological or synthetic membrane.

Many phenomena in nature are not in equilibrium and thus generate entropy. In the case of a two-component solute-solvent system the rate of entropy production can be written

$$\frac{dS}{dt} = \frac{1}{T}\left(\Delta\mu_w \frac{dN_w^i}{dt} + \Delta\mu_s \frac{dN_s^i}{dt}\right) \tag{2}$$

where N_w^i and N_s^i are the molar amounts of solvent and solute in the inner compartment, respectively. $\Delta\mu_w$ and $\Delta\mu_s$ are the differences in chemical potential between the inner and outer compartments for water (solvent) and solute, respectively. The above entropy equation may be written as a so called *dissipation function*:

$$\Phi_d = \sum_{i=1}^{n_{flows}} J_i X_i = \frac{T}{A}\frac{dS}{dt} = \Delta\mu_w \dot{n}_w + \Delta\mu_s \dot{n}_s \tag{3}$$

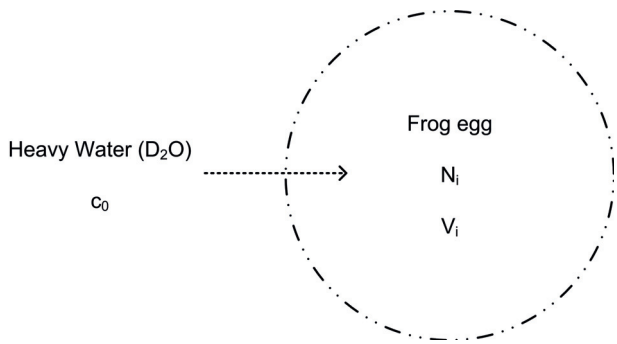

Figure 2: Heavy water D_2O in a Ringer solution diffusing into a frog egg. $N_i(t)$ is the molar amount of D_2O in the inner compartment at time t with volume V_i, P is the permeability coefficient, A the surface area and c_o the amount of D_2O in the outer solution.

which is defined as the sum of the products of forces X_i and flows J_i (cf. [97]) and

$$\dot{n}_w = \frac{1}{A}\frac{dN_w^i}{dt} \tag{4}$$

$$\dot{n}_s = \frac{1}{A}\frac{dN_s^i}{dt} \tag{5}$$

Actually, the choice of forces and flows is entirely arbitrary and thus this is indeed a case of "there is more than one way to do it". Using the approximation of an ideal dilute solution (cf. also [19]), we can write the chemical potentials or "forces" as

$$\Delta\mu_w = \nu_w\Delta P + RT\Delta ln\gamma = \nu_w\Delta P - RT\frac{\Delta c_s}{c_w} \tag{6}$$

$$\Delta\mu_s = \nu_s\Delta P + RT\Delta ln\gamma = \nu_s\Delta P + RT\frac{\Delta c_s}{c_s} \tag{7}$$

where ν_s and ν_w are partial molar volumes (i.e. the fractional contribution to the overall volume), γ is the molar fraction (i.e. the concentration in the outer compartment divided by that in the inner compartment) of the constituent and $\Delta c_s = c_s^o - c_s^i$ and c_s is the average concentration in the entire system. The definition of the average concentration c_s has varied over the years [101]. K & K proposed that if $\Delta c_s/c_i^s << 1$ then $c_s \approx (c_s^o - c_s^i)/2$ may be used. The dissipation function (sum of products of forces and flows) may now be written

$$\Phi_d = (\dot{n}_w\nu_w + \dot{n}_s\nu_s)\Delta P + \left(\frac{\dot{n}_s}{c_s} - \frac{\dot{n}_w}{c_w}\right)RT\Delta c_s \tag{8}$$

Thus, the "forces" are $X_1 = \Delta P$ and $X_2 = RT\Delta c_s$ and the flows are

$$J_1 = (\dot{n}_w \nu_w + \dot{n}_s \nu_s) \tag{9}$$

$$J_2 = \left(\frac{\dot{n}_s}{c_s} - \frac{\dot{n}_w}{c_w} \right) \tag{10}$$

Where J_1 is the net volume flow per unit membrane area A and J_2 is the "exchange flow" (relative velocity of the solute versus the solvent).

3.1 Cross coefficients

The key assumption made by K & K is that the relationship between the driving forces (differences in concentration Δc and pressure ΔP) and the resulting flows (J_1 and J_2 in mL/min) is linear

$$J_1 = L_{11} \cdot \Delta P + L_{12} \cdot \Delta c \tag{11}$$

$$J_2 = L_{21} \cdot \Delta P + L_{22} \cdot \Delta c \tag{12}$$

where L_{11}, L_{12}, L_{21} and L_{22} are the phenomenological coefficients relating the driving force to their effect on the flows. It is assumed that the coefficients are not dependent on the forces (i.e. concentration or pressure) and that they are constant (i.e. everywhere the same in the membrane). Such an assumption is a reasonable approximation if the distances are small and the medium is completely homogenous. The law of Onsager requires the equality of the cross-coefficients, $L_{ik} = L_{ki}$, and thus $L_{12} = L_{21}$. To facilitate comparison with experimental measurements, the above system of coefficients was modified and the cross-coefficients were defined as

$$L_{21} = L_{12} = -\sigma L_p \tag{13}$$

where σ is the Staverman reflection coefficient [91] and L_p is the hydraulic conductivity (i.e. $L_p A = L_p S$ is the hydraulic conductance). Thus, for example, if $\Delta c > 0$ and $\Delta P > 0$ both water and solute flow are reduced by a factor σL_p.

3.2 The practical K & K equations

For practical purposes the above system of equations was simplified by K & K. First, in a practical experimental situation we are usually more interested in the net solute flow

$\dot{n}_s = (J_1 + J_2)c_s$ (if $c_s\nu_s << 1$) than we are in J_2. Second, in a dilute solution $\nu_s \approx 0$ and $\nu_w \approx 1$ so the water flow $J_v \approx \dot{n}_w$ (mL/min) and the resulting equations can be written

$$J_v = \dot{n}_w = L_pA\left(\Delta P - \sigma RT\Delta c_s\right) \tag{14}$$

$$J_s = \dot{n}_s = L_pA\Delta P(1-\sigma)c_s + (L_{22}A - c_sL_pA)RT\Delta c_s = -PA\Delta c_s + J_v(1-\sigma)c_s \tag{15}$$

For the transport of an uncharged solute, the membrane could now be completely described by three coefficients: the hydraulic conductivity (L_p), the diffusional permeability ($P = -L_{22}RT$) and the Staverman reflection coefficient (σ).

3.3 The Patlak differential equations and the heteroselective model

Under the assumption of local (global) equilibrium and homogeneity, the membrane was essentially described by K & K as a "black box" giving rise to changes in chemical potential leading to differences in pressure, concentration and electrical charge between the two neighboring solutions. While there is no formal error in this macroscopic treatment of barrier, there are limitations in the applicability of the model equations [16][25] due to the fact that the underlying assumptions may not necessarily be true for all membranes. One limitation was the local nature of the original equations which necessitated an approximation of the average concentration profile over the (global) barrier. This matter was resolved by Patlak et al who wrote the equations in a separable differential form which, when integrated, led to an expression for the concentration profile cr over the barrier [61]. This description of the filtration barrier is - in terms of differential equations - identical to the one-dimensional steady-state convection-diffusion equation with the volume flux described by the Starling equilibrium. The system of differential equations presented by Patlak were

$$J_v = L_pA\left(\frac{dp}{dx} - \sigma RT\frac{dc}{dx}\right) \tag{16}$$

$$J_s = -DA\frac{dc}{dx} + J_v(1-\sigma)c \tag{17}$$

This is a very common system of differential equations used in the modeling of transcapillary transport phenomena [26, 38, 71, 94]. In many practical applications it is typically assumed that the pressure and concentration profiles in Equation 16 are linear ($\frac{dp}{dx} = \Delta P$ and $\frac{dc}{dx} = \Delta C$). Another limitation in K & K model, subject to much discussion over the years, is that the equations do not apply if the barrier is heteroselective (i.e. does not present the same selectivity to solutes of different sizes) [14]. As discussed by Katz et al the application of the original coefficients to a heteroselective barrier inevitably leads to an

inequality of the osmotic and solvent drag reflection coefficients [38]. For water transport, the two-pore model result is

$$J_{v,S} = \alpha_S L_p A\,(\Delta P - \sigma_S RT\Delta C) \tag{18}$$

$$J_{v,L} = \alpha_L L_p A\,(\Delta P - \sigma_L RT\Delta C) \tag{19}$$

so that the net water flux equation is

$$J_v = L_p A\,(\Delta P - \sigma_o RT\Delta C) \tag{20}$$

where the osmotic reflection coefficient is given by $\sigma_o = \alpha_S\sigma_S + \alpha_L\sigma_L$. For solute transport we have

$$J_s = -DA_S\frac{dc}{dx} + J_{v,S}(1-\sigma_S)c \tag{21}$$

$$J_s = -DA_L\frac{dc}{dx} + J_{v,L}(1-\sigma_L)c \tag{22}$$

so that the net solute flux is

$$J_s = -DA\frac{dc}{dx} + J_v(1-\sigma_d)c \tag{23}$$

where the filtration (solvent drag) reflection coefficient is given by $\sigma_d = \frac{J_{v,S}}{J_v}\sigma_S + \frac{J_{v,L}}{J_v}\sigma_L = f_S\sigma_S + f_L\sigma_L$ and $A = A_S + A_L$. Thus, if an osmotic gradient exists over a heteroselective barrier, then the volume flow through each pathway will be different from that predicted solely from the hydraulic conductance of that pathway. This phenomenon, which is sometimes referred to as *volume recirculation* (perhaps more correctly termed volume redistribution since any actual recirculation does not always occur), leads to the inequality of the fractional hydraulic conductance (α_i) and the fractional water flux (f_i) through a particular pathway [70]. This in turn means that Onsager reciprocity is (usually) not fulfilled for a heteroselective pathway since $\sigma_o \neq \sigma_d$ (unless there is no osmotic gradient). In other words, the three classic phenomenological coefficients are inadequate to describe solute transport over a heteroselective barrier [32] and the addition of a fourth phenomenological coefficient becomes necessary which gives rise to the two-pore theory of capillary permeability [71].

In the literature, observed increments in solute or water transport between the circulation and other compartments are commonly reported as an increased permeability although the permeability itself can be unchanged or even lower than baseline. Such misconceptions

Table 1: Permeability coefficients for a heteroselective barrier.

SOLUTE PERMEABILITY	SOLVENT PERMEABILITY
Diffusional permeability (P)	Osmotic reflection coefficient (σ_o)
$P = \int_0^{\Delta x} \frac{J_s}{A \cdot c(x)} dx$ when $J_v = 0$	$\sigma_o = \frac{\Delta P}{\Delta C}$ when $J_v = 0$
Convectional permeability (σ_d)	Water permeability (L_p)
$\sigma_d = 1 - \frac{J_s}{J_v c}$ when $\frac{dc}{dx} = 0$	$L_p = \frac{J_v}{A \cdot \Delta P}$ when $\frac{dc}{dx} = 0$

highlight the importance of differing between the properties of the barrier itself, the properties of the permeating fluid and the driving forces (pressure, concentration et cetera). In Table 1, the four phenomenological membrane coefficients for a heteroselective barrier are listed with their definitions. Importantly, the "solvent drag" reflection coefficient (σ_d) is different from the osmotic reflection coefficient (σ_o). For a homoselective membrane $\sigma_d = \sigma_o$ and Onsager reciprocity is fulfilled.

Transport theory

It's easy to be complicated
but very difficult to be simple.
— Debasish Mridha

4 The solute sphere

Many important questions arise when theoretical assumptions are studied in detail. If we first assume a single spherical solute molecule - which we here call a *solsphere* for convenience - suspended in a volume partition V^* of water surrounded by a larger body of water V. The net movement of such particles is a result of countless collisions with individual water atoms constantly altering the position of the solsphere. At each point along its complex trajectory in the water partition, the solsphere will experience an opposing frictional force with frictional coefficient μ. The terminal velocity U (m/s) attained by the solute molecule is simply the forces acting in the forward direction of the molecule divided by this frictional coefficient (μ)

$$U = \frac{F}{\mu} \tag{24}$$

If the dimensions of the solsphere is at least several times larger than the surrounding water molecules it can be viewed as a hydrodynamic particle [24]. The frictional coefficient for a solsphere was calculated by Sir George Stokes in the 1840ies

$$\mu = 6\pi\eta r \tag{25}$$

where r is the radius of the solsphere and η is the viscosity of the solvent [93]. Thus, according to Stokes, for a 3.6 nm molecule moving freely in a water solution $\mu \approx 48$

pNs/m. What is this body force F acting on the solsphere in a free water solution? Well, first if the particle is in equilibrium the the net force is 0 and the particle is equally likely to move anywhere in the solution. If the particle is not in equilibrium, then, according to thermodynamic laws, it generates entropy, and in the absence of any water flux we can write our dissipation function

$$T\frac{dS}{dt} = \dot{n}_s \mu_s \tag{26}$$

where μ_s is the phenomenological "force" and $\dot{n}_s$ is the solute flow. The concentration $c(x)$ of a solute is here defined as proportional to the probability of finding a certain molecule at that precise location x. Of course this definition includes the everyday definition of concentration as being the number of molecules per unit volume. An important difference is that the former definition allows us to understand the concept of a *pointwise concentration*. Making the same assumptions as before and assuming that there is no pressure gradient, the force acting on a single solsphere must be

$$F = \frac{\mu_s}{N_A} = \frac{RT}{N_A}\ln\gamma = kT\frac{d\ln c}{dx} = kT\frac{1}{c}\frac{dc}{dx} \tag{27}$$

where N_A is the constant of Avogadro and R and k have their usual meanings. If the particle is in steady motion through the water (i.e. the net force is 0) we have

$$kT\frac{d\ln c}{dx} + U\mu = 0 \tag{28}$$

The solute flow is simply the concentration multiplied by the terminal velocity and the surface (contact) area (Js=AUC) and apparently

$$J_s = \frac{kT}{6\pi\eta r}A\frac{dc}{dx} = DA\frac{dc}{dx} \tag{29}$$

which is Fick's first law with the so called Stokes-Einstein diffusion coefficient $D = \frac{kT}{6\pi\eta r}$. If the diffusion coefficient is determined experimentally, the equation can be used to calculate the radius of the diffusing solute which is called the *Stokes-Einstein radius* (SE-radius) or *hydrodynamic radius* (usually in angstroms = Å = 10^{-10} m). It is of course possible to calculate such a radius even if the solute is very far from being an ideal spherical molecule. Since the solsphere is contained within the volume partition V^* it will, in addition to the hydrostatic pressure of the water in the partition, exert a pressure on the walls of the partition according to the well known equation

$$p = RT\frac{dc}{dx} \tag{30}$$

According to Newton's third law there must also be a pressure equal in magnitude acting in the other direction (on the outside of the walls) on the partition. This is known as the *osmotic pressure*. When the osmotic pressure is calculated from the above equation it is sometimes called a Van't Hoff pressure.

5 A brief introduction to pore theory

In this section the theory for the transport of an ideal solute sphere in a long water filled pore will be summarized. Several such parallel pores represent a simple model for a porous membrane. In this situation, additional forces than those considered above will need to be taken into account due to the interaction between the solsphere and the pore walls. Transport is assumed to occur along the axial direction of the pore (x) and (as will be further developed below) no transport is assumed to occur in the radial direction (r). The friction caused by the presence of the pore walls is expressed as a drag coefficient K. Also, the presence of pore walls causes the solsphere to "lag behind" the water flux velocity (V) in the pore. In steady state, the forces acting on a solsphere are

$$kT\frac{d\ln c}{dx} + K(U - GV)\mu = 0 \tag{31}$$

The local solute flux is $N = UC$ so

$$N = -K^{-1}D\frac{dc}{dx} + GVc \tag{32}$$

If we also assume that an electric field is present in the direction of transport dE/dx then

$$-kT\frac{d\ln c}{dx} - ze\frac{dE}{dx} - K(U - GV)\mu = 0 \tag{33}$$

In Figure 3, the different forces acting on the solute molecule inside the microchannel are illustrated. Similar to the case of no electric field, if we denote the local solute flux by $N = UC$ we get

$$N = -K^{-1}D\left(\frac{dc}{dx} + \frac{ze}{kT}\frac{dE}{dx}c\right) + GVc \tag{34}$$

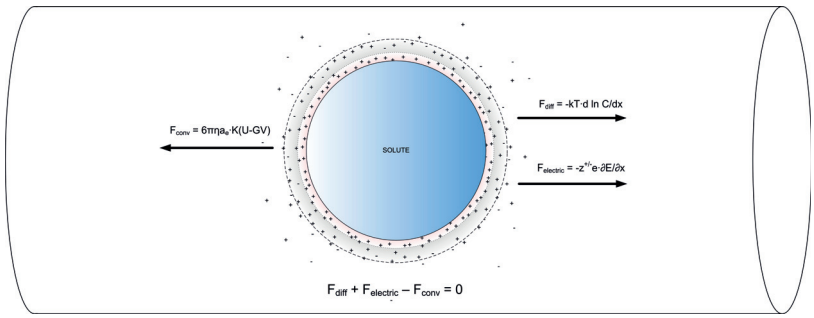

Figure 3: The three forces acting on an ideal spherical solute in a water filled pore during steady motion.

This is the Nernst-Planck equation (with the addition of convective transport) that has been modified by the factors K^{-1} and G. A fundamental assumption in pore theory is that these two coefficients are dependent on the radial position of the solsphere inside the pore and, importantly, on the ratio of the radius of the solsphere and the pore, $\lambda = r_s/r_p$. If β is the fractional radial position (r/r_p) of the solute in relation to the pore radius r_p, the fluid velocity at position β inside a long cylindrical pore can be written

$$V(\beta) = 2\bar{v}(1 - \beta^2) \tag{35}$$

assuming laminar (Poiseuille) flow. The concentration of the solute will be different at different radial positions and due to the size of the solsphere. Especially, C will vanish in the periphery of the pore cross-section (i.e. $C = 0$ for $\beta > 1 - \lambda$). Thus all 4 parameters V, G, K and C will vary with radial position and the net flux across the pore section, $\bar{N}$, must be the average of the local fluxes N

$$\bar{N} = \frac{\int_0^1 N\beta d\beta}{\int_0^1 \beta d\beta} = 2\int_0^{1-\lambda} N\beta d\beta \tag{36}$$

Inserting equation 34 into the above equation gives

$$\bar{N} = -2D\int_0^{1-\lambda} K^{-1}\frac{dc}{dx}\beta d\beta - 2D\int_0^{1-\lambda} K^{-1}\frac{ze}{kT}\frac{dE}{dx}c\beta d\beta + 4\bar{v}\int_0^{1-\lambda} G\left(1-\beta^2\right)c\beta d\beta \tag{37}$$

5.1 The radial equilibrium approximation

The *radial equilibrium approximation* [24] is based on the assumption that no net flux of solute or solvent occurs in the radial direction in the pore and thus

$$D\frac{d\tilde{c}}{e\beta} + \frac{D}{kT}\frac{d\Psi(\beta)}{d\beta}\tilde{c} = 0 \tag{38}$$

with a solution

$$\tilde{c}(\beta) = c(x)e^{-\Psi(\beta)/kT} \tag{39}$$

Thus the radial component is a Boltzmann equilibrium distribution where $\Psi(\beta)$ is the potential energy of interaction and c(x) is the concentration at $\beta = 0$. This allows the calculation of the average radial concentration in the pore

$$\bar{c} = 2 \cdot c(x) \int_0^{1-\lambda} e^{-\Psi(\beta)/kT}\beta d\beta \tag{40}$$

The radial equilibrium approximation simplifies the calculations but it neglects *Taylor dispersion* (i.e. the increased radial diffusion of a solute due to the shear flow) [24]. Anyway, the differential flux equation can now be written in terms of this average radial concentration as

$$\bar{N} = -K_d D\frac{d\bar{c}}{dx} - K_e D\frac{ze}{kT}\frac{dE}{dx}\bar{c} + K_c\overline{vc} \tag{41}$$

where

$$K_c = \frac{\int_0^{1-\lambda} G(1-\beta^2)e^{-\Psi(\beta)/kT}\beta d\beta}{\int_0^{1-\lambda} e^{-\Psi(\beta)/kT}\beta d\beta 2\int_0^1 (1-\beta^2)\beta d\beta} = 2\frac{\int_0^{1-\lambda} G(1-\beta^2)e^{-\Psi(\beta)/kT}\beta d\beta}{\int_0^{1-\lambda} e^{-\Psi(\beta)/kT}\beta d\beta} \tag{42}$$

$$K_d = \frac{\int_0^{1-\lambda} K^{-1}e^{-\Psi(\beta)/kT}\beta d\beta}{\int_0^{1-\lambda} e^{-\Psi(\beta)/kT}\beta d\beta} \tag{43}$$

$$K_e = \frac{\int_0^{1-\lambda} K^{-1}\frac{dE}{dx}e^{-\Psi(\beta)/kT}\beta d\beta}{\int_0^{1-\lambda} e^{-\Psi(\beta)/kT}\beta d\beta 2\int_0^1 \frac{dE}{dx}\beta d\beta} \tag{44}$$

As seen, if the electric field in the axial direction is constant and the electric field has no radial component then $K_e = K_d$ [64]. This latter equality has been the subject of some recent controversy. It was assumed, in the so called *electrokinetic model* of glomerular permeability, that $K_e = K_c$ [75] which indicates that $K_e >> K_d$, potentially making electrophoresis a significant transport mechanism for macromolecules [52]. There is, however, no theoretical or experimental evidence to support this assumption.

5.2 Solute partitioning and boundary conditions for the pore

The above equations need to be related to the exterior concentrations of the pore at its exit $\bar{c}(\Delta x)$ and entrance $c(0)$. Due to the axial symmetry of the pore, the exit and entrance partition coefficients can be assumed to be identical and

$$\Phi = \frac{\bar{c}(0)}{C_0} = \frac{\bar{c}(\Delta x)}{C_L} = 2\int_0^{1-\lambda} e^{-\Psi(\beta)/kT}\beta d\beta \tag{45}$$

where C_0 and C_L are the exterior concentration at $x = 0$ and $x = \Delta x$, respectively. As was discovered by Ferry [28] (and adopted by Renkin [66] in the so called *Renkin equation*), for the important case of purely steric interactions between the solute and pore wall

$$\Phi = 2\int_0^{1-\lambda} \beta d\beta = (1-\lambda)^2 \tag{46}$$

The above equation can now be integrated across the membrane with thickness Δx having a total cross sectional pore area of A_0. If the water flux is known ($J_v = \bar{v}A_0$) and $dE/dx = 0$ we get the net solute flux J_s from

$$J_s = J_v W \frac{C_0 - C_L e^{-Pe}}{1 - e^{-Pe}} \tag{47}$$

where the Péclet number (Pe) is given by

$$Pe = \frac{J_v W \Delta x}{HDA_0} \tag{48}$$

and the *hindrance factors* H and W are given by

$$H = \Phi K_d = 2\int_0^{1-\lambda} K^{-1} e^{-\Psi(\beta)/kT}\beta d\beta \tag{49}$$

$$W = \Phi K_c = 2\int_0^{1-\lambda} G(1-\beta^2)e^{-\Psi(\beta)/kT}\beta d\beta \tag{50}$$

which is identical to the result by Deen [24] and to that of Anderson and Quinn if E=0 [5].

The above notation was introduced by Deen [23, 24] and is often used for synthetic membranes. In order to translate this notation into the notation commonly used in capillary transport physiology, we define the filtration (solvent drag) reflection coefficient to be

$$\sigma_f = 1 - W \tag{51}$$

Also, the diffusion capacity (mass-transfer area coefficient) is defined as

$$PS = HD\frac{A_0}{\Delta x} \tag{52}$$

Furthermore, the water flux is written $J_v = \bar{v}A_0$ so that the Péclet number can be written

$$Pe = \frac{J_v(1-\sigma_f)}{PS} \tag{53}$$

For the case of an axial electric field $\mathbb{E}(x)$ we get

$$J_s = HDA_0\frac{C_i - C_p e^{Pe(\Delta x)}}{\int_0^{\Delta x} e^{-Pe(x)}dx} \tag{54}$$

where the Péclet number is calculated from

$$Pe(x) = \frac{J_v(1-\sigma_d)x}{PS} - \frac{ze}{kT}\mathbb{E}(x) \tag{55}$$

If the field is constant ($\mathbb{E} = -E_{cap}/\Delta x$) then the a modified Patlak equation can be used

$$J_s = J_v\,(1-\xi_z)\,\frac{c_p - c_i e^{-Pe}}{1-e^{-Pe}} \tag{56}$$

where the modified Péclet number is $Pe = \frac{J_v(1-\xi_z)}{PS}$ and the 'reflection coefficient' ξ_z is given by

$$\xi_z = \sigma - \frac{PS}{J_v}\frac{ze}{kT}E_{cap} \tag{57}$$

6 Fiber-matrix theory

The ability of a solute to enter a gel fiber matrix (or for a pore system, to enter the pore) is described by its partition coefficient

$$\Phi = \frac{C_{im}}{C_e} \tag{58}$$

where C_{im} is the equilibrium intra-membrane concentration and C_e is the external concentration (often assumed equal to the plasma water concentration). If we first consider a suspension of cylindrical fibers with length $2L$ and radius r_f in water having an average number ν of fibre centers per mL. The volume density of fibers is then $\phi = 2L\pi r_f^2$ and the volume of the interfiber "gaps", the *void volume*, is $1 - \phi$. If further we assume $D = r_f + r_s + h$ is the distance between the centers of a fiber with radius r_f and a solute with radius r_s and, furthermore, that h is the distance between the peripheries of the fiber and spherical solute) the result by Ogston (cf. eqn 12a in [58]) can be rewritten

$$\Phi = e^{-\phi\left(1-\frac{r_s}{r_f}\right)^2} \tag{59}$$

The partition coefficient is different from the reflection coefficient since it does not take into account the frictional drag and the lag of the solute as it is transported through the membrane. In the fiber matrix theory it is assumed to be equal to the probability of penetration. In the current work it has been estimated that the osmotic reflection coefficient is given by

$$\sigma = (1 - \Phi)^2 \tag{60}$$

Although, strictly only valid for a porous membrane (see [24]), this expression was used by Curry and Michel [21] and later also by Jeansson et al [37] and in Study I [57].

Methods

Education is an admirable thing,
but it is well to remember from time to time
that nothing that is worth knowing
can be taught.
— Oscar Wilde

7 Experimental data

In studies I-III on the permeability of the GFB, data from previous experiments were analyzed in which a bolus dose of FITC labelled Ficoll was given together with FITC Inulin (to calculate the fractional clearance) and 51Cr-EDTA (to calculate GFR) followed by a continuous infusion (3 mL/h) to maintain adequate marker concentrations in plasma. The experimental protocol can be found in [10] and will only be described briefly here. There is also an excellent description available in [7].

7.1 Brief protocol

Monitoring of mean arterial pressure and heart rate was performed by means of a polygraph (model 7B; Grass Instruments, Quincy, MA) attached to the tail artery. Blood samples were obtained via the left carotid artery (via a PE-50 cannula) and infusions were given via the left jugular vein. A small abdominal incision was made via which the left ureter is cannulated (PE-10 cannula) and used for continuous sampling of urine. Prior to cannulation of the ureter, a dose of furosemide (Furosemide Recip 375 µg/kg BW) was administered in order to increase urine production which facilitates cannulation. Equilibration was allowed for at least 20 min before the start of measurements. After the initial rest period, urine was collected for 5 min during which a mid-point (2.5 min) blood sample is collected. Urine flow is calculated simply as the urine volume divided by 5. By measuring the gamma activity of 51Cr-EDTA in both urine and plasma water, the glomerular filtration rate can easily be

obtained as is described in any basic text book. Blood and urine samples are analyzed using high pressure size exclusion chromatography (HPSEC) where a phosphate buffer is used as the mobile phase. The FITC-marked polysaccharides were separated according to their size in an Ultrahydrogel-500 column (Waters, Milford, MA) and their relative concentrations are determined by the detection of fluorescence (Waters 2475). The use of FITC inulin mainly serves the purpose of determining where the sieving coefficient is unity (defined as the ratio between the urine and plasma water concentration for FITC-inulin).

8 Non-linear regression

For the theoretical models used in study I-III, non-linear regression is used to fit the sieving coefficients calculated from theory to the experimental sieving coefficients. The experimental data consists of 327 data points giving the molecular size (in Å) and the corresponding sieving coefficient (θ). The dataset also included the calculated clearance of Cr-EDTA (GFR) for each animal. A weighted objective function was used

$$\sum_{j=1}^{npoints} \frac{1}{\theta_{j,data}^2} \left(\theta_{j,data} - \theta_{j,model}\right)^2 \tag{61}$$

in order to compensate for the fact that the data $\theta_{j,data}^2$ spans several orders of magnitude. The MINPACK software library was used for the regression (using standard settings) [53].

9 Statistics

The current author believes that statistical hypothesis testing for very small numbers of subjects, like in the current Study I-III, has a limited value. More insight can usually be gained by just looking at the data itself. Nevertheless, differences between groups were tested using non-parametric tests. For repeated measures scenarios the Friedman test was used. For comparison between two groups or post-hoc analysis and, the Mann-Whitney [57] or a variant of the Wilcoxon test was used [56], respectively. Despite the use of non-parametric methods, values are typically expressed as arithmetic mean +/- SE.

Results

It is not knowledge
but the act of learning
not possession
but the act of getting there
which grants the greatest enjoyment.
— Carl Friedrich Gauss

10 The glomerular filtration barrier modeled as a charged fiber-matrix

In Study I we explore the electrostatic hindrance of charge modified Ficoll in the rat GFB. By modeling the barrier as a charged fiber-matrix, the surface charge density of the barrier (the fiber matrix) was estimated to be between 5-20 mC/m^2, similar to many proteins in the body. The results of this study indicate that electrical charge may be of less importance in the hindrance of charged molecules in the GFB than previously thought.

For the data analysis, two different diameters for the individual fibers in the model was assumed, 5Å and 10Å (see also Table 2). Only the small pore system was considered in the data analysis (cf. also [10]). The analysis gave the best fit for the small 5Å fibers.

11 A distributed two-pore model of the GFB

In Study II [56], we construct a distributed two-pore model and use it to analyze Ficoll sieving data from the rat GFB. As seen in Figure 5, the model (solid line) provided a very good visual fit to Ficoll sieving data. This is in contrast to the classic two-pore model which usually provides a poor visual fit for solutes between 45-65 in hydrodynamic size.

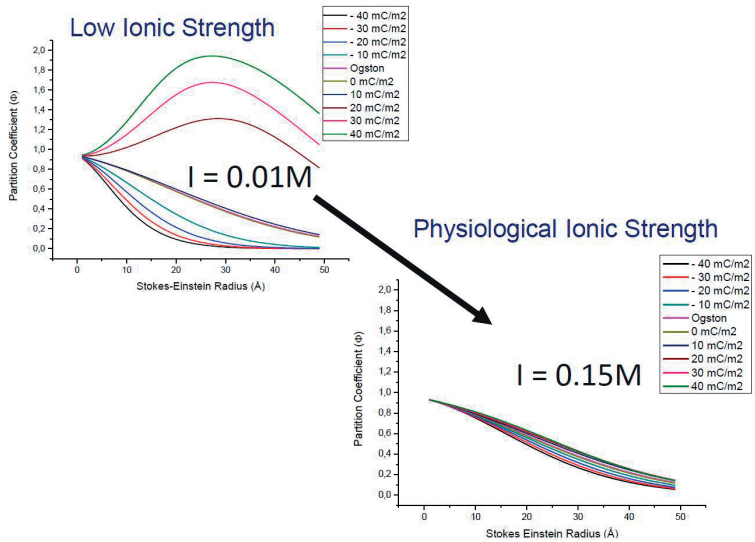

Figure 4: The effects of varying the ionic strength (and thus the Debye screening length) in the theoretical fiber-matrix model. At physiological (high) ionic strengths, the effects of charge on the permeability of anionic Ficoll is small.

It is hypothesized that the wide distribution obtained in the analysis may be due to a variation in solute size rather than a true variation in pore size. This could in part explain the large difference in sieving coefficients between plasma proteins [49, 94] and polysaccharides [6]. This hypothesis is further analyzed in Study III. In addition to the data analysis, several theoretical results are presented such as Poiseuille's law for a distributed pore population

$$K_f = \frac{A_0}{\Delta x}\frac{u^2}{8\eta}e^{6\ln^2 s} \tag{62}$$

12 A distributed solute model - application to the glomerular sieving of Ficoll

In study III, the classic heteroporous model by Deen, Bridges, Brenner and Myers [26] was extended by introducing size distributions on the solute molecules, making them flexible in their conformation. By contrast, in the original model, the size-distribution was applied only to the pores, not to the solute molecules. Experimental sieving data (θ vs. SE-radius) for Ficoll, both from the rat glomerulus and from precision-made nanopore membranes [29, 30], were analyzed using the model. The variation in solute size was quantified in terms of the geometric standard deviation (gSD) of the (log-normal) solute size distribution. The glomerular capillary was included in the modeling according to the classic model by Deen and colleagues [27].

Table 2: Uncharged fiber-matrix parameters. $A_0/\Delta x$ effective pore area over unit diffusion path-length; LpS hydraulic conductance of the fiber array; χ^2 = "Goodness of fit". Additional symbols are given in the text. **p<0.01.

	5Å	10 Å
Fractional void-volume	0.884 ± 0.001	0.591 ± 0.003
$\frac{A_0}{\Delta x}$, cm/g	18 ± 2	41 ± 4
L_pS, mL/min/mmHg	0.13 ± 0.01	0.14 ± 0.01
GFR	0.65 ± 0.05	0.65 ± 0.05
Pearson χ^2	0.036 ± 0.002**	0.048 ± 0.002

In Study III, we show, for the first time, that a variation of only 15-17% in the size of the molecule is sufficient to explain the difference in glomerular permeability between negatively charged albumin and neutral Ficoll 36Å. Furthermore, we demonstrate that the effects of applying a size distribution on the solute molecule are only evident when the molecular size is close to the size of the selective elements of the barrier. This is well in line with experimental data, both from the GFB and from synthetic membranes [30]. In conclusion, molecular size, structure and conformation seem to be far more important than electrical charge for the glomerular permeability of macromolecules.

13 Optimizing Automated Peritoneal Dialysis (APD) using an extended three-pore model

It is well known that the efficiency of APD can be increased by more frequent and rapid exchanges [1, 31]. However, the time spent during the fill and drainage cycles of each dwell leads to a reduction in the effective contact time between the dialysate and the peritoneal membrane. Too frequent exchanges will reduce the efficacy of the treatment and, above all, lead to increased costs due to the increased consumption of dialysis fluid. The three-pore model by Rippe [69] is a widely applied model of peritoneal dialysis [4, 98, 102, 103]. In Study IV, an extended version of the classical model is derived and used to model automated peritoneal dialysis for a wide range of different scenarios. The extended model features an additional "bag" compartment acting as a reservoir for the unused and spent dialysis fluid.

The most important conclusion from Study IV is that the glucose absorption of APD-prescriptions can be reduced by >20% using moderately higher dialysate flows and by utilizing a so called bi-modal treatment regime. In addition, for most patients, the dialysate flow rate should exceed 1.5-2L/h in order to optimize osmotic water transport (UF), small-solute removal (Kt/V) while maintaining a low glucose absorption. It would however appear that DFRs over 3L/h seem to provide little benefit for most patients while increasing the cost of the treatment.

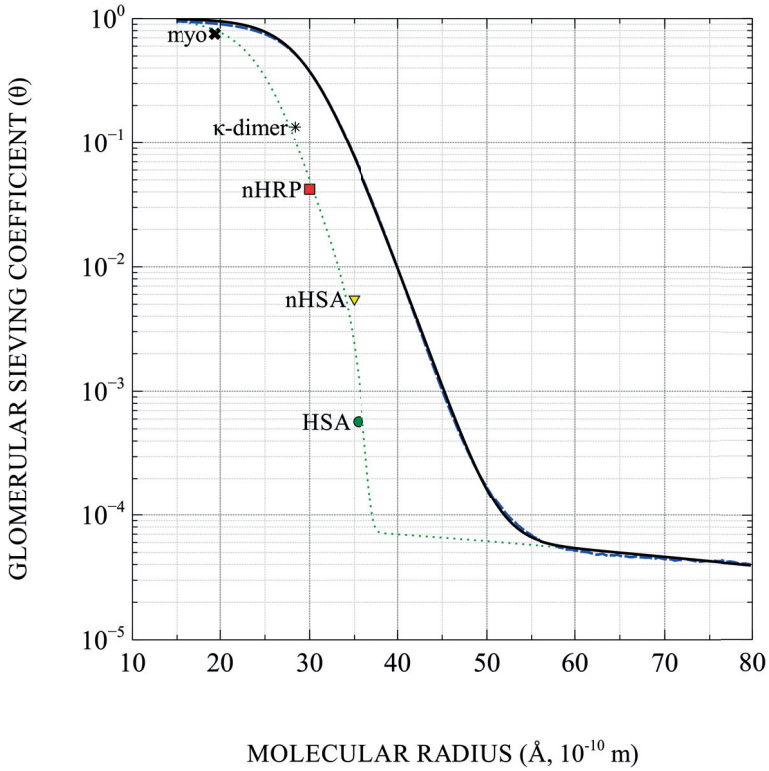

Figure 5: Sieving coefficient (θ) versus Stokes-Einstein radius (a_e) for the experimental data (dashed line) and the best fit for the regression of the distributed two-pore model (solid line). The dotted line represents a simulated scenario were the small-pore spread (s_S) and $A0/\Delta x$ have been decreased to match the sieving data for five different globular proteins (according to Lund et al. [49]: myoglobin (myo; 19.4 Å), human myeloma dimeric κ-chain (κ-dimer; 28.4 Å), nHRP (30.4 Å), neutralized Human Serum Albumin (nHSA; 35.0 Å), and HSA (35.5 Å).

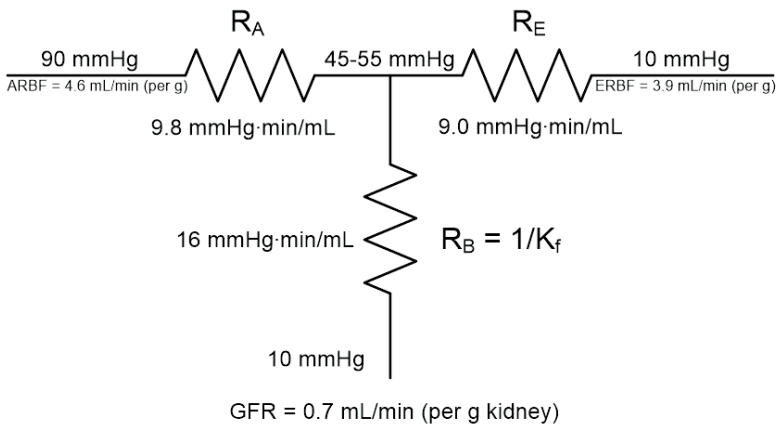

Figure 6: The glomerular capillary was included in the modeling in Study III according to the classic model by Deen and colleagues [27]. Symbols: R_A afferent arteriolar resistance, R_E efferent arteriolar resistance, ARBF afferent renal blood flow, ERBF efferent renal blood flow

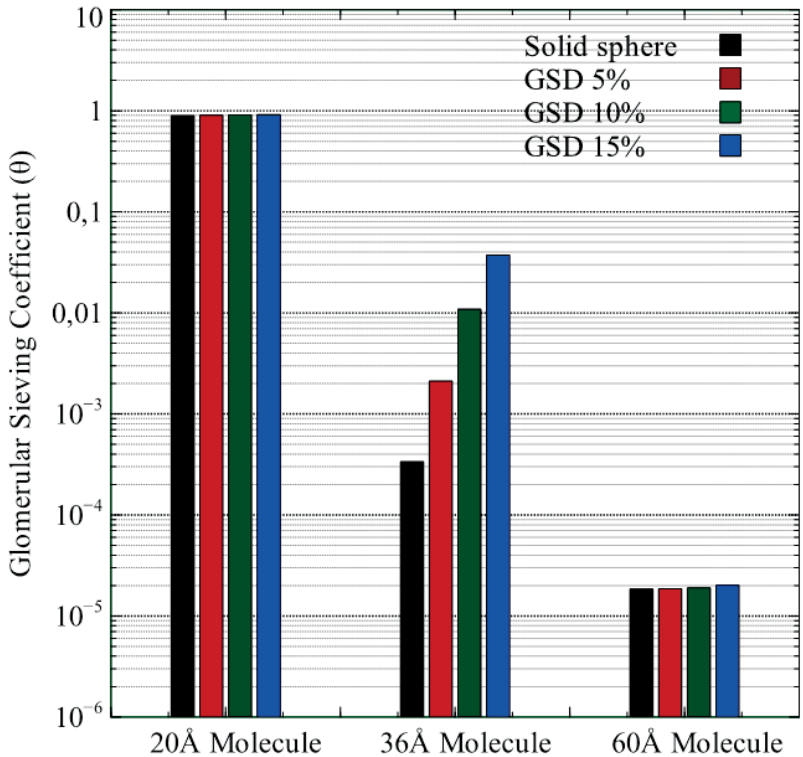

Figure 7: Effects of varying the "softness" of the Ficoll molecule (the gSD parameter) for three differently sized molecules having radii 20Å, 36 (cf. albumin) and 60Å. Variation in the solute distribution standard deviation (gSD) of the smaller 20 and the larger 60 solute molecules has virtually no effect on their permeability across the GFB. The opposite holds true for the 36 molecule which has a radius close to the pore radius.

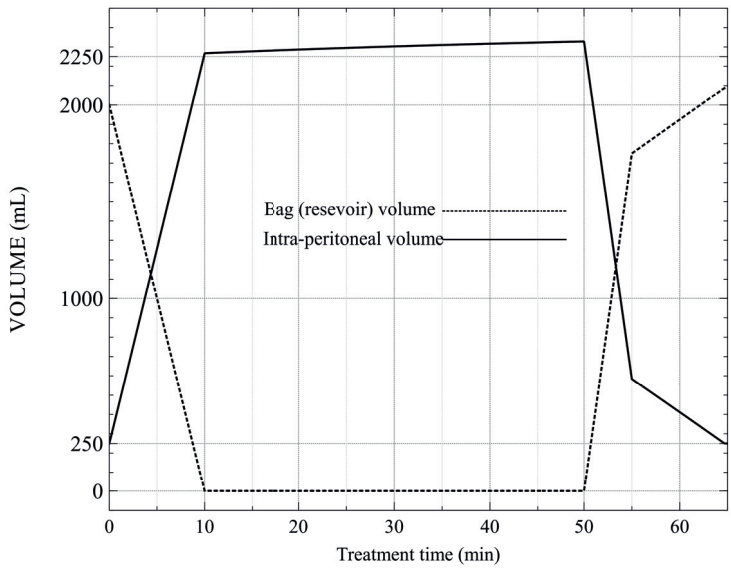

Figure 8: The simultaneous volume changes in the fluid resevoir (bag) and the peritoneal cavity during the course of a dwell.

Discussion

Logic will get you from A to B.
Imagination will take you everywhere.
— Albert Einstein

14 What are the differences between the peritoneal barrier and the GFB?

The human kidney is an impressive biological cross-flow filter comprised of 1 million glomeruli coupled in parallel. Compared to peripheral capillaries, which have a filtration fraction of only about 0.4-0.5%, glomerular capillaries have an extremely high hydraulic conductance, filtering about 20% of the received blood flow in to Bowman's space. Also, in contrast, peripheral capillaries allow passage of 50% of the plasma proteins while glomerular capillaries show a fractional clearance of albumin of only 0.01%. This remarkable selectivity to albumin is likely accomplished mainly by a size-selective mechanism which implies that the glomerular filtration barrier is a highly regular structure. This is exemplified by the sieving coefficient of inulin being 1. A barrier having a distribution in the size-selective elements would sieve inulin due to the presence of pores close to/smaller than the size of inulin (implying a sieving coefficient < 1).

In the current thesis, these two very different transport barriers are investigated using simplified models of "equivalent barriers" with which the transport over the actual biological barriers can be compared. Little effort is made to model the actual structure of the barriers. In general, the transport of solutes over the peritoneal barrier during peritoneal dialysis is by means of diffusion, except for solutes that are close to equilibrium with the plasma compartment (such as Na^+ [36, 47, 100]). This relative dominance of diffusion as the main transport mechanism is thus a result of the large concentration gradients that are (artificially) created during PD.

The transport of small solutes in the glomerular filtration barrier, a biological "cross-flow"

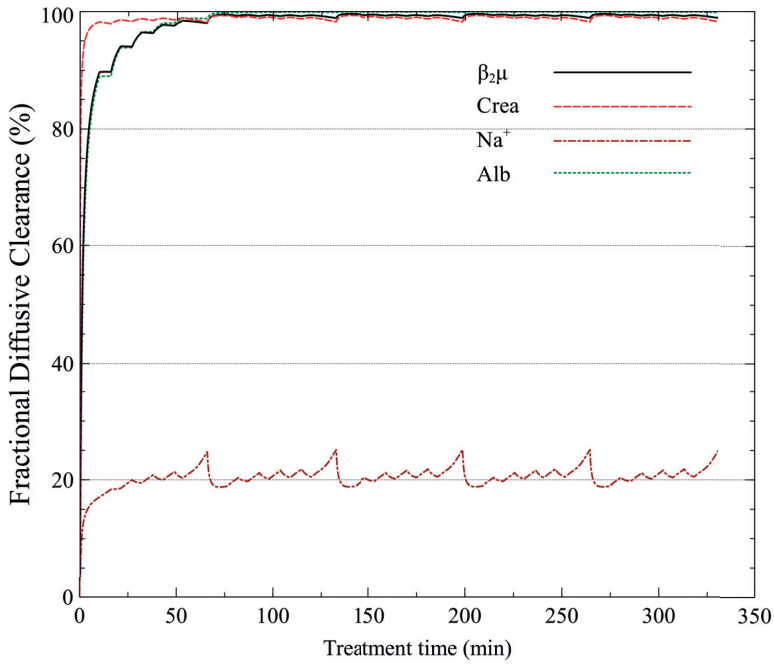

Figure 9: A tidal PD regime (25 consecutive dwells) from the simulations. The mechanism of transport is entirely diffusive for most solutes except for sodium since the concentration gradient is smaller and the MTAC is lower (4.5 mL/min) than expected from theory (17 mL/min).

filter, is very different in this regard. Smaller solutes are severely flow limited during their transport across the GFB. Only solutes that are sieved by the barrier are transported by means of diffusion. Thus, proteins such as albumin, orosomucoid and myoglobin are transported by means of diffusion (cf. also [88]). For a molecule the size of FITC inulin, approximately 40% of the transport is diffusive at a normal GFR. For small solutes like urea, glucose, creatinine and electrolytes, the transport is almost entirely convective. Flow limitation occurs also over peripheral capillaries during hi-flow conditions. As was reviewed by Rippe, this phenomenon falsely led pioneering researchers to believe that there was no diffusional hindrance for small solutes in the capillary wall (cf. Pappenheimer's dilemma). By contrast, the capillary wall has a marked diffusional hindrance for small solutes, which can easily be shown during conditions in which the concentration gradient is large and the volume flow is lower than the diffusion capacity of the solute.

15 Pappenheimer's pore puzzle

As is discussed at some length in Study II, the $\frac{A_0}{\Delta x}$ parameter clearly does not represent the unrestricted pore area per unit path length but is rather a lumped parameter containing sev-

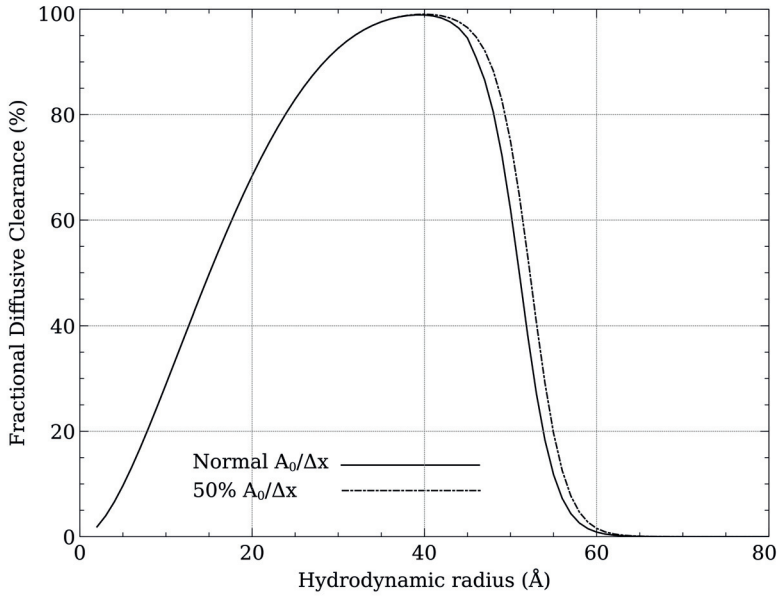

Figure 10: The fractional diffusive clearance of Ficoll over the GFB. Smaller solutes are severely flow limited during their transport.

eral other factors. Thus, $\frac{A_0}{\Delta x}$ confounds both with the pore radius and, for the distributed models, also with the distribution standard deviation. In other words, we cannot be sure that any of these latter parameters represent actual properties of the membrane. Nevertheless, it can be assumed a priori that the $\frac{A_0}{\Delta x}$ parameter is different than what can be deduced from the water permeability (LpS) of the filter [11]. There are several reasons for this. First, there is good evidence showing that the permeate has a higher viscosity [13] which leads to a further reduction in the diffusion capacity than what is predicted from pore theory. Second, the geometry and structure of the GFB and the peritoneal barrier is markedly different from that of a porous membrane, meaning that it is unlikely that LpS and $\frac{A_0}{\Delta x}$ will be commensurate for any other barrier than an ideal porous membrane with very large pores compared to the solute. Lastly, the pore radius is determined by the behavior of solutes with radii that are close to the pore radius (in the GFB, this is the case also for the $\frac{A_0}{\Delta x}$ parameter). For such solutes the membrane will of course show a marked hindrance, leading to low concentrations in the permeate which translates to larger errors in the measurement of their concentration. Thus, for any realistic modeling approach, there will always be some degree of inconsistency between the model parameters.

16 We know there are no pores - but what are they and how are they affected in glomerular disease?

In the GFB, the single pore radius approach and the distributed approach may represent structural extremes, at least for the determination of pore radius (i.e. a small pore radius r_p implies a large $\frac{A_0}{\Delta x}$ and vice-versa). If adopting such a view, the "true" small pore radius is between 36-46Å and it likely has a small variation (< 5%) in the pore sizes. Charge effects may be important but, according to the current results, only as a threshold phenomenon. The location for this charge selectivity is likely in the luminal end of the filter, maybe in the endothelial glycocalyx which may form an important part of the small-pore pathway. The GBM and the slit membrane at the podocyte level likely also contribute to the small pore pathway [34]. Thus, we can expect changes in small-pore permeability if there are 1) actual structural damages in the barrier and possibly also 2) alterations in the endothelial glycocalyx. According to the two-pore model, leakage of albumin through the small-pores will lead to (selective) proteinuria if only slight perturbations of the effective pore radius occur. Indeed, if there is a threshold effect as was hypothesized in Study II, it may explain the occurrence of selective proteinuria. Furthermore, the threshold effect may also arise as a consequence of slight alterations in the structural correlates of the small-pore pathway - for example an increased heteroporosity (increase spread) in the small pores or larger small pore radius. For the rather unselective large-pores, charge phenomena are most likely not important. By contrast, large-pores seem to be regulated by the contractile elements of the cells lining (i.e. endothelial and epithelial cells) and supporting (i.e. mesangial cells) the glomerular filtration barrier [7-9]. Also, in a number of in vitro studies it has been demonstrated that glomerular permeability may indeed change rapidly and reversibly [22, 50, 83, 86]. Arguably, the endothelial glycocalyx would not appear to play important role in the selectivity of the large-pores. Since the large-pores can form rapidly and reversibly, they may in part explain the occurrence of physiological proteinuria, which will vary according to circadian rhythm [46], food intake [15], physical exercise [54] and so on. Also, a pathological activation of the large-pore pathway (form example during diabetic kidney disease [48]) may represent an important pathophysiological mechanism since proteinuria may in itself be harmful for the tubulointerstitium [2, 62]. Thus, reduction of proteinuria, for example by using RAS-blockade, will typically slow the progression of renal disease [44, 84, 85]. In addition to the large pores, several studies indicate the presence of "shunt pathways" through which very large proteins such as IgM [12, 95].

17 The three-pore model - facts, fallacies and fables

17.1 Lymphatic flux

In the current simulations, the lymphatic absorption of fluid volume from the peritoneal cavity was set to 0.3 mL/min which is slightly higher than that measured in patients [78]. According to the 3-pore model, the total fluid flux into the peritoneal cavity is the sum of the fluxes arising from the perturbed Starling equilibria (equations 10-12) subtracted by the lymph flow (L).

$$TotalUF = J_{vc} + J_{vs} + J_{vL} - L \tag{63}$$

Thus, for a given 3-pore system, choosing a higher value for L will imply a lower filtration coefficient and a higher reflection coefficient for glucose [92]. A large part of the reflection coefficient for glucose is due to the occurrence of aquaporines in the peritoneal "membrane" which is, for example, elegantly demonstrated in a study by Ni et al [55] using aquaporine knock-out mice. From the results in their study, it can be shown that only 3% of the hydraulic conductance in the barrier is due to aquaporins, setting an upper limit for the reflection coefficient for glucose (σ_g) on the order of 0.04-0.06. However, the clearance of a large intraperitoneal volume marker such as RISA is 4-5-fold larger than the lymphatic fluid flow. If the reflection coefficient for glucose is 0.03 this implies that this clearance of the molecular species does not represent a net fluid flux out of the PC, but rather, marker molecules have a 4-5-fold larger distribution volume than the IPV, reflecting their entrapment in periperitoneal tissues. A possible mechanism for this entrapment may be the so called volume recirculation mechanism [74]. Thus, in conclusion, where the macromolecules go from the peritoneal cavity, water does not necessarily need to follow.

17.2 The interstitium

Both an advantage and a disadvantage of the three-pore model is that it is a lumped parameter model [77], treating the peritoneum as an "equivalent porous barrier" with which a researcher or clinician can compare the transport over the actual peritoneal barrier. One clear advantage is thus its simplicity - the computations are straight-forward and it is possible for clinicians without mathematical training to use the model to make calculations on transport and clearances et cetera. However, the transport of water and solute matter from the circulation to the different tissues in the body occurs not only via the capillary wall but also through the interstitial space. Therefore, a disadvantage of the three-pore model is that it does not take the interstitial compartment into consideration and thus any time-dependent changes in interstitial concentration and pressure profiles are ignored

[89]. If it is this simplification that leads to the observed difference in the disappearance of the osmotic gradient and the glucose gradient [79] is not known to the author, but time-dependent changes in interstitial glucose concentration may be worth considering it as a likely candidate for this phenomenon.

17.3 Constant plasma solute concentrations

Since the plasma solute concentrations are assumed to be constant, the current modeling does not take in to account the fact that plasma levels of removed solutes will change during the course of the treatment. However, by simple application of the mean value theorem, it can be shown that there is a certain concentration, lower than the initial concentration, at which the transport will be identical to that which would arise if the plasma concentrations were allowed to vary with time. Therefore, adding the plasma compartments will not increase the descriptive power of the three-pore model since simply adjusting the constant plasma concentrations will have the same effect. In addition, correctly modeling the complex plasma kinetic behavior of many solutes, especially electrolytes, is not an easy task and choosing a "mean value" approach may be more feasible.

17.4 Electrolyte transport

The apparent diffusion capacities (MTACs) of small ions such as Na^{+} and Ca^{++} is far lower than what could be expected from their diffusion coefficients. Their small size and low molar weight would thus imply much higher values. For example, according to the three-pore model, Na+ should have a mass transfer area coefficient (MTAC, K_{BD} or PS) close to 17 mL/min which is approximately twice than that measured using low-sodium fluids (8-9 mL/min) and 4-5 times more than that obtained using standard fluids (4-5 mL/min). Although several explanations have been proposed for this difference in transport, the exact mechanisms remain to be elucidated. Surely, the main difference between the sodium ion and a neutral molecule of roughly the same SE-radius (1.8 Å) is electric charge. Thus, most likely, the main reason for the noted discrepancy is that electrolyte transport is not taken into account in the transport equations [80]. The three-pore solute flux equations can be extended to include electrodiffusion (resulting in a modified Nernst-Planck equation) as follows

$$J_{s,S,i} = -H_{S,i}D_i\left(\frac{dc_i}{dx} + \frac{z_i e}{kT}\frac{\partial \mathbb{E}}{\partial x}c_i\right) + J_v W_{S,i}c_i \tag{64}$$

$$J_{s,L,i} = -H_{L,i}D_i\left(\frac{dc_i}{dx} + \frac{z_i e}{kT}\frac{\partial \mathbb{E}}{\partial x}c_i\right) + J_v W_{L,i}c_i \tag{65}$$

Table 3: Tentative effects of increased IPP from previous studies. For volumes up to 3L, an increased IPV seems to increase both osmotic water transport (UF) and small solute removal (UreaR).

Mechanism during elevated IPP	Effect on "UF"	Effect on UreaR
Venous compression	$\Rightarrow$	$\Rightarrow$
Peritoneal surface recruitment [18, 43]	$\Downarrow$	$\Uparrow$
Reduced peritoneal blood flow [82]	$\Uparrow$	$\Downarrow$
Tissue hydration [35, 105]	$\Downarrow$	$\Downarrow$
Increased IPV [43, 99]	$\Uparrow\Uparrow\Uparrow$	$\Uparrow\Uparrow$

where z_i is the valence of solute i, e is the elementary charge ($\approx 1.602 \cdot 10^{-16} mC$), k is Boltzmanns constant and T is body temperature (310°K) and $\frac{\partial \mathbb{E}}{\partial x}$ is the electric field gradient (for a linear potential field $\frac{\partial \mathbb{E}}{\partial x} = -\frac{E_{cap}}{\Delta x}$ where E_{cap} is the capillary potential). If the blood plasma and peritoneal cavity is to remain electroneutral, no net electrical current can flow over the peritoneal barrier and thus

$$\frac{1}{60} \sum_{i=1}^{n} F z_i \left(J_{s,S,i} + J_{s,L,i} \right) = 0 \; mA \tag{66}$$

where ($F \approx 96485$ mC/mmol) is Faradays constant. A priori, this will exert an electrical hindrance on cations such as the sodium ion, mainly because of the plasma anion gap (12-15 mEq/L). The result of applying the above equations would thus be an apparently low MTAC for cations such as Na^+ and Ca^{++}. In addition cations would not, in general, equilibrate with plasma water (unless the plasma anion gap has vanished) and their dialysate concentration will be lower than that in plasma water. On the other hand, with time, dialysate concentrations of anions such as Cl^- can be predicted to exceed those in the plasma water.

17.5 The controversial effects of an increased intra-peritoneal pressure

As the peritoneal cavity is filled with dialysate, the intraperitoneal pressure will rise, typically to about 7-8 mmHg for a fill volume of 2L. First, this will lead to compression of the veins in the peritoneal cavity and most of the venous pressure will be transmitted back to the capillary pressure [67, 80, 81].

Thus, an increase in 5 mmHg in the peritoneum will result in an increase of, at least, 4 mmHg in the capillary. Secondly, the larger the intra-peritoneal pressure, the more surface area will be recruited in the peritoneum [43]. Third, since the blood vessels in the peritoneal cavity are compressed this will reduce the peritoneal blood flow. And, lastly, the increased pressure leads to tissue hydration [90].

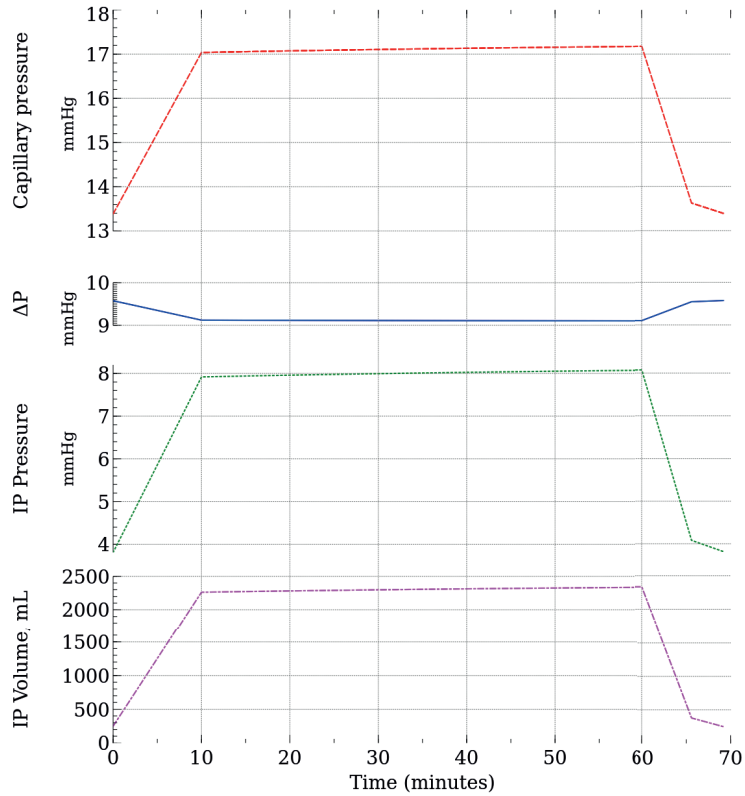

Figure 11: Simulated variations in intraperitoneal pressure (IPP). As seen, the IPP increases when then peritoneal cavity is filled with fluid. Since the venous pressure is also increased, this will increase the capillary pressure almost to the same extent. This means that the pressure difference (i.e. the driving pressure for volume flow across the peritoneal filtration barrier) is essentially unchanged when IPP is raised due to an increased intraperitoneal volume.

On the other hand, if the cause of the increased IPP is an increased IPV, the increase in the glucose mass in the peritoneal cavity will typically increase the osmotic water transport (UF). In conclusion, if the IPP is increased due to posture [96] or compression of the abdomen , the expected effect is a decreased UF. If the IPP is increased due to a higher IPV (up to at least 2L but probably also up to 3L [43]) the net effect of an increased IPP is an increased osmotic water transport (UF).

18 Methodological challenges in modeling

It is well-known that there are no actual pores in the peritoneal barrier (except aquaporins) or in the GFB. Thus, pore models are obviously phenomenological. So why the use of pores? First, it is likely impossible to discern the true nature of the size- and charge-selective elements of the GFB by analyzing transport data. Stated differently, there is no

way of telling whether the hindrance of a molecular species was caused by a pore, a fibrous membrane, a gel or more exotic structures. In addition, decades of imaging studies using electron microscopy have not succeeded in revealing the real size- and charge selective structures of the GFB. Secondly, the hydrodynamic theory of hindered transport is most completely developed for the simple case of spherical solute molecules in a long cylindrical pore while transport in other media is much less completely understood.

A challenge in modeling various phenomena in nature is the unavoidable need to make simplifying assumptions. Some of these assumptions will have little impact on the end results, such as disregarding effects of the well-known relativity theory. Although present in all of our experiments, effects of relativity will, in general, be negligible. Other assumptions will have a larger impact and, typically, by not including effects that indeed are important, the models may show a poor fit to data. In addition, seemingly paradoxical results may arise since the parameters of the model will typically be perturbed in order to compensate for the lack of detail in the model. Another challenge, which might be seen as contrary to the problem of making simplifications (which may lead to "underfitting" the data) is the problem of overfitting the data due to a very detailed model having many parameters. Indeed, analyzing the distribution of the "large pores" using the distributed models in Study II-III fall into this category as one would need data also for larger solutes, that are closer to (and larger than) the large-pore radius, in order to determine both the mean radius (which is determined by the cut-off) and the distribution spread (which is determined by the "end" of the cut-off). Overfitting is perhaps even more problematic than underfitting since it is usually difficult to tell the difference between an overfit and a "perfect" fit. In conclusion, a model should ideally not have too many parameters, but not too few.

19 References

1. **Aasarod K, Wideroe TE, and Flakne SC.** A comparison of solute clearance and ultrafiltration volume in peritoneal dialysis with total or fractional (50%) intraperitoneal volume exchange with the same dialysate flow rate. Nephrology, dialysis, transplantation : official publication of the European Dialysis and Transplant Association - European Renal Association 12: 2128-2132, 1997.

2. **Abbate M, Zoja C, and Remuzzi G.** How does proteinuria cause progressive renal damage? Journal of the American Society of Nephrology 17: 2974-2984, 2006.

3. **Agre P, Preston GM, Smith BL, Jung JS, Raina S, Moon C, Guggino WB, and Nielsen S.** Aquaporin CHIP: the archetypal molecular water channel. The American journal of physiology 265: F463-476, 1993.

4. **Amici G, Mastrosimone S, Da Rin G, Bocci C, and Bonadonna A.** Clinical validation of PD Adequest software: modeling error assessment. Peritoneal dialysis international : journal of the International Society for Peritoneal Dialysis 18: 317-321, 1998.

5. **Anderson JL, and Quinn JA.** Restricted Transport in Small Pores - Model for Steric Exclusion and Hindered Particle Motion. Biophys J 14: 130-150, 1974.

6. **Asgeirsson D.** Permeability of the glomerular filtration barrier in relation to the size, shape, charge and deformability of the permeating molecules. Lund University, 2009.

7. **Axelsson J.** Dynamics of the glomerular filtration barrier-Physiological and pathophysiological aspects. Lund University, 2011.

8. **Axelsson J, Rippe A, and Rippe B.** Acute hyperglycemia induces rapid, reversible increases in glomerular permeability in nondiabetic rats. American journal of physiology Renal physiology 298: F1306-1312, 2010.

9. **Axelsson J, Rippe A, Öberg CM, and Rippe B.** Rapid, dynamic changes in glomerular permeability to macromolecules during systemic Angiotensin II (AngII) infusion in rats. American journal of physiology Renal physiology 303: F790-F799, 2012.

10. **Axelsson J, Sverrisson K, Rippe A, Fissell W, and Rippe B.** Reduced diffusion of charge-modified, conformationally intact anionic Ficoll relative to neutral Ficoll across the rat glomerular filtration barrier in vivo. American journal of physiology Renal physiology 301: F708-712, 2011.

11. **Axelsson J, Öberg CM, Rippe A, Krause B, and Rippe B.** Size-selectivity of a synthetic high-flux and a high cut-off dialyzing membrane compared to that of the rat glomerular filtration barrier. J Membrane Sci 2012.

12. **Bakoush O, Torffvit O, Rippe B, and Tencer J.** High proteinuria selectivity index based upon IgM is a strong predictor of poor renal survival in glomerular diseases. Nephrology, dialysis, transplantation : official publication of the European Dialysis and Transplant Association - European Renal Association 16: 1357-1363, 2001.

13. **Bowen WR, and Welfoot JS.** Modelling the performance of membrane nanofiltration - critical assessment and model development. Chem Eng Sci 57: 1121-1137, 2002.

14. **Bresler EH, and Groome LJ.** On equations for combined convective and diffusive transport of neutral solute across porous membranes. The American journal of physiology 241: F469-476, 1981.

15. **Buzio C, Mutti A, Capani F, Andrulli S, Perazzoli F, Alinovi R, Negro A, and Rustichelli R.** Circadian rhythm of proteinuria: effects of an evening meat meal. Nephrology, dialysis, transplantation : official publication of the European Dialysis and Transplant Association - European Renal Association 4: 266-270, 1989.

16. **Caplan SR.** Principles and Models of Biological Transport - Friedman,Mh. Nature 326: 255-255, 1987.

17. **Castrop H, and Schiessl IM.** Novel routes of albumin passage across the glomerular filtration barrier. Acta Physiol (Oxf) 2016.

18. **Chagnac A, Herskovitz P, Ori Y, Weinstein T, Hirsh J, Katz M, and Gafter U.** Effect of increased dialysate volume on peritoneal surface area among peritoneal dialysis patients. Journal of the American Society of Nephrology : JASN 13: 2554-2559, 2002.

19. **Cook G, and Dickerson RH.** Understanding the Chemical-Potential. Am J Phys 63: 737-742, 1995.

20. **Crone C, and Lassen NA.** Capillary permeability. Munksgaard Kopenhagen, 1970.

21. **Curry FE, and Michel CC.** A fiber matrix model of capillary permeability. Microvascular research 20: 96-99, 1980.

22. **Dahly-Vernon AJ, Sharma M, McCarthy ET, Savin VJ, Ledbetter SR, and Roman RJ.** Transforming growth factor-beta, 20-HETE interaction, and glomerular injury in Dahl salt-sensitive rats. Hypertension 45: 643-648, 2005.

23. **Dechadilok P, and Deen WM.** Hindrance factors for diffusion and convection in pores. Ind Eng Chem Res 45: 6953-6959, 2006.

24. **Deen WM.** Hindered Transport of Large Molecules in Liquid-Filled Pores. Aiche J 33: 1409-1425, 1987.

25. **Deen WM, Bohrer MP, and Brenner BM.** Macromolecule transport across glomerular capillaries: application of pore theory. Kidney international 16: 353-365, 1979.

26. **Deen WM, Bridges CR, Brenner BM, and Myers BD.** Heteroporous model of glomerular size selectivity: application to normal and nephrotic humans. The American journal of physiology 249: F374-389, 1985.

27. **Deen WM, Robertson CR, and Brenner BM.** A model of glomerular ultrafiltration in the rat. The American journal of physiology 223: 1178-1183, 1972.

28. **Ferry JD.** Statistical Evaluation of Sieve Constants in Ultrafiltration. The Journal of general physiology 20: 95-104, 1936.

29. **Fissell WH, Dubnisheva A, Eldridge AN, Fleischman AJ, Zydney AL, and Roy S.** High-Performance Silicon Nanopore Hemofiltration Membranes. J Memb Sci 326: 58-63, 2009.

30. **Fissell WH, Manley S, Dubnisheva A, Glass J, Magistrelli J, Eldridge AN, Fleischman AJ, Zydney AL, and Roy S.** Ficoll is not a rigid sphere. American journal of physiology Renal physiology 293: F1209-1213, 2007.

31. **Freida P, and Issad B.** Continuous cyclic peritoneal dialysis prescription and power. Contributions to nephrology 129: 98-108, 1999.

32. **Groome LJ, Kinasewitz GT, and Diana JN.** Diffusion and convection across heteroporous membranes: a simple macroscopic equation. Microvascular research 26: 307-322, 1983.

33. **Grotte G.** Passage of dextran molecules across the blood-lymph barrier. Acta chirurgica Scandinavica Supplementum 211: 1-84, 1956.

34. **Haraldsson B, Nystrom J, and Deen WM.** Properties of the glomerular barrier and mechanisms of proteinuria. Physiological reviews 88: 451-487, 2008.

35. **Imholz AL, Koomen GC, Struijk DG, Arisz L, and Krediet RT.** Effect of an increased intraperitoneal pressure on fluid and solute transport during CAPD. Kidney international 44: 1078-1085, 1993.

36. **Imholz ALT, Koomen GCM, Struijk DG, Arisz L, and Krediet RT.** Fluid and Solute Transport in Capd Patients Using Ultralow Sodium Dialysate. Kidney international 46: 333-340, 1994.

37. **Jeansson M, and Haraldsson B.** Glomerular size and charge selectivity in the mouse after exposure to glucosaminoglycan-degrading enzymes. Journal of the American Society of Nephrology 14: 1756-1765, 2003.

38. **Katz MA, Schaeffer RC, Jr., Gratrix M, Mucha D, and Carbajal J.** The glomerular barrier fits a two-pore-and-fiber-matrix model: derivation and physiologic test. Microvascular research 57: 227-243, 1999.

39. **Kedem O, and Katchalsky A.** Permeability of Composite Membranes .1. Electric Current, Volume Flow and Flow of Solute through Membranes. T Faraday Soc 59: 1918-1930, 1963.

40. **Kedem O, and Katchalsky A.** Permeability of Composite Membranes .2. Parallel Elements. T Faraday Soc 59: 1931-1940, 1963.

41. **Kedem O, and Katchalsky A.** Permeability of Composite Membranes .3. Series Array of Elements. T Faraday Soc 59: 1941-1953, 1963.

42. **Kedem O, and Katchalsky A.** Thermodynamic Analysis of the Permeability of Biological Membranes to Non-Electrolytes. Biochim Biophys Acta 27: 229-246, 1958.

43. **Keshaviah P, Emerson PF, Vonesh EF, and Brandes JC.** Relationship between body size, fill volume, and mass transfer area coefficient in peritoneal dialysis. Journal of the American Society of Nephrology 4: 1820-1826, 1994.

44. **Kramer BK, and Schweda F.** Ramipril in non-diabetic renal failure (REIN study). Ramipril Efficiency in Nephropathy study. Lancet 350: 736; author reply 736-737, 1997.

45. **Landis EM, Jonas L, Angevine M, and Erb W.** The Passage of Fluid and Protein through the Human Capillary Wall during Venous Congestion. The Journal of clinical investigation 11: 717-734, 1932.

46. **Landis EM, Jonas L, Angevine M, and Erb W.** The Passage of Fluid and Protein through the Human Capillary Wall during Venous Congestion. The Journal of clinical investigation 11: 717-734, 1932.

47. **Lemm G, Kuppers J, Frey R, Wingender W, and Kuhlmann J.** Monitoring of proteinuria in phase I studies in healthy male subjects. European journal of clinical pharmacology 54: 287-294, 1998.

48. **Leypoldt JK, Charney DI, Cheung AK, Naprestek CL, Akin BH, and Shockley TR.** Ultrafiltration and solute kinetics using low sodium peritoneal dialysate. Kidney international 48: 1959-1966, 1995.

49. **Lubbad L, Öberg CM, Dhanasekaran S, Nemmar A, Hammad F, Pathan JY, Rippe B, and Bakoush O.** Reduced glomerular size selectivity in late streptozotocin-induced diabetes in rats: application of a distributed two-pore model. Physiological reports 3: 2015.

50. **Lund U, Rippe A, Venturoli D, Tenstad O, Grubb A, and Rippe B.** Glomerular filtration rate dependence of sieving of albumin and some neutral proteins in rat kidneys. Am J Physiol-Renal 284: F1226-F1234, 2003.

51. **McCarthy ET, Sharma R, Sharma M, Li JZ, Ge XL, Dileepan KN, and Savin VJ.** TNF-alpha increases albumin permeability of isolated rat glomeruli through the generation of superoxide. Journal of the American Society of Nephrology : JASN 9: 433-438, 1998.

52. **Michel CC, and Curry FE.** Microvascular permeability. Physiological reviews 79: 703-761, 1999.

53. **Moeller MJ, and Kuppe C.** Point: Proposing the electrokinetic model. Peritoneal dialysis international : journal of the International Society for Peritoneal Dialysis 35: 5-8, 2015.

54. **Moré J, Garbow B, and Hillström K.** User Guide for MINPACK-1. Argonne National Laboratory Report ANL-80-74: 1980.

55. **Nedbal J, and Seliger V.** Electrophoretic analysis of exercise proteinuria. J Appl Physiol 13: 244-246, 1958.

56. **Ni J, Verbavatz JM, Rippe A, Boisde I, Moulin P, Rippe B, Verkman AS, and Devuyst O.** Aquaporin-1 plays an essential role in water permeability and ultrafiltration during peritoneal dialysis. Kidney international 69: 1518-1525, 2006.

57. **Öberg CM, and Rippe B.** A distributed two-pore model: theoretical implications and practical application to the glomerular sieving of Ficoll. American journal of physiology Renal physiology 306: F844-854, 2014.

58. **Öberg CM, and Rippe B.** Quantification of the electrostatic properties of the glomerular filtration barrier modeled as a charged fiber matrix separating anionic from neutral Ficoll. American journal of physiology Renal physiology 304: F781-787, 2013.

59. **Ogston AG.** The Spaces in a Uniform Random Suspension of Fibres. T Faraday Soc 54: 1754-1757, 1958.

60. **Pappenheimer JR.** Passage of Molecules through Capillary Walls. Physiological reviews 33: 387-423, 1953.

61. **Pappenheimer JR, Renkin EM, and Borrero LM.** Filtration, diffusion and molecular sieving through peripheral capillary membranes; a contribution to the pore theory of capillary permeability. The American journal of physiology 167: 13-46, 1951.

62. **Patlak CS, Goldstein DA, and Hoffman JF.** The flow of solute and solvent across a two-membrane system. J Theor Biol 5: 426-442, 1963.

63. **Peterson JC, Adler S, Burkart JM, Greene T, Hebert LA, Hunsicker LG, King AJ, Klahr S, Massry SG, and Seifter JL.** Blood pressure control, proteinuria, and the progression of renal disease. The Modification of Diet in Renal Disease Study. Annals of internal medicine 123: 754-762, 1995.

64. **Prescott DM, and Zeuthen E.** Comparison of Water Diffusion and Water Filtration across Cell Surfaces. Acta physiologica Scandinavica 28: 77-94, 1953.

65. **Pujar NS, and Zydney AL.** Electrostatic and Electrokinetic Interactions during Protein-Transport through Narrow Pore Membranes. Ind Eng Chem Res 33: 2473-2482, 1994.

66. **Renkin EM.** Capillary transport of macromolecules: pores and other endothelial pathways. J Appl Physiol 58: 315-325, 1985.

67. **Renkin EM.** Filtration, diffusion, and molecular sieving through porous cellulose membranes. The Journal of general physiology 38: 225-243, 1954.

68. **Rippe B.** Is intraperitoneal pressure important? Periton Dialysis Int 26: 317-319, 2006.

69. **Rippe B.** Relationships between diffusion and convection across capillary walls. 1978.

70. **Rippe B.** A three-pore model of peritoneal transport. Peritoneal dialysis international : journal of the International Society for Peritoneal Dialysis 13 Suppl 2: S35-38, 1993.

71. **Rippe B, and Haraldsson B.** Fluid and protein fluxes across small and large pores in the microvasculature. Application of two-pore equations. Acta physiologica Scandinavica 131: 411-428, 1987.

72. **Rippe B, and Haraldsson B.** Transport of macromolecules across microvascular walls: the two-pore theory. Physiological reviews 74: 163-219, 1994.

73. **Rippe B, Haraldsson B, and Folkow B.** Evaluation of the 'stretched pore phenomenon' in isolated rat hindquarters. Acta physiologica Scandinavica 125: 453-459, 1985.

74. **Rippe B, Kamiya A, and Folkow B.** Transcapillary passage of albumin, effects of tissue cooling and of increases in filtration and plasma colloid osmotic pressure. Acta physiologica Scandinavica 105: 171-187, 1979.

75. **Rippe B, and Öberg CM.** Albumin Turnover in Peritoneal and Hemodialysis. Seminars in dialysis 29: 458-462, 2016.

76. **Rippe B, and Öberg CM.** Counterpoint: Defending pore theory. Peritoneal dialysis international : journal of the International Society for Peritoneal Dialysis 35: 9-13, 2015.

77. **Rippe B, Rosengren BI, Carlsson O, and Venturoli D.** Transendothelial transport: the vesicle controversy. J Vasc Res 39: 375-390, 2002.

78. **Rippe B, and Stelin G.** Simulations of peritoneal solute transport during CAPD. Application of two-pore formalism. Kidney international 35: 1234-1244, 1989.

79. **Rippe B, Stelin G, and Ahlmen J.** Lymph flow from the peritoneal cavity in CAPD patients. In: Frontiers in peritoneal dialysisSpringer, 1986, p. 24-30.

80. **Rippe B, Stelin G, and Haraldsson B.** Computer simulations of peritoneal fluid transport in CAPD. Kidney international 40: 315-325, 1991.

81. **Rippe B, Venturoli D, Simonsen O, and de Arteaga J.** Fluid and electrolyte transport across the peritoneal membrane during CAPD according to the three-pore model. Periton Dialysis Int 24: 10-27, 2004.

82. **Rippe B, and Öberg CM.** Is Adapted APD Theoretically More Efficient Than Conventional APD? Peritoneal dialysis international : journal of the International Society for Peritoneal Dialysis 2016.

83. **Rosengren BI, and Rippe B.** Blood flow limitation in vivo of small solute transfer during peritoneal dialysis in rats. Journal of the American Society of Nephrology : JASN 14: 1599-1604, 2003.

84. **Salmon AH, Neal CR, Bates DO, and Harper SJ.** Vascular endothelial growth factor increases the ultrafiltration coefficient in isolated intact Wistar rat glomeruli. The Journal of physiology 570: 141-156, 2006.

85. **Schiessl IM, and Castrop H.** Acute changes in glomerular albumin filtration during systemic infusion of angiotensin II - a multiphoton microscopy study. Faseb J 27: 2013.

86. **Schiessl IM, and Castrop H.** Angiotensin II AT(2) receptor activation attenuates AT(1) receptor-induced increases in the glomerular filtration of albumin: a multiphoton microscopy study. Am J Physiol-Renal 305: F1189-F1200, 2013.

87. **Sharma R, Khanna A, Sharma M, and Savin VJ.** Transforming growth factor-beta1 increases albumin permeability of isolated rat glomeruli via hydroxyl radicals. Kidney international 58: 131-136, 2000.

88. **Shirley HH, Jr., Wolfram CG, Wasserman K, and Mayerson HS.** Capillary permeability to macromolecules: stretched pore phenomenon. The American journal of physiology 190: 189-193, 1957.

89. **Smithies O.** Why the kidney glomerulus does not clog: a gel permeation/diffusion hypothesis of renal function. Proceedings of the National Academy of Sciences 100: 4108-4113, 2003.

90. **Stachowska-Pietka J, Waniewski J, Flessner MF, and Lindholm B.** Computer simulations of osmotic ultrafiltration and small-solute transport in peritoneal dialysis: a spatially distributed approach. American journal of physiology Renal physiology 302: F1331-1341, 2012.

91. **Stachowska-Pietka J, Waniewski J, Flessner MF, and Lindholm B.** Distributed model of peritoneal fluid absorption. American journal of physiology Heart and circulatory physiology 291: H1862-1874, 2006.

92. **Staverman AJ.** The Theory of Measurement of Osmotic Pressure. Recl Trav Chim Pay B 70: 344-352, 1951.

93. **Stelin G, and Rippe B.** A phenomenological interpretation of the variation in dialysate volume with dwell time in CAPD. Kidney international 38: 465-472, 1990.

94. **Stokes G.** On the Effect of the Internal Friction of Fluids on the Motion of Pendulums. Transactions of the Cambridge Philosophical Society 9: 8, 1851.

95. **Tencer J, Frick IM, Oquist BW, Alm P, and Rippe B.** Size-selectivity of the glomerular barrier to high molecular weight proteins: upper size limitations of shunt pathways. Kidney international 53: 709-715, 1998.

96. **Tofik R.** Urinary Biomarkers and Patient Outcome in Chronic Kidney Disease and Atherosclerotic Heart Disease: The value of IgM-uria and IgG-uria. Lund University, 2014.

97. **Twardowski ZJ, Prowant BF, Nolph KD, Martinez AJ, and Lampton LM.** High volume, low frequency continuous ambulatory peritoneal dialysis. Kidney international 23: 64-70, 1983.

98. **Wallenius G.** Renal clearance of dextran as a measure of glomerular permeability. Acta Societatis Medicorum Upsaliensis Supplementum 59: 1-91, 1954.

99. **Van Biesen W, Carlsson O, Bergia R, Brauner M, Christensson A, Genestier S, Haag-Weber M, Heaf J, Joffe P, Johansson AC, Morel B, Prischl F, Verbeelen D, and Vychytil A.** Personal dialysis capacity (PDC(TM)) test: a multicentre clinical study. Nephrology, dialysis, transplantation : official publication of the European Dialysis and Transplant Association - European Renal Association 18: 788-796, 2003.

100. **Wang T, Heimburger O, Cheng H, Waniewski J, Bergstrom J, and Lindholm B.** Effect of increased dialysate fill volume on peritoneal fluid and solute transport. Kidney international 52: 1068-1076, 1997.

101. **Wang T, Waniewski J, Heimburger O, Werynski A, and Lindholm B.** A quantitative analysis of sodium transport and removal during peritoneal dialysis. Kidney international 52: 1609-1616, 1997.

102. **Waniewski J.** Mathematical modeling of fluid and solute transport in hemodialysis and peritoneal dialysis. J Membrane Sci 274: 24-37, 2006.

103. **Verrina E, Amici G, Perfumo F, Trivelli A, Canepa A, and Gusmano R.** The use of the PD Adequest mathematical model in pediatric patients on chronic peritoneal dialysis. Peritoneal dialysis international : journal of the International Society for Peritoneal Dialysis 18: 322-328, 1998.

104. **Vonesh EF, Story KO, and O'Neill WT.** A multinational clinical validation study of PD ADEQUEST 2.0. PD ADEQUEST International Study Group. Peritoneal dialysis international : journal of the International Society for Peritoneal Dialysis 19: 556-571, 1999.

105. **Yudilevich DL, and Alvarez OA.** Water, sodium, and thiourea transcapillary diffusion in the dog heart. The American journal of physiology 213: 308-314, 1967.

106. **Zakaria ER, and Rippe B.** Peritoneal fluid and tracer albumin kinetics in the rat. Effects of increases in intraperitoneal hydrostatic pressure. Peritoneal dialysis international : journal of the International Society for Peritoneal Dialysis 15: 118-128, 1995.

Conclusions

What goes up,
must come down.
— Isaac Newton

20 Study I-III

- The two-pore model is mainly useful for the quantification of the transport occuring over the selective pathway (small pore) and the non-selective pathway (large pore and shunt). It gives no information regarding the actual structure of the GFB.
- The selective pathway (the small pores) is the main filtration barrier in the kidney. It is highly selective towards large molecules such as albumin. Also the structure and conformation of the solute seem to be very important. Charge may play a role as a threshold phenomenon but it cannot explain the difference in transport between polysaccharides and proteins. Changes in the properties of the small-pore is typically associated with structural damage to the glomerulus.
- The permeability through the weakly selective pathway (the large pores) can change rapidly and reversibly. It is the main route for proteins during normal conditions. A pathological activation of large pore permeability, for example during diabetic kidney disease, may accelerate kidney disease.
- For permeability studies of the GFB during normal filtration fractions it is not necessary to model transport along the glomerular capillary.

21 Study IV

- The glucose absorption of APD-prescriptions can be greatly reduced by using moderately higher dialysate flows and by utilizing a bi-modal treatment regime. Further research should assess whether such optimized bi-modal regimes are feasible and safe.
- By using DFRs higher than standard prescriptions (1.5-2L/h), improvements in small-solute clearance and UF are typically possible, although the relative benefits in UF and Kt/V seem to be relatively small compared to the increased cost of the treatment.
- The complexity of a physiological model is limited by the quality of the experimental input data. In the case of PD, the large variablity in input data makes a more sophisticated approach than the three-pore model difficult to justify at present.

Scientific publications

This thesis is based on the following studies which are referred to in the text according to their Roman numerals (I-IV).

Paper I: Quantification of the electrostatic properties of the glomerular filtration barrier modeled as a charged fiber matrix separating anionic from neutral Ficoll

Paper II: A distributed two-pore model: Theoretical implications and practical application to the glomerular sieving of Ficoll

Paper III: A distributed solute model: an extended two-pore model with application to the glomerular sieving of Ficoll

Paper IV: Optimizing automated peritoneal dialysis (APD) using an extended three-pore model

Study 1

Am J Physiol Renal Physiol 304: F781–F787, 2013.
First published January 9, 2013; doi:10.1152/ajprenal.00621.2012.

Quantification of the electrostatic properties of the glomerular filtration barrier modeled as a charged fiber matrix separating anionic from neutral Ficoll

Carl M. Öberg and Bengt Rippe

Department of Nephrology, University Hospital of Lund, Lund, Sweden

Submitted 1 November 2012; accepted in final form 7 January 2013

Öberg CM, Rippe B. Quantification of the electrostatic properties of the glomerular filtration barrier modeled as a charged fiber matrix separating anionic from neutral Ficoll. *Am J Physiol Renal Physiol* 304: F781–F787, 2013. First published January 9, 2013; doi:10.1152/ajprenal.00621.2012.—In the current study we explore the electrostatic interactions on the transport of anionic Ficoll (aFicoll) vs. neutral Ficoll (nFicoll) over the glomerular filtration barrier (GFB) modeled as a charged fiber matrix. We first analyze experimental sieving data for the rat glomerulus, and second, we explore some of the basic implications of a theoretical model for the electrostatic interactions between a charged solute and a charged fiber-matrix barrier. To explain the measured difference in glomerular transport between nFicoll and aFicoll (Axelsson J, Sverrisson K, Rippe A, Fissell W, Rippe B. *Am J Physiol* 301: F708–F712, 2011), the present simulations demonstrate that the surface charge density needed on a charged fiber matrix must lie between -0.005 C/m^2 and -0.019 C/m^2, depending on the surface charge density of the solute. This is in good agreement with known surface charge densities for many proteins in the body. In conclusion, the current results suggest that electrical charge makes a moderate contribution to glomerular permeability, while molecular size and conformation seem to be more important. Yet, the weak electrical charge obtained in this study can be predicted to nearly totally exclude albumin from permeating through "high-selectivity" pathways in a charged-fiber matrix of the GFB.

capillary permeability; fiber matrix; anionic Ficoll; charge selectivity

THE RELATIVE IMPORTANCE OF electrical charge in the sieving of plasma proteins across the glomerular filtration barrier (GFB) has been a matter of debate over the last few decades. The seminal data of Brenner an colleagues (8, 10), using differently charged dextran thus suggested that the glomerular transport of negatively charged, sulfated dextran molecules be much lower than that of neutral dextran of the same size (8). However, several authors have questioned these results. Thus some fractions of sulfated dextran seem to bind to plasma proteins or glomerular cells (18, 33). In addition, it has been shown that polysaccharides (such as dextran and Ficoll) exhibit a flexible molecular conformation, making them hyperpermeable compared with more rigid solutes, such as proteins, at least for molecular radii approaching the pore radius (1, 12). Ficoll apparently shows glomerular sieving characteristics somewhere between those of dextran and proteins (34). Several findings also suggest that polysaccharides undergo significant conformational changes during charge modification, making them even more flexible. Hence, Asgeirsson et al. (2) conducted an experiment investigating the glomerular sieving of carboxymethylated (CM) anionic Ficoll (aFicoll) and "unmodified" neutral Ficoll (nFicoll) in rats. The glomerular permeability to negatively charged CM-Ficoll was markedly enhanced compared with that of its neutral counterpart. In addition, size separation using high-performance size exclusion chromatography showed that the aFicoll tested eluted earlier than nFicoll, indicating that the charge-modification process had indeed increased the molecular radius (and altered the conformation) of Ficoll (2).

Schaeffer and colleagues (16, 31) published experiments showing that the difference in permeability between anionic and neutral dextran was negligible. In contrast to these results, there are extensive experimental results from both synthetic membranes and the glomerulus that demonstrate that globular proteins are selected based both on their size and charge (19, 34). Using anionic 5.8- and 20-nm (pore radius) silicon nanopore membranes, Fissell and colleagues (17) showed a charge-dependent permselectivity for aFicoll. Using the same charge-modification technique for CM-Ficoll, our own experiments have demonstrated a reduced transport of aFicoll relative to nFicoll across the rat GFB (4). Bhalla and Deen (6) published an elegant theoretical model for the transport of charged solutes over a regular array of charged fibers, and their results showed that the osmotic reflection coefficient for BSA was much larger than that for an uncharged system.

It is well-recognized that some of the major structural components of the GFB (e.g., perlecan, agrin, entactin/nidogen, and proteoglycans of the glycocalyx) and important plasma proteins, such as albumin and orosomucoid, carry a net negative charge during physiological conditions. Numerous experiments using charged barriers have demonstrated large to moderate effects of electrical charge in the hindrance of charged solutes, with the difference being strongly dependent on the ionic strength of the solution. Pujar and Zydney (27) showed that the clearance of BSA through a 100,000 molecular weight cutoff membrane decreased by nearly two orders of magnitude as the ionic strength (salt concentration) was reduced from 150 to 1.5 mM. At physiologic ("high") ionic strengths the electrical field of the solute will be condensed and the "screening distance" for charge at which significant charge effects occur (i.e., the so-called Debye length, being ~8 Å at physiological ionic strength) will be reduced (9). Isolated glomerular basement membranes (GBM) have failed to show charge selectivity at physiological ionic strengths when probed with neutral and negatively charged Ficoll (7). At the ionic strengths of 1.0, 0.11, and 0.01 M, Johnson et al. (22) demonstrated that the hindrance due to charge of BSA, ovalbumin, and lactalbumin was moderate in a charged agarose gel. The partition coefficient for BSA with an estimated net charge of -37 was reduced from 0.67 to 0.47 when the ionic strength was lowered from 1.0 to 0.11 M (22).

In the current study, the model of Johnson and Deen (23) as modified by Jeansson and Haraldsson (21) is used to analyze the sieving data for 20–35 Å (radius) aFicoll and nFicoll based

Address for reprint requests and other correspondence: B. Rippe, Dept. of Nephrology, Lund Univ., Univ. Hospital of Lund, S-211 85 Lund, Sweden (e-mail: Bengt.Rippe@med.lu.se).

Table 1. *Dimensionless coefficients*

Dimensionless Coefficient	Definition
β	$\frac{r_s}{r_f}$
τ	$r_s\kappa$
η	$h\kappa$
σ_s	$\frac{r_s F}{\varepsilon RT} q_s$
σ_f	$\frac{r_f F}{\varepsilon RT} q_f$

Nondimensionalized coefficients for the fiber radius (r_f), ratio of solute radius to Debye length (τ), separation distance (η), and the surface charge densities of the solute (σ_s) and fiber (σ_f), respectively. Additional symbols are explained in the text.

on experimental data from Axelsson et al. (4) to determine the charge density needed in a fibrous barrier to account for the measured results. To our knowledge, this is the first attempt to calculate the surface charge density of the GFB. It will be shown that, in a randomly oriented anionic fiber matrix fitting to the mentioned Ficoll data, if the difference between the sieving coefficient of nFicoll and that of negatively charged albumin would be due to charge only, this would require a very highly charged barrier. In such a case, surface potentials exceeding −200 mV would be needed, which is equivalent to that of a charged spherical 35.5 Å (radius) solute with a net charge of approximately −200. Still, the electrical charge of the GFB certainly has a distinct effect on the glomerular permeability to charged solutes. The importance of this charge effect relative to the size selectivity will be explored in this study.

METHODS

Theory. The fiber-matrix model of Ogston supposes a barrier consisting of a random array of fibers of thickness r_f. The partition coefficient was determined from

$$\Phi = \int_0^\infty g(h)dh \tag{1}$$

where $g(h)$ is the probability density function (PDF) for finding the closest fiber at a surface-to-surface distance h from the solute sphere with radius r_s. For Ogston's original model for random fibrous media, the PDF is

$$g(h) = \frac{2\phi(h + r_f + r_s)}{r_f^2} e^{-\phi\left[\frac{(h + r_f + r_s)}{r_f}\right]^2} \tag{2}$$

Here ϕ is the volume fraction of fibers, often expressed in terms of the fractional void volume $\varepsilon = 1 - \phi$. As explained in Johnson and Deen (23), a Boltzmann factor $e^{-E(h)/kT}$ can be introduced describing the relative probabilities of various energy states in the solute-fiber system.

$$\Phi = \int_0^\infty e^{-E(h)/kT} g(h)dh \tag{3}$$

where $E(h)$ is the electrostatic free energy associated with moving a charged sphere to a certain distance h from the fiber. The free-energy was calculated from the expression

$$E(h) = \varepsilon_r r_s \left(\frac{RT}{F}\right)^2 \Delta G \tag{4}$$

where ε_r is the dielectric permittivity of the solvent and

$$\Delta G = A_1(\beta, \tau, \eta)\sigma_s\sigma_f + A_2(\beta, \tau, \eta)\sigma_s^2 + A_3(\beta, \tau, \eta)\sigma_f^2 \tag{5}$$

The nondimensionalized parameters β, τ, η, σ_s, and σ_f are described in Table 1. The coefficients A_i are given by

$$A_i(\beta, \tau, \eta) = a_i \beta^{b_i} \tau^{-c_i} e^{-d_i \eta} \tag{6}$$

where the coefficients are given by Table 1 in Johnson and Deen (23).

Charged fiber-matrix + large-pore model. The data were analyzed using a modified version of the theoretical model by Johnson and Deen (23), based on the extended Ogston model, as developed by Jeansson and Haraldsson (21). In this model, the theoretical sieving coefficients (θ_{model}) were calculated from the nonlinear global convection/diffusion equation (*30*) according to

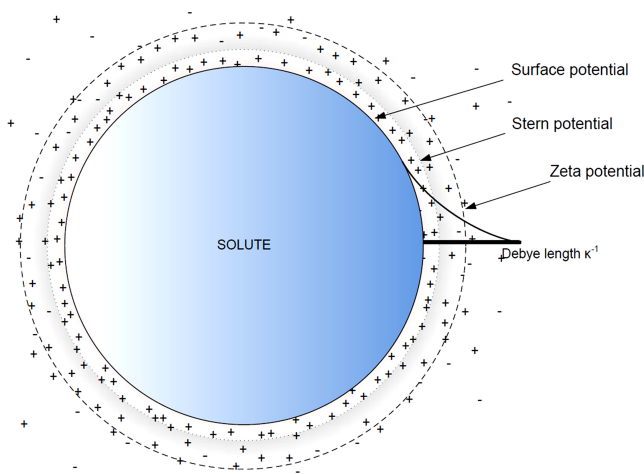

Fig. 1. Illustration of the electrical double layer in a liquid at contact with a negatively-charged solid. The zeta potential is the potential at the slipping plane that separates mobile fluid from fluid that remains attached to the solute.

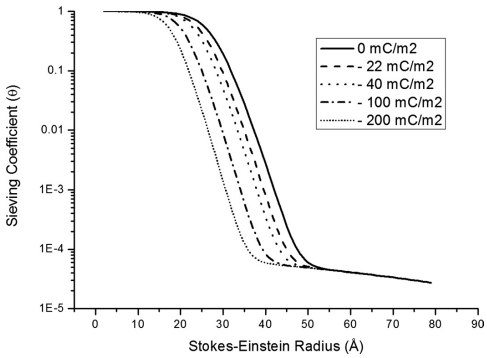

Fig. 2. Glomerular sieving curves at different surface charge densities on the fibers of the glomerular barrier modeled as a random fiber matrix characterized by the (uncharged) physical properties listed in Table 2.

$$\theta_{\text{model}} = f_{\text{fib}}\frac{1-\sigma_{\text{fib}}}{1-\sigma_{\text{fib}}e^{-Pe_{\text{fib}}}} + f_{\text{L}}\frac{1-\sigma_{\text{L}}}{1-\sigma_{\text{L}}e^{-Pe_{\text{L}}}} \quad (7)$$

where f_{fib} is the fractional volume flow ($J_{\text{v,fib}}/J_{\text{v}}$) through the fiber-matrix pathway and $f_{\text{L}} = 1 - f_{\text{fib}}$ represents the fraction of volume transported via the large-pore system. The Peclet numbers are defined by

$$Pe_{\text{fib}} = f_{\text{fib}}\frac{\text{GFR}(1-\sigma_{\text{fib}})}{PS_{\text{fib}}} \quad (8)$$

$$Pe_{\text{L}} = f_{\text{L}}\frac{\text{GFR}(1-\sigma_{\text{L}})}{PS_{\text{L}}} \quad (9)$$

For the fiber-matrix pathway, the reflection coefficient was estimated from the partition-coefficient (Φ) using the simple relation

$$\sigma = (1-\Phi)^2 \quad (10)$$

The permeability-surface area coefficient was calculated from

$$PS_{\text{fib}} = D\frac{A_0}{\Delta x}\Phi \quad (11)$$

For the large-pore system, the hydrodynamic estimates recommended for porous membranes (*Eqs. 16* and *18*) by Dechadilok and Deen (11) were used. The definitions of constants and symbols are essentially the same as those used in the two-pore model according to Rippe and Haraldsson (30). The hydraulic conductance through the fibrous pathway was estimated using the Kozeny-Carman equation

$$L_{\text{p}}S = \alpha_{\text{fib}}^{-1}\frac{A_{0,\text{S}}}{A_0}\frac{A_0}{\Delta x}\frac{r_{\text{f}}^2\varepsilon^3}{4G\eta(1-\varepsilon)^2} \quad (12)$$

where ε is the fractional void volume, η is the viscosity of the filtrate (water) at 310° K, and G is the Kozeny constant. The fractional total cross-sectional area over the large pores can be calculated using [cf. also *Eq. 27* in Rippe and Haraldsson (30)]

$$\frac{A_{0,\text{L}}}{A_{0,\text{S}}} = \frac{2\alpha_{\text{L}}r_{\text{f}}^2\varepsilon^3}{\alpha_{\text{fib}}r_{\text{L}}^2G(1-\varepsilon)^2} \quad (13)$$

Optimal values for the fractional fiber volume $\phi = (1-\varepsilon)$, $A_0/\Delta x$, r_{L}, and α_{L} were calculated with the nonlinear regression method of Levenberg and Marquardt using the well-known MINPACK software library (25) with standard settings. For the data analysis of the aFicoll, only the fiber-matrix pathway was considered so that $f_{\text{L}} = 0$ and the nonlinear regression scheme was limited to the parameters ϕ and $A_0/\Delta x$. Due to the confounding effects of the other model parameters, only the barrier surface charge density (q_{f}) was allowed to vary between the charged and uncharged models. Taking into account that the oncotic pressure gradient is different over different pathways (cf. *Eqs. 3–11*; Ref. 29), the volume flux through a pathway i in a heteroselective barrier can be approximated from

$$J_{\text{v},i} = \alpha_i\left[L_{\text{p}}S(\sigma_o - \sigma_{i,\text{albumin}})\Delta\pi + \text{GFR}\right] \quad (14)$$

where $\sigma_{\text{o}} = \Sigma\alpha_i\sigma_i$ is the osmotic reflection coefficient and a plasma oncotic pressure $\Delta\pi$ of 28 mmHg is assumed. The improper integral in *Eq. 3* was evaluated numerically using a 21-point Gauss-Kronrod quadrature. Numerical calculations were performed using the software package GNU Science Library (14).

Physical properties of aFicoll. The net charge of human serum albumin during physiological conditions is −22 (26). By approximating its surface area to that of a sphere, using a Stokes-Einstein radius of 35.5 Å, a surface charge density of approximately −0.022 C/m^2 can be calculated. The electric charge of the aFicoll used in the experiments has been quantified in terms of the zeta potential ζ (see Fig. 1), which is the electric potential at the slipping plane, with values of −40 mV and −45 mV for CM-Ficoll 70 and CM-Ficoll 400, respectively (17). The surface charge density can be approximated using the Grahame equation

$$q_{\text{s}} = \zeta\varepsilon_{\text{r}}\kappa \quad (15)$$

where ε_{r} is the dielectric permittivity of the solvent and κ^{-1} is the Debye length. If assuming a relative permittivity of 74.3 for the solvent at 310° K (13) and an ionic strength of 0.15 M, a surface charge density of −0.033 C/m^2 for Ficoll 70 and −0.037 C/m^2 for Ficoll 400 can be calculated. The general problem of estimating the net charge of a protein is not trivial (35), but the use of the Grahame equation provides a good estimate at high ionic strengths (9). Since the perfusate used in the experiments consisted of both Ficoll 70 and Ficoll 400, the surface charge density is estimated as the arithmetic mean of the above values, i.e., −0.035 C/m^2. This charge density is equivalent to that of a 36 Å spherical molecule with a net charge of approximately −37. As described in Axelsson et al. (4), aFicoll showed a slight increase in molecular diameter as measured by the difference in elution time. This effect was compensated for in the current analysis by subtracting the measured difference in Stokes-Einstein radius from the aFicoll data. In addition, the glomerular filtration rate differed in the experiments using nFicoll from that in the anionic group. To compensate for this, the same glomerular filtration rate for both Ficoll species was used in the theoretical model.

Table 2. *Uncharged 5 Å fiber-matrix + large-pore parameters*

	5 Å
Fractional void volume	0.884 ± 0.001
$A_0/\Delta x$, cm/g × 10^{-5}†	15.87 ± 0.74
$A_{0,\text{L}}/A_0 \times 10^6$	0.12 ± 0.0
$L_{\text{p}}S$, ml·min^{-1}·mmHg	0.12 ± 0.01
$\alpha_{\text{L}} \times 10^5$	2.2 ± 0.2
J_{vL}/GFR (f_{L}) × 10^5	10.8 ± 1.1
$J_{\text{vL,iso}}$, μl/min	0.05 ± 0.01
Large-pore radius, Å	162.2 ± 8.5
Kozeny constant (G)	5
Pearson χ^2	0.077 ± 0.008

Values are given as means ± SE. $A_0/\Delta x$, effective pore area over unit diffusion path-length; $A_{0,\text{L}}/A_0$, fractional large-pore area; $L_{\text{p}}S$, hydraulic conductance of the fiber array; α_{L}, fractional large-pore hydraulic conductance; f_{L}, fractional large-pore volume flux; $J_{\text{vL,iso}}$, "volume recirculation" term, see Ref. 31); χ^2, "goodness of fit"; GFR, glomerular filtration rate. Additional symbols are given in the text. †Refers to g kidney for the rat glomerulus.

Statistical Analysis

Parameter values are presented as means ± SE. Differences among the models were tested using a nonparametric Mann-Whitney test. A Pearson χ^2-test was used for testing the "goodness of fit" for the data fitted to the model. Significance levels were set at $P < 0.05$, $P < 0.01$, and $P < 0.001$. All statistical calculations were made using the computer software R version 2.14.2 for Linux.

RESULTS

Theoretical analysis. In Fig. 2, several different fiber surface charge densities are simulated for a solute having a charge density similar to that of albumin (−22 mC/m^2) utilizing as starting point the optimized parameters calculated for nFicoll (or aFicoll) in an uncharged fiber matrix with characteristics shown in Table 2 (4). The rightmost sieving curve is the best-fitting curve to experimental data for nFicoll according to the charged fiber-matrix + large-pore model. A very low value (0.077) of the Pearson χ^2 indicates a good data fit to the model. The leftmost curve represents an extreme scenario, where the barrier has a surface charge of −200 mC/m^2. With this charge,

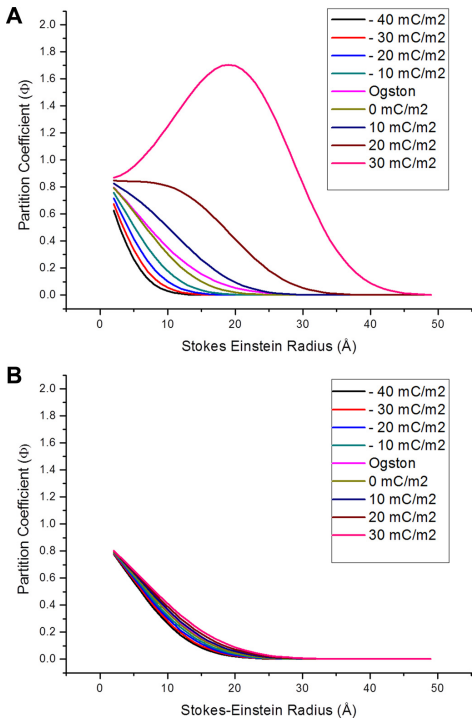

Fig. 3. *A*: partition coefficient for different solute charge densities on a fiber matrix with size-selective sieving characteristics listed in Table 2 at a low ionic strength of 10 mM. A positively charged barrier enhances the transport of an anionic solute. *B*: partition coefficient for different solute charge densities at a high ionic strength (similar to that in plasma) of 0.15 M.

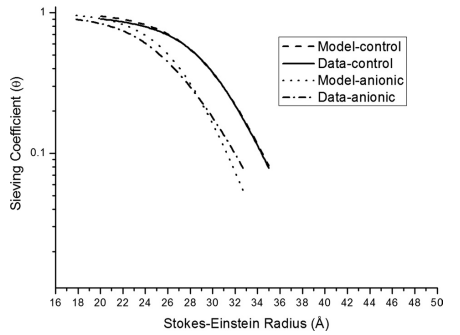

Fig. 4. Model fit to experimental sieving data for anionic Ficoll vs. neutral Ficoll in the molecules of radius range $20 < a_e < 35$ Å.

the theoretical aFicoll$_{35.5Å}$ sieving coefficient is on the order of $1 \cdot 10^{-5}$ (cf. albumin). In Fig. 3, *A* and *B*, the importance of ionic strength in screening the surface potential on a charged solute is demonstrated by plotting the partition coefficient vs. solute radii for different solute charge densities (q_s) at low (Fig. 3*A*) and physiologic (Fig. 3*B*) ionic strengths. As expected, the importance of charge on the partition coefficient is moderate at physiologic ("high") ionic strengths. In these plots, it can also be seen that there is a slight difference between the original Ogston model and the charged fiber-matrix model, even for an uncharged molecule. However, this difference becomes negligible at physiologic ionic strengths.

Data analysis. The sieving curves for the model best-fit versus the experimental data are shown in Fig. 4. The optimized model parameters for the uncharged random fiber-matrix model are shown in Table 3, whereas the parameters for the charged fiber-matrix model are shown in Table 4. Since the Grahame equation only gives a rough estimate of the actual surface charge density, two different solute surface charge densities were used in the models, −0.022 C/m^2 (albumin) and −0.035 C/m^2 (Ficoll approximation). Expectedly, a more anionic solute resulted in a lower charge density for the filtration barrier of about −5 mC/m^2. Interestingly, assuming the solute to have a charge similar to that of serum albumin gave values for fiber charge in the vicinity of known surface charge densities for many anionic plasma proteins. Only solute radii in the range 20–35 Å were analyzed. Two different fiber radii, 5 and 10 Å, were used in the modeling. For the neutral Ficoll data, the 5-Å fiber-radius model showed a better goodness of fit

Table 3. *Uncharged fiber-matrix parameters*

	5 Å	10 Å
Fractional void volume	0.884 ± 0.001	0.591 ± 0.003
$A_0/\Delta x$, cm/g × 10^{-5}†	17.51 ± 1.68	41.22 ± 4.09
L_pS, ml·min^{-1}·mmHg	0.13 ± 0.01	0.14 ± 0.01
Kozeny constant (*G*)	5	1
GFR, ml/min	0.65 ± 0.05	0.65 ± 0.05
Pearson χ^2	0.036 ± 0.002**	0.048 ± 0.002

Values are given as means ± SE. Additional symbols are given in the text. Statistical differences between 5- and 10-Å models: **$P < 0.01$. †Refers to g kidney for the rat glomerulus.

Table 4. *Charged fiber-matrix parameters*

Parameters				
Fiber radius (r_f), Å	5	5	10	10
Solute charge density (q_s), C/m^2	−0.022	−0.035	−0.022	−0.035
Fiber charge density (q_f), C/m^2	−0.019 ± 0.002	−0.004 ± 0.002	−0.017 ± 0.002	−0.005 ± 0.001
Pearson χ^2	0.823 ± 0.181	0.936 ± 0.189	0.943 ± 0.216	1.070 ± 0.229

Values are given as means ± SE. Additional symbols are given in the text.

than the 10-Å model. It can also be seen that the fractional void volume is much lower for the 10-Å model, which is to be expected since the partition coefficient (*Eq. 1*) is an increasing function of r_f, i.e., a more dense fiber array is needed for an array of large fibers to achieve the same partition coefficient as that of an array of thinner fibers. The hydraulic conductance was calculated assuming a Kozeny constant of 5 for the 5 Å-model, which yields a reasonable value for hydraulic conductance of the fiber array (LpS) of 0.13 ml·min^{-1}·mmHg, which is equivalent of a glomerular net pressure gradient of 5–7 mmHg. In the 10-Å model, a Kozeny constant of 1 was needed to achieve a similar gradient.

DISCUSSION

The essential result of the present modeling is that the magnitude of negative charge present on the fibers in a charged fiber-matrix model separating aFicoll from nFicoll in the intact rat GFB (4) is predicted to be of the same order of magnitude as that obtained for a majority of anionic proteins in plasma, such as albumin or orosomucoid. At normal (physiologic) ionic strengths, electrical charge effects thus appear to contribute only moderately to glomerular permeability, whereas molecular size and conformation are more important. A factor of ~2–3 difference in the sieving coefficient, as in the current study, is moderate compared with that of several other researchers, both historically (8) and recently, for example in Haraldsson et al. (19) where a factor of ~20, for a solute charge density similar to that of albumin, was suggested. This does not deny the fact that in a more "tight" fiber matrix with a higher size selectivity, as that assessed for neutral proteins (corresponding to an equivalent small-pore radius of ~37.4 Å), a negative electrical charge may critically exclude albumin from passing through "high-selectivity" pathways, redirecting albumin to rare "large-pore" pathways (24). In terms of Debye screening lengths (being ~8 Å at physiologic ionic strength), the charge effect in this study was found to be only ~20% of that predicted from the simple Debye-Hückel theory of ion-ion interactions. Hence, using pore theory and adding 1.5 Å (20% of 8 Å) to the molecules of radius of albumin (35.5 Å) and subtracting 1.5 Å from the small-pore radius (37.4 Å) implies that even the small charge effects obtained in the current study will totally screen out albumin from the "small-pore" pathway, thus, making the large-pore system the only pathway in the GFB for proteins of a similar or larger size than albumin under normal conditions. Leakage of albumin and large plasma solutes may, however, occur across the small pores in conditions where they are less selective, as has been observed in dialyzer membranes (5) or in the GFB after high doses of angiotensin II (3).

The mathematical model used in this study assumes a very simple structure of the GFB as a negatively charged barrier with random fibers (fiber matrix) and an idealized uniformly charged spherical "hard" solute (21). Conceivably, the former approximation should be more accurate for proteins than for polysaccharide molecules, such as dextran or Ficoll. For opposing surface charges, the single fiber-single sphere approach will tend to underestimate the restriction when there is significant interaction with several fibers, i.e., at a low void volume. Therefore, this approach should be most accurate at small Debye lengths (high ionic strengths) and/or at low fiber densities. Technically, the construction of a more complex model is always possible, but on the other hand, such models would have an increasing number of phenomenological parameters that would need to be approximated more or less arbitrarily, since the exact structure of the GFB is not known. In addition, a good model should be able to reproduce real experimental data. Despite the simplicity of the model used in this study, it shows a very good fit to the neutral Ficoll data for molecules of radius 20–35 Å. Thus, in a functional sense, the real and theoretical barriers are comparable. Only one model parameter, the surface charge density (q_f), was allowed to vary between the charged and uncharged barriers (due to the confounding effects of the other parameters). This may, in part, explain why the model fit for the aFicoll data was not as good as that for nFicoll since there are also small [cf. Axelsson et al. (4)] differences in the other parameters.

Given the lack of charge selectivity of isolated GBM (7), and the fact that the total abolition of the negatively charged GBM proteoglycans, agrin, and perlecan does not seem to affect the permeability of albumin across the GFB (15, 20), the endothelial glycocalyx may be implicated as the major charge barrier of the GFB. Actually, the best fit of nFicoll data to the fiber-matrix model was for a fiber radius of 5 Å and a fiber density of 11%, which would approximately fit the composition of a fiber matrix of glycoproteins, proteoglycans, and glucosaminoglycans, rather than a matrix of the much thicker collagen-IV and laminin molecules of the GBM. The glycocalyx, representing a cell surface coat of the composition mentioned above, is important for several basic cell functions, such as immunologic recognition of "self" and "nonself," sensing of shear stress, and the presentation of receptors and adhesion molecules on the cell surface (32). The glycocalyx can be regarded as a dynamic network in which soluble plasma proteins and endothelial derived components are incorporated to form an even larger endothelial surface layer (ESL). Being in direct contact with the circulation, the ESL is continuously remodeled due to both enzymatic and shear-induced shedding (28). This means that the glycocalyx, and the ESL in toto, can hardly be viewed as a static structure. Still, the glycocalyx may be regarded as at least one of the structural candidates to the charged fiber-matrix concept in this study.

Examining glomerular permeability by studying the sieving of plasma proteins is complicated by the fact that there is extensive tubular processing of the glomerular ultrafiltrate with almost complete tubular reabsorption of filtered proteins. Furthermore, the sieving of a large number of proteins of discrete molecules of radii (a_e) has to be assessed to create a protein glomerular sieving curve. We have therefore preferred to use polysaccharides, uncharged and charged, as probe molecules, to estimate the sieving properties of the GFB. Polysaccharides are minimally processed by the renal tubule, and they allow the assessment of sieving of molecules of a wide range of a_e. Unfortunately, polysaccharides in general apparently exhibit a glomerular "hyperpermeability," especially when a_e approaches the radius of the size-selective structures in the GFB. We have found, however, that Ficoll apparently behaves as a hard sphere (cf. proteins) for λ values (solute radius over pore radius) $\leq$0.65, implying that Ficoll data and protein data are similar for solutes up to a radius of 25 Å, i.e., across the "small-pore equivalent" of the GFB. Furthermore, Ficoll and proteins seem to be handled in a similar fashion for an a_e interval of 50–75 Å, i.e., in the equivalent "large-pore pathway" (pore radius ~120 Å). Thus, as already discussed above, the size selectivity of the GFB measured using intermediately sized Ficoll molecules of radius of 25–50 Å might be in error. If instead the small-pore radius estimate determined for neutral protein permeation across the GFB (24), i.e., 37.4 Å, were correct, this implies that Ficoll molecules >37.4 Å would actually permeate the membrane in an anomalous fashion, conceivably by (increased) molecular deformability. In the present study we found that the sieving coefficients for aFicoll $\geq$35 Å in radius (for λ approaching or exceeding 1) significantly deviated from those predicted by the charged fiber-matrix model, in that sieving coefficients for aFicoll approached those for nFicoll. A similar phenomenon has been observed for aFicoll vs. nFicoll in artificial membranes (17). This may indicate that charge restriction effects tend to be markedly reduced in magnitude when the size of the charged molecules approaches the size of the transport limiting structures of the barrier or that charge selectivity is much more complex than predicted from a charged fiber-matrix model.

The present results suggest that electrical charge only makes a moderate contribution to glomerular permselectivity and that molecular size and conformation are far more important in this respect. In fact, in the present study it was shown that a supraphysiological surface charge density (q_f), being nearly -0.2 C/m^2, is needed to account for the difference in the sieving coefficients between nFicoll and (negatively) charged albumin, if charge-dependent restriction were the only factor affecting the glomerular sieving of albumin vs. Ficoll. For a more compact fiber matrix than that fitting to the sieving characteristics measured for nFicoll, i.e., a fiber matrix fitting to (neutral) protein data, the moderate negative charge determined in this study may still critically affect the permeation of albumin from blood to urine. In such a model, a weak electrical charge will more or less totally exclude albumin from a high-selectivity fiber matrix, to redirect it to some very rare low-selectivity glomerular transport pathways.

ACKNOWLEDGMENTS

We gratefully thank Josefin Axelsson for technical aid and Kerstin Wihlborg for expert secretarial assistance.

GRANTS

This study was supported by grants from the Swedish Research Council Grant 08285, Heart and Lung Foundation, and Medical Faculty at Lund University (ALF Grant).

DISCLOSURES

No conflicts of interest, financial or otherwise, are declared by the author(s).

AUTHOR CONTRIBUTIONS

Author contributions: C.M. and B.R. conception and design of research; C.M. analyzed data; C.M. and B.R. interpreted results of experiments; C.M. prepared figures; C.M. and B.R. drafted manuscript; C.M. and B.R. edited and revised manuscript; C.M. and B.R. approved final version of manuscript.

REFERENCES

1. **Asgeirsson D, Axelsson J, Rippe C, Rippe B.** Similarity of permeabilities for Ficoll, pullulan, charge-modified albumin and native albumin across the rat peritoneal membrane. *Acta Physiol (Oxf)* 196: 427–433, 2009.
2. **Asgeirsson D, Venturoli D, Rippe B, Rippe C.** Increased glomerular permeability to negatively charged Ficoll relative to neutral Ficoll in rats. *Am J Physiol Renal Physiol* 291: F1083–F1089, 2006.
3. **Axelsson J, Rippe A, Oberg CM, Rippe B.** Rapid, dynamic changes in glomerular permeability to macromolecules during systemic angiotensin II (ANG II) infusion in rats. *Am J Physiol Renal Physiol* 303: F790–F799, 2012.
4. **Axelsson J, Sverrisson K, Rippe A, Fissell W, Rippe B.** Reduced diffusion of charge-modified, conformationally intact anionic Ficoll relative to neutral Ficoll across the rat glomerular filtration barrier in vivo. *Am J Physiol Renal Physiol* 301: F708–F712, 2011.
5. **Axelsson J, Öberg CM, Rippe A, Krause B, Rippe B.** Size-selectivity of a synthetic high-flux and a high cut-off dialyzing membrane compared to that of the rat glomerular filtration barrier. *J Membrane Sci* 413–414: 29–37, 2012.
6. **Bhalla G, Deen WM.** Effects of charge on osmotic reflection coefficients of macromolecules in fibrous membranes. *Biophys J* 97: 1595–1605, 2009.
7. **Bolton GR, Deen WM, Daniels BS.** Assessment of the charge selectivity of glomerular basement membrane using Ficoll sulfate. *Am J Physiol Renal Physiol* 274: F889–F896, 1998.
8. **Brenner BM, Hostetter TH, Humes HD.** Glomerular permselectivity: barrier function based on discrimination of molecular size and charge. *Am J Physiol Renal Fluid Electrolyte Physiol* 234: F455–F460, 1978.
9. **Butt HJ, Kappl M.** *Physics and Chemistry of Interfaces*. Weinheim, Germany: Wiley-VCH Verlag, 2006.
10. **Chang RL, Deen WM, Robertson CR, Brenner BM.** Permselectivity of the glomerular capillary wall: III. Restricted transport of polyanions. *Kidney Int* 8: 212–218, 1975.
11. **Dechadilok P, Deen WM.** Hindrance factors for diffusion and convection in pores. *Ind Eng Chem Res* 45: 6953–6959, 2006.
12. **Fissell WH, Manley S, Dubnisheva A, Glass J, Magistrelli J, Eldridge AN, Fleischman AJ, Zydney AL, Roy S.** Ficoll is not a rigid sphere. *Am J Physiol Renal Physiol* 293: F1209–F1213, 2007.
13. **Freitas RA.** *Nanomedicine*. Basel, Switzerland: Karger, 2004.
14. **Galassi M.** *GNU Scientific Library Reference Manual* (3rd ed). UK: Network Theory, 2009.
15. **Goldberg S, Harvey SJ, Cunningham J, Tryggvason K, Miner JH.** Glomerular filtration is normal in the absence of both agrin and perlecan-heparan sulfate from the glomerular basement membrane. *Nephrol Dial Transplant* 24: 2044–2051, 2009.
16. **Gratrix ML, Mucha DR, Carbajal JM, Schaeffer RC Jr.** The rat glomerular filtration barrier does not show negative charge selectivity. *FASEB J* 12: 1998.
17. **Groszek J, Li L, Ferrell N, Smith R, Zorman CA, Hofmann CL, Roy S, Fissell WH.** Molecular conformation and filtration properties of anionic Ficoll. *Am J Physiol Renal Physiol* 299: F752–F757, 2010.
18. **Guasch A, Deen WM, Myers BD.** Charge selectivity of the glomerular filtration barrier in healthy and nephrotic humans. *J Clin Invest* 92: 2274–2282, 1993.

19. **Haraldsson B, Nystrom J, Deen WM.** Properties of the glomerular barrier and mechanisms of proteinuria. *Physiol Rev* 88: 451–487, 2008.
20. **Harvey SJ, Jarad G, Cunningham J, Rops AL, van der Vlag J, Berden JH, Moeller MJ, Holzman LB, Burgess RW, Miner JH.** Disruption of glomerular basement membrane charge through podocyte-specific mutation of agrin does not alter glomerular permselectivity. *Am J Pathol* 171: 139–152, 2007.
21. **Jeansson M, Haraldsson B.** Glomerular size and charge selectivity in the mouse after exposure to glucosaminoglycan-degrading enzymes. *J Am Soc Nephrol* 14: 1756–1765, 2003.
22. **Johnson EM, Berk DA, Jain RK, Deen WM.** Diffusion and partitioning of proteins in charged agarose gels. *Biophys J* 68: 1561–1568, 1995.
23. **Johnson EM, Deen WM.** Electrostatic effects on the equilibrium partitioning of spherical colloids in random fibrous media. *J Colloid Interface Sci* 178: 749–756, 1996.
24. **Lund U, Rippe A, Venturoli D, Tenstad O, Grubb A, Rippe B.** Glomerular filtration rate dependence of sieving of albumin and some neutral proteins in rat kidneys. *Am J Physiol Renal Physiol* 284: F1226–F1234, 2003.
25. **Moré J, Garbow B, Hillström K.** User guide for MINPACK-1. *Argonne National Laboratory Report ANL-80–74*: Argonne, IL: Argonne National Laboratory, 1980.
26. **Peters T.** *All About Albumin: Biochemistry, Genetics, and Medical Applications.* New York: Elsevier, 1996.
27. **Pujar NS, Zydney AL.** Electrostatic and Electrokinetic Interactions during Protein-Transport through Narrow Pore Membranes. *Ind Eng Chem Res* 33: 2473–2482, 1994.
28. **Reitsma S, Slaaf DW, Vink H, van Zandvoort MA, Egbrink MG.** The endothelial glycocalyx: composition, functions, and visualization. *Pflügers Arch* 454: 345–359, 2007.
29. **Rippe B, Haraldsson B.** Fluid and protein fluxes across small and large pores in the microvasculature. Application of two-pore equations. *Acta Physiol Scand* 131: 411–428, 1987.
30. **Rippe B, Haraldsson B.** Transport of macromolecules across microvascular walls: the two-pore theory. *Physiol Rev* 74: 163–219, 1994.
31. **Schaeffer RC Jr, Gratrix M, Mucha D, Carbajal J.** The rat glomerular filtration barrier does not show negative charge selectivity. *Microcirculation* 9: 329–342, 2002.
32. **Schmidt EP, Lee WL, Zemans RL, Yamashita C, Downey GP.** On, around, and through: neutrophil-endothelial interactions in innate immunity. *Physiology* 26: 334–347, 2011.
33. **Tay M, Comper WD, Singh AK.** Charge selectivity in kidney ultrafiltration is associated with glomerular uptake of transport probes. *Am J Physiol Renal Fluid Electrolyte Physiol* 260: F549–F554, 1991.
34. **Venturoli D, Rippe B.** Ficoll and dextran vs. globular proteins as probes for testing glomerular permselectivity: effects of molecular size, shape, charge, and deformability. *Am J Physiol Renal Physiol* 288: F605–F613, 2005.
35. **Winzor DJ.** Determination of the net charge (valence) of a protein: a fundamental but elusive parameter. *Anal Biochem* 325: 1–20, 2004.

Study II

Am J Physiol Renal Physiol 306: F844–F854, 2014.
First published February 12, 2014; doi:10.1152/ajprenal.00366.2013.

A distributed two-pore model: theoretical implications and practical application to the glomerular sieving of Ficoll

Carl M. Öberg and Bengt Rippe

Department of Nephrology, University Hospital of Lund, Lund University, Lund, Sweden

Submitted 1 July 2013; accepted in final form 9 February 2014

Öberg CM, Rippe B. A distributed two-pore model: theoretical implications and practical application to the glomerular sieving of Ficoll. *Am J Physiol Renal Physiol* 306: F844–F854, 2014. First published February 12, 2014; doi:10.1152/ajprenal.00366.2013.—In the present study, an extended two-pore theory is presented where the porous pathways are continuously distributed according to small- and large-pore mean radii and SDs. Experimental glomerular sieving data for Ficoll were analyzed using the model. In addition, several theoretical findings are presented along with analytic solutions to many of the equations used in distributed pore modeling. The results of the data analysis revealed a small-pore population in the glomerular capillary wall with a mean radius of 36.6 Å having a wide arithmetic SD of ~5 Å and a large-pore radius of 98.6 Å with an even wider SD of ~44 Å. The small-pore radius obtained in the analysis was close to that of human serum albumin (35.5 Å). By reanalyzing the data and setting the distribution spread of the model constant, we discovered that a narrow distribution is compensated by an increased mean pore radius and a decreased pore area-to-diffusion length ratio. The wide distribution of pore sizes obtained in the present analysis, even when considering electrostatic hindrance due to the negatively charged barrier, is inconsistent with the high selectivity to proteins typically characterizing the glomerular filtration barrier. We therefore hypothesize that a large portion of the variance in the distribution of pore sizes obtained is due to the molecular "flexibility" of Ficoll, implying that the true variance of the pore system is lower than that obtained using flexible probes. This would also, in part, explain the commonly noted discrepancy between the pore area-to-diffusion length ratio and the filtration coefficient.

two-pore model; log-normal distributed model; capillary permeability; Ficoll; standard deviation

THE TWO-PORE MODEL of capillary permeability has been successfully applied to describe the transport of water and plasma solutes in a large number of different organs (8, 19, 26, 32, 33, 35, 36) and, recently, dialyzer membranes as well (7). The classic two-pore model assumes that the transcapillary transport of plasma solutes and water occurs over two distinct porous pathways, small pores and large pores, each having a fixed (discrete) pore radius. In contrast, distributed pore models assume that the pore radii are continuously distributed around a mean radius with a distribution spread [standard deviation (SD)] (1, 7, 9, 11, 20, 21). In most distributed models, only the small-pore system has been considered, whereas the large-pore pathway has been modeled as an unselective shunt pathway, theoretically allowing free passage of all solutes regardless of molecular size [to our knowledge the only exception is (1), where both the small-pore and large-pore systems are distributed]. However, when analyzing the glomerular transport of large globular proteins using the discrete two-pore model, Tencer et al. (36) found that there seems to be an upper size limit for molecular radii on the order of ~110–115 Å. This implies that very large plasma proteins, such as IgM (molecular radius: ~120 Å), will not pass the glomerular filtration barrier (GFB) at all under normal circumstances (36). Similarly, while studying the glomerular transport of globular proteins, Lund and colleagues (24) found a good fit for a (discrete) large-pore radius (r_L) of 110 Å.

Distributed pore models usually assume that the underlying pore size distribution can be characterized by a log-normal distribution, which has the advantage that it is defined only for positive pore radii, in contrast to the standard (Gaussian) normal distribution, which, if applied, would (per definition) also include negative pore radii. Often, it has been noted that biological mechanisms induce log-normal distributions, as when, for instance, the causative effects are multiplicative rather than additive (22). Indeed, the seminal work by Deen and colleagues (11) indicated that the log-normal distribution provides a better fit to the experimental data than other continuous distributions (i.e., normal distribution or gamma-distribution). In addition, the classic (discrete) two-pore model (regarding the goodness of fit) is superior to either a log-normal distributed model or an isoporous (single discrete pore radius) model in describing glomerular transport data, especially in nephrotic patients (11). Despite a superior goodness of fit (low χ^2-value) to the experimental data (7, 11), the discrete two-pore model typically shows a poor visual fit in the region between ~50 and 65 Å (cf. Ref. 34), which has been attributed to the molecular flexibility of the Ficoll molecule in this region. Due to the poor fit, data in this "knee" region are sometimes excluded from regression analysis (34).

Most models for diffusion and filtration of solute molecules over a porous (or fibrous) barrier assume that the solute molecules behave like rigid spheres. Thus, compared with a rigid sphere, flexible polysaccharide molecules, such as dextran and, to a lesser degree, Ficoll, are hyperpermeable across the GFB, whereas less flexible, globular proteins, such as albumin, behave more similar to a rigid sphere (13, 14, 38). In terms of the discrete pore model, this means that the small-pore radius (r_S) will be overestimated when analyzing the sieving of polysaccharide probe molecules (7), while, to the best of our knowledge, a similar overestimation of the mean pore radius (u) in the distributed model has not been observed. Hence, it has been noted that the mean small-pore radius for Ficoll in distributed models is ~35–39 Å, which is very close to that obtained using the discrete two-pore model to describe protein sieving data (~37 Å) (24). At the same time, the width of the small-pore distribution [usually specified in terms of the geometric SD (commonly denoted "s")] has been quite large, 1.15–1.19, corresponding to an arithmetic SD (σ_S) of ~5–7 Å.

Address for reprint requests and other correspondence: C. M. Öberg, Dept. of Nephrology, Lund Univ., Univ. Hospital of Lund, Lund S-211 85, Sweden (e-mail: carl.oberg@med.lu.se).

The reason behind the observed hyperpermeability of the Ficoll molecule is not known. Conceivably, Ficoll may have several intermediate shapes and/or an increased molecular deformability, which may give the molecules an ability to change shape under pressure (13). Interestingly, a recent study by Georgalis et al. (16) indicated the coexistence of two closely spaced diffusive modes in Ficoll 70 solutions.

A widely used parameter in pore theory is $A_0/\Delta x$ (sometimes denoted "*fS*/*l*"), which represents the total pore area available for diffusive transport (A_0) divided by the diffusion length (Δx). From this parameter, the total volume flow can be approximated (e.g., by using Poiseuille's law). Often, it has been noted that the volume flow approximated from the diffusive solute transport ($A_0/\Delta x$) differs from that actually measured experimentally [e.g., the glomerular filtration rate (GFR) for glomerular capillaries]. This discrepancy is particularly evident in nonglomerular capillaries, as previously reviewed (31, 33), and in distributed pore models (20, 21, 34). In an early pioneering experiment, Lambert et al. (21) studied the glomerular sieving of radiolabeled polyvinylpyrrolidone and calculated values for $A_0/\Delta x$ that were up to one order of magnitude larger for the log-normal distributed model than that of the discrete model. In addition, the mean pore radius was lower for the distributed model (21). Jeansson and Haraldsson (20) studied glomerular size selectivity in the mouse using Ficoll and found a similar discrepancy between the two-pore model and the log-normal distributed + shunt model. In line with these results, our own experiments have yielded comparable results for the log-normal distributed + shunt model (5, 7, 34). The inflation of the $A_0/\Delta x$ parameter leads to an inconsistency among $A_0/\Delta x$ [as calculated from the filtration coefficient (L_pS)] and the value for $A_0/\Delta x$ as determined by the model regression on sieving data. Indeed, similar inconsistencies have been a classic controversy in the field of capillary physiology over several decades [cf. "Pappenheimer's pore puzzle" (29)].

It is reasonable to assume that there should be at least some variation in the pore radii and also an upper size limitation in the large-pore system. Thus, the present study aimed to combine the two "classic" models for glomerular transport (two-pore and log-normal + shunt) by the application and theoretical analysis of a distributed two-pore model. The model was used to analyze sieving data from Axelsson et al. (6) to determine the mean pore radius and the distribution spread of both the small-pore and large-pore systems in the GFB. The discrete two-pore model typically yields lower values for L_pS and $A_0/\Delta x$ and usually a mean small-pore radius that is ~7–8 Å higher than that of the distributed + shunt model. Analysis of data with the discrete two-pore model is equivalent to using the distributed two-pore model with the spread parameter set to unity. To discern the effects of using a constant spread, the data were analyzed again setting the spread of the model constant. This revealed if there were any other differences between distributed and discrete (or fixed spread) pore modeling apart from the previously noted differences in $A_0/\Delta x$ and small-pore radius.

Glossary

α_i	Fractional hydraulic conductance for the *i*th pore population
α_L	Fractional hydraulic conductance for the large-pore population (i.e., K_{fL}/K_f)
α_S	Fractional hydraulic conductance for the small-pore population (i.e., K_{fS}/K_f)
η	Viscosity of the solvent (in Pa·s) (e.g., $\eta_{water} \approx$ 0.7 mPa·s)
θ	Sieving coefficient
$\theta_{j,data}$	Experimental sieving coefficient of the data
$\theta_{j,model}$	Theoretical sieving coefficient of the model
λ	Solute-to-pore radius ratio (e.g., a_e/r_s)
μ_L	Arithmetic mean pore radius for the large-pore population
μ_S	Arithmetic mean pore radius for the small-pore population
$\Delta\pi$	Osmotic pressure gradient (in mmHg)
σ	Reflection coefficient
σ_f	Solvent-drag reflection coefficient
$\sigma_{h,L}$	Homoporous large-pore reflection coefficient
$\sigma_{h,S}$	Homoporous small-pore reflection coefficient
$\sigma_{i,net}$	Net osmotic reflection coefficient
σ_L	Arithmetic SD for the large-pore population
σ_o	Osmotic reflection coefficient
$\sigma_{o,net}$	Ensemble osmotic reflection coefficient for all solutes and all pathways
σ_S	Arithmetic SD for the small-pore population
a_e	Molecular (Stokes-Einstein) radius (in Å)
A	Effective surface area available for restricted diffusion (i.e., $A_0 \geq A$)
A_0	Total cross-sectional pore area
A/A_0	Diffusive transport restriction coefficient (effective-to-total area ratio)
B^n	Analytical solution
c(x)	Concentration profile along the length of the pore (in mol/ml)
C_i	Downstream (filtrate) concentration (in mol/ml)
C_p	Plasma concentration (in mol/ml)
D	Free diffusion coefficient (in cm^2/min)
erf	Error function
f_L	Fractional volume flux across the large-pore population (i.e., J_{vL}/J_v)
f_S	Fractional volume flux across the small-pore population (i.e., J_{vS}/J_v)
g(r)	Log-normal probability density function
G^n	Analytical solution (defined in *Eq. 23*)
GFR	Glomerular filtration rate
GFB	Glomerular filtration barrier
H	Alternate notation of A/A_0
HSA	Human serum albumin
$J_{convection}$	Flux through convective transport
$J_{diffusion}$	Flux through diffusive transport
J_s	Total solute flux across the entire barrier (in mol/min)
J_v	Total volume flux across the entire barrier (in ml/min)
J_{vi}	Volume flux across the *i*th pore population in a heteroselective barrier (in ml/min)
J_{vL}	Volume flux across the large-pore population (in ml/min)
$J_{vL,iso}$	Isogravimetric flux for large-pore population (in μl/min) ($J_{vS,iso} = -J_{vL,iso}$)
J_{vS}	Volume flux across the small-pore population (in ml/min)
k	Boltzmann constant

K_f	See L_pS
L_p	Total hydraulic conductivity (in ml·min^{-1}·mmHg^{-1}·cm^{-2})
L_pS	Filtration coefficient; total hydraulic conductance (in ml·min^{-1}·mmHg^{-1})
n	Any real number
N	Total number of pores per unit weight kidney (in g) (or unit area for a membrane)
nHRP	Neutral horseradish peroxidase
P	Permeability coefficient; $D/\Delta x$ (in cm/min)
Pe	Péclet number
Pe_L	Péclet numbers for the large-pore system
Pe_S	Péclet numbers for the small-pore system
PS	Permeability-surface (diffusion capacity) coefficient (in ml/min)
PS_L	Permeability-surface (diffusion capacity) coefficient for the large-pore system
PS_S	Permeability-surface (diffusion capacity) coefficient for the small-pore system
ΔP	Hydraulic pressure gradient (in mmHg)
ΔP_{net}	Net pressure gradient ($\Delta P - \sigma\Delta\pi$)
r	Log-normally distributed radius
R	Natural logarithm of r
s	Geometric pore SD
s_L	Geometric large-pore SD
s_S	Geometric small-pore SD
S	Barrier surface area (in cm^2) per unit weight kidney (or unit area for a membrane)
SD	Standard deviation
T	Temperature (in K) (body temperature = 310 K)
u	Geometric mean pore radius
u_L	Geometric mean large-pore radius (in Å)
u_S	Geometric mean small-pore radius (in Å)
W	Alternative notation of 1-σ
x	Distance (in cm)
Δx	Total barrier thickness (in cm)

METHODS

Experimental sieving data from Axelsson et al. (controls) (6) for the rat glomerulus were analyzed using a novel extended two-pore model where each pore population is distributed around a central tendency, u_S and u_L, respectively, each with a small-pore and large-pore SD (s_S and s_L, respectively). In summary, the mathematical construction is identical to that of the discrete two-pore model with the exception that the hindrance factors are calculated for a log-normal distribution of pore sizes instead of single discrete pore sizes.

Theoretical background. The steady-state solute transport (J_s, in mol/min) across a semipermeable barrier can be described by the convection-diffusion equation, as follows:

$$J_s = J_{diffusion} + J_{convection} = -DA\frac{dc}{dx} + J_v(1-\sigma)c \qquad (1)$$

where D is the diffusion coefficient (in cm^2/min), A is the effective area (in cm^2), J_v is the volume flux (GFR), σ is the reflection coefficient, and $c(x)$ is the concentration (in mol/ml) as a function of the distance x (in cm) from the plasma side of the barrier. Thus, J_s is the sum of the diffusive transport [according to Fick's first law, $J_{diffusion} = -DA \times dc/dx$ (in mol/min)] and the convective transport $J_{convection}$ (in mol/min) [the effective volume flux $J_v \times (1 - \sigma)$ (in ml/min) times the concentration (in mol/ml)]. All coefficients are assumed to be constant. *Equation 1* is a separable first-order ordinary differential equation that can be integrated over the barrier [ad modum Patlak et al. (30); see the APPENDIX), yielding

$$J_s = J_v(1-\sigma)\frac{c_p - c_i e^{-Pe}}{1 - e^{-Pe}} \qquad (2)$$

where C_p is the plasma concentration (in mol/ml) and C_i is the downstream (filtrate) concentration (in mol/ml). The Péclet number (Pe), the "convection-to-diffusion ratio" for a particular barrier-flux-solute combination, is defined as follows:

$$Pe = \frac{J_v(1-\sigma)}{PS} \qquad (3)$$

where the permeability-surface area coefficient (PS; in ml/min) is given by the following equation:

$$PS = \frac{D}{\Delta x}A = D\frac{A_0}{\Delta x}\frac{A}{A_0} \qquad (4)$$

The latter equality is particularly useful since hydrodynamic estimates give an expression for A/A_0 rather than $A/\Delta x$ (33). The diffusion restriction coefficient (A/A_0) represents the restriction in the diffusive transport due to the hindrance of the barrier. As an example, if $A/A_0 = 1/3$, then the clearance of a solute from $x = 0$ to $x = \Delta x$ is only one-third of that which would occur if there was no diffusive transport restriction. Assuming an ideal spherical uncharged solute, D can be estimated using the following Stokes-Einstein equation:

$$D = \frac{kT}{6\pi\eta a_e} \qquad (5)$$

where k is the Boltzmann constant, T is the temperature (in K), η the viscosity of the permeate (the permeate is assumed to have a viscosity close to that of water, i.e., ~0.7 mPa·s). and a_e is the Stokes-Einstein radius of the solute (in Å). In the present article, the term "radius" is used synonymously with Stokes-Einstein radius unless otherwise specified. During ultrafiltration, $J_s = J_v \times C_i$, so the sieving coefficient (θ; equal to C_i/C_p) can be derived from *Eq. 2*, leading to the following practical expression:

$$\theta = \frac{1-\sigma}{1-\sigma e^{-Pe}} \qquad (6)$$

The solute clearance (in ml/min) is simply $J_v \times \theta$. Thus, it is possible to relate the ultrafiltrate concentration to the plasma concentration using the following equation:

$$C_p = \theta \times C_i \qquad (7)$$

It is important to note that the solution above (*Eq. 2*) is only valid if $J_v \neq 0$. During zero flux conditions, Fick's first law can be applied directly, i.e., $J_s = -PS(C_i - C_p)$.

Log-normal distribution. The log-normal distribution has been widely used in the characterization of the pore size distribution of both synthetic and biological barriers. There has, however, been considerable differences regarding the proper functional form of the log-normal probability density function as well as concerning the interpretation of the distribution parameters (40). Arguably, the most widely adopted distribution parameters are u and s. The functional form for the probability density function for the log-normal distribution is then given as follows:

$$g(r,u,s) = \frac{1}{r\ln(s)\sqrt{2\pi}}e^{-\frac{1}{2}\left[\frac{\ln(r)-\ln(u)}{\ln(s)}\right]^2} \qquad (8)$$

The corresponding arithmetic mean (μ) and standard deviation (σ) (in Å) can be calculated by $\mu = u \times s^{1/2\,\ln s}$ and $\sigma = u \times (s^{2\,\ln s} - s^{\ln s})^{1/2}$, respectively (40). In this article, both arithmetic (μ and σ) and geometric (u and s) distribution parameters are presented in the data analysis. The

arithmetic mean and SD must not be confused with the corresponding moments for the standard normal distribution. The log-normal distribution is an asymmetric distribution with a positive skew.

Solute flux. The net θ value for the filtration barrier was calculated using the following equation:

$$\theta = f_s \frac{1-\sigma_S}{1-\sigma_S e^{-Pe_S}} + f_L \frac{1-\sigma_L}{1-\sigma_L e^{-Pe_L}} \quad (9)$$

where $f_L = 1 - f_S$ is the fraction of fluid flow passing the barrier via the large-pore pathway (i.e., $f_L = J_{vL}/GFR$), σ_S and σ_L are the reflection coefficients for the small-pore and large-pore systems, respectively, and Pe_S and Pe_L are the Péclet numbers for the small-pore and large-pore system, respectively. σ_S and σ_L values were calculated using the following equations:

$$\sigma_S = \frac{\int_0^\infty r^4 g(r, u_S, s_S)\sigma_{h,S}(r)dr}{\int_0^\infty r^4 g(r, u_S, s_S)dr} \quad (10)$$

and

$$\sigma_L = \frac{\int_0^\infty r^4 g(r, u_L, s_L)\sigma_{h,L}(r)dr}{\int_0^\infty r^4 g(r, u_L, s_L)dr} \quad (11)$$

where $\sigma_{h,L}$ and $\sigma_{h,S}$ are the homoporous small-pore and large-pore reflection coefficients, respectively. Pe_S and Pe_L were calculated using the following equations:

$$Pe_S = \frac{J_{vS}(1-\sigma_S)}{PS_S} \quad (12)$$

and

$$Pe_L = \frac{J_{vL}(1-\sigma_L)}{PS_L} \quad (13)$$

PS_S and PS_L are calculated using the following equations:

$$PS_S = D\frac{A_{0,S}}{A_0}\frac{A_0}{\Delta x}\frac{\int_0^\infty r^2\left(\frac{A}{A_0}\right)_{h,S} g(r)dr}{\int_0^\infty r^2 g(r)dr} \quad (14)$$

and

$$PS_L = D\frac{A_{0,L}}{A_0}\frac{A_0}{\Delta x}\frac{\int_0^\infty r^2\left(\frac{A}{A_0}\right)_{h,L} g(r)dr}{\int_0^\infty r^2 g(r)dr} \quad (15)$$

where $A_{0,S}/A_0 = 1 - A_{0,L}/A_0$ is the fractional cross-sectional pore area of the small-pore system and $(A/A_0)_{h,S}$ and $(A/A_0)_{h,L}$ are the (homoporous) diffusive transport restriction coefficients (cf. *Eq. 21*) for the small-pore and large-pore systems, respectively.

Volume flux. If no osmotic gradient exists over an heteroselective barrier (i.e., $\Delta\pi = 0$), then the volume flux via the ith pathway is directly proportional to the hydraulic conductance ($\alpha_i K_f$) of the pathway, as follows:

$$J_{vi:\Delta\pi=0} = \alpha_i \times GFR \quad (16)$$

where $\alpha_i = K_{f,i}/K_f$ is the fractional hydraulic conductance of the ith pathway. If there is an osmotic gradient, then the Starling equilibrium can be applied directly to the pathway, as follows:

$$J_{vi} = \alpha_i K_f(\Delta P - \sigma_{i,net}\Delta\pi) \quad (17)$$

where $\sigma_{i,net}$ is the net osmotic reflection coefficient (i.e., effective σ_o for all solutes for the ith pathway). Hence, if an osmotic gradient exists over a heteroselective barrier, then the volume flow through each pathway will be different from that predicted solely from the hydraulic conductance of that pathway. This difference, known as the isogravimetric flux (32), is thus:

$$J_{vi,iso} = J_{vi} - J_{vi:\Delta\pi=0} = \alpha_i K_f(\sigma_{o,net} - \sigma_{i,net})\Delta\pi \quad (18)$$

where $\sigma_{o,net}$ is the ensemble osmotic reflection coefficient for all solutes and all pathways. The volume flux over the ith pathway in a heteroselective filtration barrier is therefore:

$$J_{vi} = \alpha_i \times GFR + J_{vi,iso} = \alpha_i[K_f(\sigma_{o,net} - \sigma_{i,net})\Delta\pi + GFR] \quad (19)$$

In the calculations, the net reflection coefficients have been approximated to those of albumin and a net $\Delta\pi$ of 28 mmHg has been assumed. If the net reflection coefficient of a pathway is smaller than the net osmotic reflection coefficient (for the barrier), then $J_{vi,iso}$ will be negative for that pathway and the flux (J_{vi}) will be smaller than that predicted solely from the hydraulic conductance of that pathway. For some pathways, J_{vi} may be negative, and a recirculation of volume occurs. For a barrier that is nearly homoporous, such as the GFB, $J_{vi,iso}$ will typically be very small (28).

Hydrodynamic hindrance factors. The hydrodynamic hindrance factors recommended by Dechadilok and Deen for porous membranes (10) were used and are repeated here for convenience. These expressions have the advantage that they are properly averaged over the entire pore section rather than being "centerline approximations." The homoporous reflection coefficient was estimated from the following equation:

$$\sigma_h = 1 - W(\lambda) = 1 - (1-\lambda)^2\frac{1 + 3.867\lambda - 1.907\lambda^2 - 0.834\lambda^3}{1 + 1.867\lambda - 0.741\lambda^2} \quad (20)$$

according to Ennis et al. (cf. *Eq. 41* in Ref. 12). The diffusive transport restriction coefficient was calculated from

$$\frac{A}{A_0} = H(\lambda) = 1 + \frac{9}{8}\lambda\ln(\lambda) - 1.56034\lambda + 0.528155\lambda^2 + 1.91521\lambda^3 - 2.81903\lambda^4 + 0.270788\lambda^5 + 1.10115\lambda^6 + 0.435933\lambda^7 \quad (21)$$

for $\lambda \leq 0.95$ (*Eq. 16* in *Ref. 10*). For more closely fitting solutes ($\lambda > 0.95$), we used the following equation:

$$\frac{A}{A_0} = (1-\lambda)^2\frac{123}{125}\left(\frac{1-\lambda}{\lambda}\right)^{5/2} \quad (22)$$

according to the estimate by Mavrovouniotis and Brenner (cf. *Eq. 71* in Ref. 25). The hydrodynamic hindrance factors are bounded functions (per definition) in the sense that A/A_0 tends to zero and σ_h tends to unity when $\lambda \to 1$ and, in addition, that A/A_0 tends to unity and σ_h tends to zero when $\lambda \to 0$. Since A/A_0 vanishes for $r < a_e$, the integrals in the numerators of *Eqs. 14* and *15* need only be evaluated from a_e to ∞.

Analytic solutions. For the improper integrals in the denominators of Eqs. *10*, *11*, *14*, and *15*, there exists the following analytic solution:

$$G^n(u, s) = \int_0^\infty r^n g(r)dr = u^n e^{\frac{n^2\ln^2(s)}{2}} \quad (23)$$

for any real number (n) that can be derived using integration by parts (see the APPENDIX). The total cross-sectional area of a log-normal distributed porous barrier with mean radius u and spread s can then be calculated exactly as follows:

$$\frac{A_0}{\Delta x} = \frac{N}{\Delta x}\int_0^\infty \pi r^2 g(r)dr = \frac{N}{\Delta x}\pi G^2(u, s) = \frac{N\pi u^2}{\Delta x}e^{2\ln^2(s)} \quad (24)$$

where N is the total number of pores per unit weight kidney (or unit area for a membrane). Analogously, using Poiseuille's law, K_f is given by the following equation:

$$K_f = N\int_0^\infty \frac{\pi r^4}{8\eta\Delta x} g(r)\mathrm{d}r = \frac{N\pi}{8\eta\Delta x} G^4(u,s) = \frac{N\pi u^4}{8\eta\Delta x} e^{8\ln^2(s)} \quad (25)$$

If $A_0/\Delta x$ is known, N cancels so that

$$K_f = \frac{A_0}{\Delta x}\frac{u^2}{8\eta} e^{6\ln^2(s)} \quad (26)$$

With minor modifications of the proof of *Eq. 23* (see the APPENDIX), one can derive the following equation:

$$B^n(u,s,a_e) = \int_{a_e}^\infty r^n g(r)dr = \frac{1}{2}u^n e^{\frac{n^2\ln^2(s)}{2}}\left\{\mathrm{erf}\left[\frac{n\ln^2(s) - \ln\left(\frac{a_e}{u}\right)}{\sqrt{2}\ln(s)}\right] + 1\right\} \quad (27)$$

where erf is the error function. This thus makes it possible to solve both *Eqs. 14* and *15* completely for $\lambda \leq 0.95$, as follows:

$$\left(\frac{A}{A_0}\right) = \frac{\int_0^\infty r^2\left(\frac{A}{A_0}\right)g(r)\mathrm{d}r}{\int_0^\infty r^2 g(r)\mathrm{d}r} = \frac{\int_{a_e}^\infty r^2\left(\frac{A}{A_0}\right)g(r)\mathrm{d}r}{\int_0^\infty r^2 g(r)\mathrm{d}r}$$
$$= \left(B^2 + \frac{9}{16}a_e u\left(\ln\frac{a_e}{u} - \ln^2(s)\right)e^{\frac{\ln^2(s)}{2}}\left[1 - \mathrm{erf}\left(\frac{\ln\frac{a_e}{u} - \ln^2(s)}{\sqrt{2}\ln(s)}\right)\right] - \frac{9}{16}\sqrt{\frac{2}{\pi}}a_e^2\ln(s)e^{-\frac{1}{2}\left(\frac{\ln(u)-\ln(a_e)}{\ln(s)}\right)^2} - 1.56034a_eB^1 + 0.528155a_e^2B^0 + 1.91521a_e^3B^{-1} - 2.81903a_e^4B^{-2} + 0.270788a_e^5B^{-3} + 1.10115a_e^6B^{-4} - 0.435933a_e^7B^{-5}\right)/G^2 \quad (28)$$

Using *Eq. 28*, instead of approximating *Eqs. 14* and *15* numerically, reduced the computation time by ~50%. If the distribution spread is set to unity, then the above equations (*Eqs. 23–28*) reduce to those of the discrete two-pore model. Thus far, it seems as if the distributed two-pore model is identical to the discrete two-pore model when s tends to unity. All that remains is to show that *Eqs. 10* and *11* are equal to $\sigma_{h,S}$ and $\sigma_{h,L}$, respectively, when $s_S = s_L = 1$ and, in addition, that *Eqs. 14* and *15* reduce to the homoporous case also for $\lambda > 0.95$ (with the spread set to unity). This can be proven (see the APPENDIX) using the dominated convergence theorem (39) using the fact that both σ_h and A/A_0 are bounded functions. The improper integrals in the numerators of *Eqs. 10* and *11* (and *Eqs. 14* and *15* for $\lambda > 0.95$) were evaluated numerically using a 21-point Gauss-Kronrod quadrature. Numeric calculations were performed using the software package GNU Science Library (15).

Nonlinear regression. The theoretical sieving coefficients for each model were fitted to the experimental data (327 data points) using the nonlinear least-squares algorithm according to Levenberg and Marquardt to calculate the optimal values of u_S, s_S, u_L, s_L, $A_0/\Delta x$, and α_L that minimize the weighted sum of squares (objective function), as follows:

$$\sum_{j=1}^{n\text{points}} \frac{1}{\theta_{j,\text{data}}^2}\left(\theta_{j,\text{data}} - \theta_{j,\text{model}}\right)^2 \quad (29)$$

using the MINPACK library with standard settings (27). This objective function provided a better goodness of fit (lower χ^2) than using the ordinary sum of squares on log-transformed data. Because of the limited data for higher solute radii, the large-pore fit was dependent on the initial value (mainly of the large-pore spread s_L). Therefore, a large number of initial values were tried with s_L ranging from 1.10 to 1.50. From these results, the best fit (lowest χ^2-score) was selected (cf. also Ref. 11, where a similar method is used).

Statistical analysis. Parameter values are presented as means ± SE. A Pearson χ^2-test was used for testing the goodness of fit for the data fitted to the discrete and distributed two-pore models. Statistical differences between the different models (discrete; narrow spread: $s_S = 1.05$ and $s_L = 1.15$; wide spread: $s_S = 1.10$ and $s_L = 1.30$) were tested using a nonparametric Friedman test followed by post hoc testing using a Wilcoxon-Nemenyi-McDonald-Thompson test. Holm-Bonferroni corrections for multiple comparisons were made. Significance levels were set at $P < 0.05$, $P < 0.01$, and $P < 0.001$. All statistical calculations were made using the computer software R (version 3.0.0) for Linux.

RESULTS

Experimental data analysis. The optimal parameters for the distributed two-pore model analysis of the Ficoll data are shown in Table 1. The corresponding arithmetic parameters are $\mu_S = 36.9$ Å and $\sigma_S = 4.7$ Å for the small-pore system and $\mu_L = 106.6$ Å and $\sigma_L = 44.0$ Å for the large-pore system. L_pS was calculated from $A_0/\Delta x$ (per g kidney) in the distributed model using *Eq. 26*. A value for L_pS of 0.44 ml·min^{-1}·mmHg^{-1}·g^{-1} corresponds to a mean pressure gradient of only ~1.5 mmHg, which is very low compared with measured values (37). Figure 1 shows θ versus a_e for the experimental data (dashed line) and the best fit for the regression of the distributed two-pore model (solid line). The dotted line represents a simulated scenario where *1*) $A_0/\Delta x$ has been decreased to ~3×10^5 cm to match the θ value of myoglobin (the value of s_S has very little effect in this range of solute radii) and *2*) the spread of the small pore has been decreased to ~1.017 to match the sieving data for four different proteins [human myeloma dimeric κ-chain (κ-dimer, 28.4 Å), nHRP (30.4 Å), HSA (35.5 Å), and neutralized HSA (35.0 Å)] and all other parameters were set according to the best model fit for the Ficoll sieving data. The fractional clearances of the proteins are

Table 1. *Distributed two-pore parameters*

Model Parameter	Regression Result
u_S, Å	36.6 ± 0.3
s_S, Å	1.13 ± 0.00
u_L, Å	98.6 ± 4.2
s_L, Å	1.49 ± 0.03
$A_0/\Delta x$, $\times 10^{-5}$*	20.6 ± 2.1
L_pS, ml·min^{-1}·mmHg^{-1}*	0.44 ± 0.04
α_L, $\times 10^5$	0.6 ± 0.1
J_{vL}/GFR, $\times 10^5$	9.3 ± 1.2
$J_{vL,iso}$, μl/min*	0.06 ± 0.01
$A_{0,L}/A_0$, $\times 10^6$	0.4 ± 0.1
$A_{0,L}$, $\times 10^3$ mm^2	2.5 ± 0.0
GFR, ml/min*	0.65 ± 0.4
Goodness of fit, χ^2	0.147 ± 0.018

u_S, geometric mean small-pore radius; s_S, geometric small-pore SD; u_L, geometric mean large-pore radius; s_L, geometric large-pore SD; $A_0/\Delta x$, effective pore area over unit diffusion path length; L_pS, hydraulic conductance (calculated from $A_0/\Delta x$); α_L, fractional large-pore hydraulic conductance; J_{vL}, volume flux across the large-pore population; GFR, glomerular filtration rate; $J_{vL,iso}$, isogravimetric flux for the large-pore population; $A_{0,L}/A_0$, fractional large pore area; $A_{0,L}$, cross-sectional area for the large-pore pathway (calculated from $A_{0,L}/A_0$ and $A_0/\Delta x$ assuming a barrier thickness of 0.3 μm). *Gram kidney.

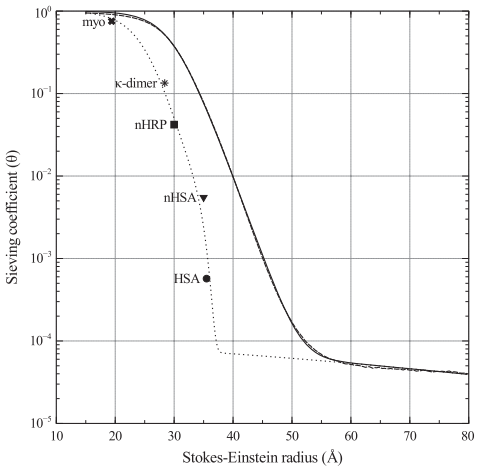

Fig. 1. Sieving coefficient (θ) versus Stokes-Einstein radius (a_e) for the experimental data (dashed line) and the best fit for the regression of the distributed two-pore model (solid line). The dotted line represents a simulated scenario were the small-pore spread (s_S) and $A_0/\Delta x$ have been decreased to match the sieving data for five different globular proteins (according to Lund et al. (24): myoglobin (myo; 19.4 Å), human myeloma dimeric κ-chain (κ-dimer; 28.4 Å), nHRP (30.4 Å), neutralized HSA (nHSA; 35.0 Å), and HSA (35.5 Å). See the *Glossary* for abbreviations.

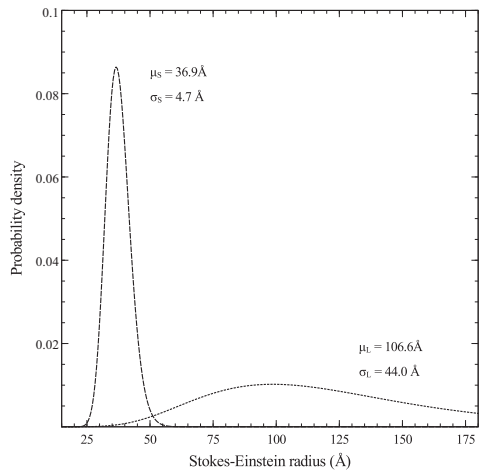

Fig. 2. The probability density function (cf. *Eq. 8*) for the small-pore (dashed line) and large-pore (dotted line) size distributions. The distributions are not to scale.

according to Lund et al. (24). Again, using *Eq. 26* to calculate L_pS from the "protein curve" yields a filtration coefficient of ~0.06 ml·min^{-1}·mmHg^{-1}·g^{-1}, corresponding to a mean pressure gradient of ~10 mmHg. In this simulated scenario, the corresponding arithmetic parameters are μ_S = 36.6 Å and σ_S = 0.6 Å for the small-pore pathway. The probability density functions (*Eq. 8*) for the small-pore (dashed line) and large-pore (dotted line) size distributions are shown in Fig. 2.

The data were reanalyzed using distributed two-pore models where s_S and s_L were set to constant values. Figure 3 shows θ versus a_e for this analysis. Along with the data (dotted line), three different scenarios are shown where the spread of the distributions have been held constant during the regression: s_S = 1.00 and s_L = 1.00 (dashed line), s_S = 1.05 and s_L = 1.15 (solid line), and s_S = 1.10 and s_L = 1.30 (dashed-dotted line). The knee region is expanded as the spread is decreased, leading to an increasingly poorer fit in this region, as has been previously noted using the classic two-pore-model (34). Interestingly, for the "wide" scenario (s_S = 1.10 and s_L = 1.30), a very low χ^2-value (0.086) was obtained. The optimized model parameters for the three different scenarios are shown in Table 2. As expected, as the spread of the model increases, both the small- and large-pore radius get smaller and $A_0/\Delta x$ gets larger for the widest scenario. No other significant differences among the three "fixed-spread" models were found. Despite the difference between $A_0/\Delta x$ in the groups, the fractional large-pore area remains relatively constant. $A_{0,L}/A_0$ is larger for the "constant-spread" models than that obtained in the full analysis above (~0.4 × 10^{-6}).

Theoretical analysis. Figure 4 shows the effect of altering the breadth of the distribution by plotting several different scenarios from the discrete case (s_S = 1.00 and s_L = 1.00, dotted line) to increasingly wider distributions (s_S = 1.05 and s_L = 1.15, dashed-dotted line; s_S = 1.10 and s_L = 1.30, dashed line; and s_S = 1.15 and s_L = 1.45, solid line). For the small-pore system, a more narrow distribution leads to a

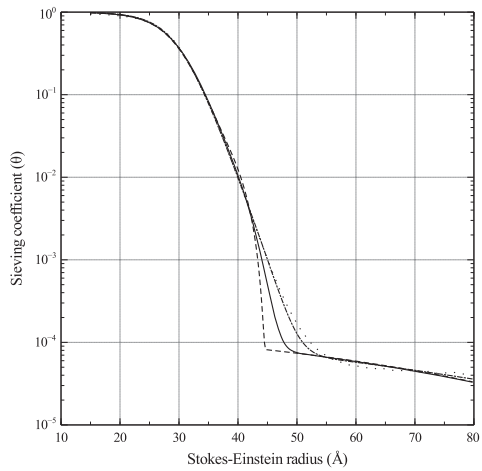

Fig. 3. Results of the analysis of the experimental data using constant values for the small-pore and large-pore spread parameters. Along with the data (dotted line), three different scenarios are plotted: s_S = 1.00 and s_L = 1.00 (dashed line), s_S = 1.05 and s_L = 1.15 (solid line), and s_S = 1.10 and s_L = 1.30 (dashed-dotted line). See the *Glossary* for abbreviations.

Table 2. *"Constant-spread" analysis parameters*

	Discrete (s_S = 1.00 and s_L = 1.00)	Narrow (s_S = 1.05 and s_L = 1.15)	Wide (s_S = 1.10 and s_L = 1.30)
u_S, Å	44.7 ± 0.1	43.3 ± 0.1‡	40.0 ± 0.1‡
u_L, Å	141.3 ± 7.0	128.0 ± 5.7	113.3 ± 7.9
$A_0/\Delta x$, $\times 10^{-5}$*	7.2 ± 0.5	7.1 ± 0.9†	11.5 ± 0.7†
L_pS, ml·min^{-1}·mmHg^{-1}*	0.21 ± 0.01	0.20 ± 0.02†	0.28 ± 0.01†
α_L, $\times 10^5$	1.7 ± 0.1	2.1 ± 0.1	1.3 ± 0.1
J_{vL}/GFR (f_L), $\times 10^5$	12.2 ± 0.1	13.6 ± 0.1	12.2 ± 0.1
$A_{0,L}/A_0$, $\times 10^6$	1.7 ± 0.2	2.3 ± 0.4	1.3 ± 0.3
$A_{0,L}$, $\times 10^3$ mm^2	3.7 ± 0.0	4.9 ± 0.4	4.5 ± 0.0
Goodness of fit, χ^2	0.257 ± 0.018	0.168 ± 0.03	0.086 ± 0.01‡

Values are given as mean ± SE. *Gram kidney. †$P < 0.05$; ‡$P < 0.01$.

steeper cutoff. As expected, with a wide distribution in the large-pore system, the selectivity approaches that of the shunted models (a horizontal line). It can also be seen that the transport of smaller solutes below 25 Å (such as VEGF and many other small peptide hormones) is largely unaffected by the width of the distribution of pore sizes.

To quantify the theoretical increase in $A_0/\Delta x$ due to an increased distribution spread, $A_0/\Delta x$ was plotted as a function of the distribution spread using *Eq. 24* (Fig. 5*A*). Similarly, Fig. 5*B* shows the GFR per gram kidney versus the distribution spread plotted using *Eq. 25* and assuming a net filtration pressure of 10 mmHg. N was set to 10^{18} pores/g, and u was set at 36.6 Å. When these theoretical predictions of the increase of $A_0/\Delta x$ and/or K_f, due to the distribution spread only are compared, it can be seen that the theoretical increase is much smaller than that obtained from the analysis of the experimental data (Table 2).

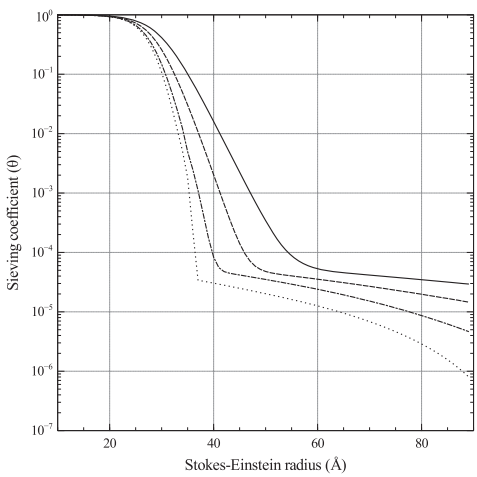

Fig. 4. Effects of altering the spread of the distribution. Several different scenarios are plotted, from the discrete case (s_S = 1.00 and s_L = 1.00, dotted line) to increasingly wider distributions (s_S = 1.05 and s_L = 1.15, dashed-dotted line; s_S = 1.10 and s_L = 1.30, dashed line; and s_S = 1.15 and s_L = 1.45, solid line). See the *Glossary* for abbreviations.

DISCUSSION

We have presented here an extended two-pore theory where the porous pathways are continuously distributed according to u_S and u_L and their corresponding s_S and s_L, thus considering effects caused by an apparent (or actual) distribution in pore sizes. The results of the data analysis revealed a small-pore population with a wide distribution in pore sizes having an arithmetic SD of ~5 Å. Such a wide pore size distribution, even when considering the electrostatic hindrance due to a negative pore charge (28), would not be consistent with the high selectivity to proteins normally characterizing the GFB (24, 34). To account for this contradiction, we hypothesize the following:

1. A large part of the variance in the distribution of pore sizes in the present analysis is due to the molecular flexibility of the Ficoll molecule, implying that the true variance of the pore system is lower than that obtained when using a flexible probe molecule.

2. The mean pore radius is near that of the true effective radius of the GFB, implying that the highly selective filtration barrier favors the filtration of Ficoll molecules having a "mean radius" close to the actual mean pore radius.

3. The inflation of $A_0/\Delta x$ (due to the wide distribution) can be explained, almost entirely, by the flexibility of the molecule (see below). Thus, the surface increase in distributed models compared with discrete models is due to the flexibility of the molecule, not the wide distribution of the pore population.

We have shown that the classic (discrete) two-pore model represents a special case of the distributed two-pore model where both s_S and s_L are set equal to unity. With the use of constant values for the spread parameters (s_S and s_L), our results revealed that a smaller distribution spread leads to a larger mean pore radius and a lower $A_0/\Delta x$ parameter. This result may be expected since *1*) the discrete small-pore radius is usually ~43–47 Å (2, 4, 5, 7, 28), whereas a common value for the mean pore radius of the log-normal + shunt model is only ~35–39 Å (5, 7, 34), and *2*) $A_0/\Delta x$ is typically two to three times higher in the distributed models than what is commonly found using the discrete two-pore model (5, 7, 34). Thus, in line with previous results, the data analysis in the present article yielded a high value for $A_0/\Delta x$ (~21×10^5 cm/g) for the distributed model, which leads to an unreasonably high value for L_pS (calculated from $A_0/\Delta x$). A more reasonable value (~3×10^5 cm/g) was obtained using a simulated scenario where the small-pore spread and $A_0/\Delta x$ were lowered to match the θ values of five proteins. We also derived a practical

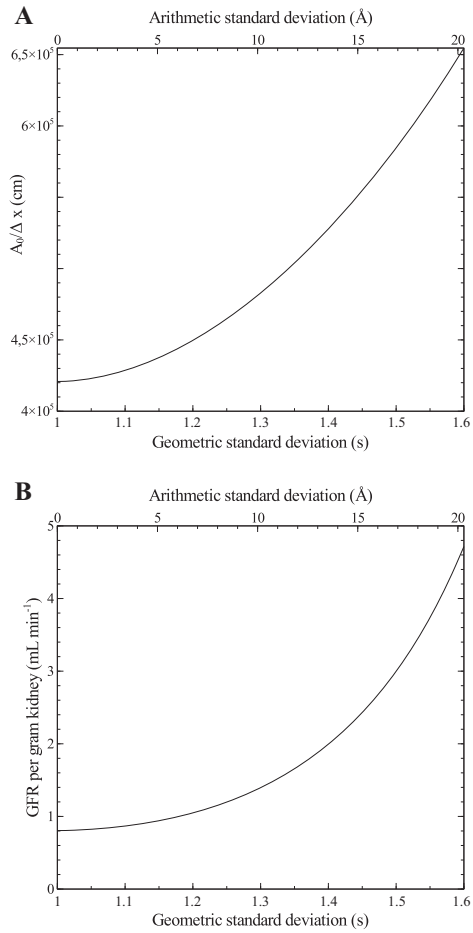

Fig. 5. *A*: $A_0/\Delta x$ (in cm) plotted as a function of s using *Eq. 24*. *B*: GFR (in ml/min) plotted as a function of s using *Eq. 25* and assuming a net filtration pressure of 10 mmHg. See the *Glossary* for abbreviations.

equation (see *Eq. 24*) showing that $A_0/\Delta x$ is, as expected, directly dependent on the pore size distribution (both spread and mean radius) so that an inflated distribution spread leads to inflation in $A_0/\Delta x$ as well. However, this theoretical increase in $A_0/\Delta x$ is much smaller than what could be expected from the measured differences between the discrete and distributed models. What is the reason behind the (often noted) inflated $A_0/\Delta x$ values in the distributed models? Interestingly, the larger pore radius for the discrete two-pore model (compared with the distributed model) leads to less restriction to the diffusive transport (i.e., larger A/A_0) in the small-pore system. As an example, for a 30-Å solute, the small-pore A/A_0 parameter is $\sim 2.4 \times 10^{-3}$ for the distributed two-pore model (using *Eq. 28* with $u = 36.6$ Å and $s = 1.13$) compared with $\sim 7.4 \times 10^{-3}$ for the discrete two-pore model (using *Eq. 28* with $u = 44.7$ Å and $s = 1.00$ or *Eq. 21*). This gives a factor of ~3 between the A/A_0 parameters of the distributed and discrete models, which is sufficient to explain (see *Eq. 4*) the discrepancy between the distributed and discrete two-pore models in this article. In conclusion, if the distribution in pore sizes is caused by the flexibility of the solute, then the increased area is apparent and does not reflect the real pore area of the membrane. Conversely, if there is an actual distribution in pore sizes, the ultrafiltration coefficient of the barrier, as calculated theoretically (from $A_0/\Delta x$ using *Eq. 26*), should more closely match the measured ultrafiltration coefficient.

The selective mechanisms of the GFB are based on the separation of molecular species depending on size, charge, and conformation. Recently, we quantified the electrostatic properties of the GFB in terms of the surface charge density of the barrier (in C/m^2) and found it to be similar to that of known surface charge densities for many proteins in the body (~5–20 mC/m^2) (28). This is a much lower value than that suggested by Haraldsson et al. (200 mC/m^2) (17). Indeed, the latter charge density would be required if most of the difference in the glomerular permeability between Ficoll and globular proteins were due to charge effects. If the wide distribution measured in the present investigation represents the actual pore size distribution in a weakly/moderately charged GFB (i.e., ~5–20 mC/m^2), then one would have to add ~15–19 Å to the effective radius of the albumin molecule to achieve the same fractional clearance as that actually measured. In contrast, if the distribution of pore sizes in the GFB is narrow, as is proposed in the present study, then a "threshold effect" is possible (due to the similarity of the mean small-pore radius, 36.6 Å, and molecular radius of albumin, 35.5 Å), so that even a moderate surface charge density on the barrier (similar to that on many plasma proteins) is sufficient exclude albumin from passing through the small-pore system. According to the hypothesis in this study, conformation plays a crucial part in how molecular species are transported across the GFB. As an example, bikunin, a 36-Å (radius) elongated protein, had ~80 times higher fractional clearance (θ) than albumin despite similar size and charge (23).

The GFB is a dynamic barrier in which the permeability can change dramatically even in a short period of time (2–5). The physiological and pathophysiological mechanisms behind the changes in permeability seem to be mediated primarily by the large-pore system. Despite the apparent role of the large-pore pathway in the regulation of the permeability of the GFB, very little is known about the underlying mechanisms or the equivalent biological structure. The permeability of the large-pore system is typically increased when the glomeruli are injured by disease [f_L (equal to J_{vL}/GFR) can increase several orders of magnitude within minutes]. In contrast to peripheral capillaries, the permeability of the large-pore system in glomerular capillaries is normally very low. This means that, in healthy glomerular capillaries, only very small amounts of large probe molecules are filtered into the urinary space, making direct measurement of the selectivity of the large-pore system difficult. Indeed, the value for the large-pore parameters in the present analysis should be interpreted carefully due to the limited range of the data in the large-pore region. In addition,

the large SD (~44 Å) may involve other factors than those suggested for the small-pore pathway above. For example, the data itself show their greatest variation in the large-pore portion of the sieving curve, which should contribute to the observed variance in the pore size distribution. It has been suggested that $Ficoll_{400}$ is more similar to a random coil than a hard sphere (13). In light of this, $Ficoll_{400}$ may be an inappropriate probe for measuring the size-selective properties of the large-pore system. On the other hand, if the hypothesis in this article is correct, as shown in Fig. 4 (and from the fact that large $Ficoll_{400}$ molecules have a similar θ value as that of HSA in Fanconi syndrome (37); see Fig. 1), f_L can be predicted with good accuracy using $Ficoll_{400}$.

What are the physiological and pathophysiological roles of the small-pore system? We (5) have recently reported measurements of glomerular permeability during systemic angiotensin II infusion in rats. The analysis (using the log-normal distributed + shunt model) showed that the width of the small-pore distribution was markedly increased (corresponding to an increase in σ_S from 4.9 to ~7–8 Å) when high doses of angiotensin II were administered. This increased heteroporosity of the small-pore system can also be seen in puromycin aminonucleoside nephrosis and is usually accompanied by a marked increase in the large-pore permeability (f_L) (18). Indeed, the widening of the small-pore distribution may be a general phenomenon, occurring after large increases in glomerular permeability. In addition, widening of the small-pore distribution (e.g., as shown in Figs. 3 and 4) may be a major pathophysiological mechanism in selective proteinuria.

The distributed pore model presented in the present article assumes a very simple structure of the glomerular capillary wall with two different size-selective modalities: small- and large-pore populations. If the experimental data were produced using this "equivalent" barrier (i.e., instead of the rat glomerulus), they would have the properties shown in Table 1. Given what is known about the actual structure of the glomerular capillary wall, the use of pores is obviously phenomenological. Nonetheless, pore theory is arguably the most popular paradigm for describing glomerular sieving and remains one of the simplest ways to model the transport of both solvent (as laminar flow) and solutes (using hydrodynamic restriction coefficients). In addition, since the model in the present article is based on established models and concepts, it is possible to directly compare new results with previous findings. Despite the differences in physical structure between the glomerular capillary wall and the distributed two-pore model, both the goodness-of-fit analysis and visual fit suggest that, in a functional sense, the barriers are remarkably similar.

The actual distribution of the size-selective structures in the GFB is not known. However, as shown in Fig. 1, over the course of just a few angstroms, the θ value (for proteins) was reduced ~200-fold from 0.13 (human myeloma κ-dimer, 28.4 Å) to 6×10^{-4} (HSA, 35.5 Å). Arguably, such an impressive cutoff is not consistent with a heteroselective small-pore pathway unless the size distribution of the selective elements (pores, fibers, slits, etc.) is very narrow. Thus, in the present investigation, a narrow distribution in the small-pore system ($s_S \approx 1.017$ and $u_S \approx 36.6$) matched the sieving data of five globular proteins, giving an estimated 95.5% confidence interval of 35.4–37.9 Å for the "real" pore radius, which has been estimated by Lund et al. (24) to be 37.4 Å. In comparison, the hydrodynamic (Stokes-Einstein) radius of HSA is ~35.5 Å. We (28) have previously reported that the electrostatic repulsion between the negative electric charge on the GFB and the anionic sites on the albumin molecule may add only a few angstroms to the apparent size of the albumin molecule. Indeed, if the estimate of the actual pore radius in this article is accurate, this means that albumin is effectively excluded from the small-pore pathway in healthy glomerular capillaries. In an ideal model for glomerular permeability, the GFR, as predicted by the solute flow, should match the measured GFR [thus resolving Pappenheimer's pore puzzle (29)]. In the present study, the measured GFR (0.65 $ml \cdot min^{-1} \cdot g^{-1}$) did not match theoretical GFRs (calculated from $GFR = L_pS \times \Delta P_{net}$) unless a very low ΔP_{net} is assumed. Lowering s_S and $A_0/\Delta x$, as in the protein sieving scenario, leads to a better match between the GFR as calculated from the solute flow and the measured GFR.

In summary, we have shown that the permeability of the GFB can be described by a distributed two-pore model, assuming that the size-selective structures of the glomerular capillary wall are log-normally distributed small-pore and large-pore populations. In the case of Ficoll, there seems to be *a distribution effect* related to the flexible structure of the molecule, since the wide distribution obtained is inconsistent with the high selectivity characterizing healthy glomerular capillaries. Furthermore, both $A_0/\Delta x$ and K_f are, as could be expected, directly dependent the pore size distribution (both spread and mean radius). Practical equations (*Eqs. 24–26*) for both of these entities have been proved analytically, eliminating the need for numeric approximations. These equations are by no means limited to a capillary wall but are actually a generalization of the Hagen-Poiseuille equation for any porous membrane with a log-normal distribution of pore sizes. We have also demonstrated that a smaller distribution spread leads to *1*) an increased mean pore radius and *2*) a decreased $A_0/\Delta x$. The latter effect is mainly due to the increased diffusive hindrance of the small-pore pathway in the distributed two-pore model leading to an inflation of $A_0/\Delta x$. Finally, we have shown that the classic (discrete) two-pore model is actually a special case of the distributed two-pore model where $s_S = s_L = 1.00$.

APPENDIX A

The Patlak equation. Define a function $h(c) = [J_v(1 - \sigma)c - J_s]/DA$. *Equation 1* can then be rewritten as follows:

$$\frac{dc}{dx} = h(c) \tag{30}$$

which can be integrated over the barrier, from the plasma concentration (C_p) to the interstitial concentration (C_i), as follows:

$$\int_{c_p}^{c_i} \frac{1}{h(c)} dc = \int_0^{\Delta x} dx \tag{31}$$

where Δx is the membrane thickness [i.e., $c(\Delta x) = C_i$]. The result of this integration is the following equation:

$$DA \frac{\ln\left|J_v(1-\sigma)c_i - J_s\right| - \ln\left|J_v(1-\sigma)c_p - J_s\right|}{J_v(1-\sigma)} = \Delta x \tag{32}$$

which can be rewritten as follows:

$$J_s = J_v(1-\sigma)\frac{c_p - c_i e^{-J_v(1-\sigma)\Delta x/DA}}{1 - e^{-J_v(1-\sigma)\Delta x/DA}}$$

Analytic solution. To find the primitive function of the integrand, we start by using the integration of parts:

$$F(r) = \int r^n g(r)\mathrm{d}r = \frac{1}{2} r^n \operatorname{erf}\left[\frac{\ln(r) - \ln(u)}{\sqrt{2}\ln(s)}\right] - \int \frac{1}{2} n r^{n-1} \operatorname{erf}\left[\frac{\ln(r) - \ln(u)}{\sqrt{2}\ln(s)}\right]\mathrm{d}r \quad (33)$$

The change of variables $R = \ln(r)$ gives the following equation:

$$\int \frac{1}{2} n r^{n-1} \operatorname{erf}\left[\frac{\ln(r) - \ln(u)}{\sqrt{2}\ln(s)}\right]\mathrm{d}r = \int \frac{1}{2} n e^{nR} \operatorname{erf}\left[\frac{R - \ln(u)}{\sqrt{2}\ln(s)}\right]\mathrm{d}R = \frac{1}{2} e^{\frac{1}{2}\left\{\left[\frac{\ln(u) + n\ln^2(s)}{\ln(s)}\right]^2 - \left[\frac{\ln(u)}{\ln(s)}\right]^2\right\}} \operatorname{erf}\left[\frac{R - \ln(u) - n\ln^2(s)}{\sqrt{2}\ln(s)}\right] - \frac{1}{2} e^{nR} \operatorname{erf}\left[\frac{R - \ln(u)}{\sqrt{2}\ln(s)}\right] \quad (34)$$

where erf is the error function. Inserting erf into *Eq. 33* gives the following equation:

$$F(r) = \frac{1}{2} e^{\frac{1}{2}\left\{\left[\frac{\ln(u) + n\ln^2(s)}{\ln(s)}\right]^2 - \left[\frac{\ln(u)}{\ln(s)}\right]^2\right\}} \operatorname{erf}\left[\frac{\ln(r) - \ln(u) - n\ln^2(s)}{\sqrt{2}\ln(s)}\right] \quad (35)$$

so that

$$G^n(u, s) = \int_0^\infty r^n g(r)dr = \lim_{r\to\infty} F(r) - \lim_{r\to 0} F(r) = e^{\frac{1}{2}\left\{\left[\frac{\ln(u) + n\ln^2(s)}{\ln(s)}\right]^2 - \left[\frac{\ln(u)}{\ln(s)}\right]^2\right\}} \quad (36)$$

which can be rearranged to the following equation:

$$G^n(u, s) = u^n e^{\frac{n^2\ln^2(s)}{2}} \quad (37)$$

When s tends to unity. Suppose $f(r)$ is an integrable real-valued bounded function. We wish to prove that

$$\lim_{s\to 1} \int_0^\infty \frac{e^{-\frac{1}{2}\left[\frac{\ln(r) - \ln(u)}{\ln(s)}\right]^2}}{r\ln(s)\sqrt{2\pi}} f(r)\mathrm{d}r = f(u) \quad (38)$$

The change of variables $X = k[\ln(r) - \ln(u)]$, where $k = 1/\ln(s)$, gives the following equation:

$$\lim_{s\to 1} \int_0^\infty \frac{e^{-\frac{1}{2}\left[\frac{\ln(r) - \ln(u)}{\ln(s)}\right]^2}}{r\ln(s)\sqrt{2\pi}} f(r)\mathrm{d}r = \lim_{k\to\infty} \int_{-\infty}^\infty \frac{e^{-\frac{1}{2}X^2}}{\sqrt{2\pi}} f(ue^{X/k})\mathrm{d}X \quad (39)$$

Since $f(r)$ is bounded, there is a real number (m) such that

$$\left|\frac{e^{-\frac{1}{2}X^2}}{\sqrt{2\pi}} f(ue^{X/k})\right| \le \frac{m}{\sqrt{2\pi}} \quad (40)$$

for all k and all X. Under these conditions, the dominated convergence theorem (39) is applicable so that the limit may be taken under the integral sign, as follows:

$$\lim_{k\to\infty} \int_{-\infty}^\infty \frac{e^{-\frac{1}{2}X^2}}{\sqrt{2\pi}} f(ue^{X/k})\,\mathrm{d}X = \int_{-\infty}^\infty \lim_{k\to\infty} \frac{e^{-\frac{1}{2}X^2}}{\sqrt{2\pi}} f(ue^{X/k})\,\mathrm{d}X = f(u) \quad (41)$$

ACKNOWLEDGMENTS

The authors gratefully thank Josefin Axelsson for generously providing the Ficoll sieving data and Kerstin Wihlborg for expert secretarial assistance. The authors also thank Fredrik Nilsson (Unit of Medical Statistics and Epidemiology, Region Skåne) for valuable advice.

GRANTS

This work was supported by Swedish Research Council Grant 08285, the Heart and Lung Foundation, and the Medical Faculty at Lund University (ALF Grant).

DISCLOSURES

No conflicts of interest, financial or otherwise, are declared by the author(s).

AUTHOR CONTRIBUTIONS

Author contributions: C.M.Ö. and B.R. conception and design of research; C.M.Ö. analyzed data; C.M.Ö. and B.R. interpreted results of experiments; C.M.Ö. prepared figures; C.M.Ö. drafted manuscript; C.M.Ö. and B.R. edited and revised manuscript; C.M.Ö. and B.R. approved final version of manuscript.

REFERENCES

1. **Arturson G, Groth T, Grotte G.** Human glomerular membrane porosity and filtration pressure: dextran clearance data analysed by theoretical models. *Clin Sci* 40: 137–158, 1971.
2. **Axelsson J, Mahmutovic I, Rippe A, Rippe B.** Loss of size selectivity of the glomerular filtration barrier in rats following laparotomy and muscle trauma. *Am J Physiol Renal Physiol* 297: F577–F582, 2009.
3. **Axelsson J, Rippe A, Rippe B.** Transient and sustained increases in glomerular permeability following ANP infusion in rats. *Am J Physiol Renal Physiol* 300: F24–F30, 2011.
4. **Axelsson J, Rippe A, Venturoli D, Sward P, Rippe B.** Effects of early endotoxemia and dextran-induced anaphylaxis on the size selectivity of the glomerular filtration barrier in rats. *Am J Physiol Renal Physiol* 296: F242–F248, 2009.
5. **Axelsson J, Rippe A, Öberg CM, Rippe B.** Rapid, dynamic changes in glomerular permeability to macromolecules during systemic angiotensin II (ANG II) infusion in rats. *Am J Physiol Renal Physiol* 303: F790–F799, 2012.
6. **Axelsson J, Sverrisson K, Rippe A, Fissell W, Rippe B.** Reduced diffusion of charge-modified, conformationally intact anionic Ficoll relative to neutral Ficoll across the rat glomerular filtration barrier in vivo. *Am J Physiol Renal Physiol* 301: F708–F712, 2011.
7. **Axelsson J, Öberg CM, Rippe A, Krause B, Rippe B.** Size-selectivity of a synthetic high-flux and a high cut-off dialyzing membrane compared to that of the rat glomerular filtration barrier. *J Membr Sci* 413–414: 29–37, 2012.
8. **Bark BP, Öberg CM, Grände PO.** Plasma volume expansion by 0.9% NaCl during sepsis/SIRS, after hemorrhage, and during a normal state. *Shock* 40: 59–64, 2013.
9. **Blouch K, Deen WM, Fauvel JP, Bialek J, Derby G, Myers BD.** Molecular configuration and glomerular size selectivity in healthy and nephrotic humans. *Am J Physiol Renal Physiol* 273: F430–F437, 1997.
10. **Dechadilok P, Deen WM.** Hindrance factors for diffusion and convection in pores. *Ind Eng Chem Res* 45: 6953–6959, 2006.
11. **Deen WM, Bridges CR, Brenner BM, Myers BD.** Heteroporous model of glomerular size selectivity: application to normal and nephrotic humans. *Am J Physiol Renal Physiol* 249: F374–F389, 1985.
12. **Ennis J, Zhang H, Stevens G, Perera J, Scales P, Carnie S.** Mobility of protein through a porous membrane. *J Membr Sci* 119: 47–58, 1996.
13. **Fissell WH, Hofmann CL, Smith R, Chen MH.** Size and conformation of Ficoll as determined by size-exclusion chromatography followed by multiangle light scattering. *Am J Physiol Renal Physiol* 298: F205–F208, 2010.
14. **Fissell WH, Manley S, Dubnisheva A, Glass J, Magistrelli J, Eldridge AN, Fleischman AJ, Zydney AL, Roy S.** Ficoll is not a rigid sphere. *Am J Physiol Renal Physiol* 293: F1209–F1213, 2007.
15. **Galassi M.** *GNU Scientific Library Reference Manual* (3rd ed.). Bristol, UK: Network Theory, 2009.
16. **Georgalis Y, Philipp M, Aleksandrova R, Kruger JK.** Light scattering studies on Ficoll PM70 solutions reveal two distinct diffusive modes. *J Colloid Interface Sci* 386: 141–147, 2012.
17. **Haraldsson B, Nystrom J, Deen WM.** Properties of the glomerular barrier and mechanisms of proteinuria. *Physiol Rev* 88: 451–487, 2008.
18. **Hjalmarsson C, Ohlson M, Haraldsson B.** Puromycin aminonucleoside damages the glomerular size barrier with minimal effects on charge density. *Am J Physiol Renal Physiol* 281: F503–F512, 2001.

19. **Ibrahim R, Nitsche JM, Kasting GB.** Dermal clearance model for epidermal bioavailability calculations. *J Pharm Sci* 101: 2094–2108, 2012.
20. **Jeansson M, Haraldsson B.** Glomerular size and charge selectivity in the mouse after exposure to glucosaminoglycan-degrading enzymes. *J Am Soc Nephrol* 14: 1756–1765, 2003.
21. **Lambert PP, Verniory A, Gassee JP, Ficheroulle P.** Sieving equations and effective glomerular filtration pressure. *Kidney Int* 2: 131–146, 1972.
22. **Limpert E, Stahel WA, Abbt M.** Log-normal distributions across the sciences: keys and clues. *Bioscience* 51: 341–352, 2001.
23. **Lindstrom KE, Blom A, Johnsson E, Haraldsson B, Fries E.** High glomerular permeability of bikunin despite similarity in charge and hydrodynamic size to serum albumin. *Kidney Int* 51: 1053–1058, 1997.
24. **Lund U, Rippe A, Venturoli D, Tenstad O, Grubb A, Rippe B.** Glomerular filtration rate dependence of sieving of albumin and some neutral proteins in rat kidneys. *Am J Physiol Renal Physiol* 284: F1226–F1234, 2003.
25. **Mavrovouniotis GM, Brenner H.** Hindered sedimentation, diffusion, and dispersion coefficients for brownian spheres in circular cylindrical pores. *J Colloid Interface Sci* 124: 269–283, 1988.
26. **Miller NE, Michel CC, Nanjee MN, Olszewski WL, Miller IP, Hazell M, Olivecrona G, Sutton P, Humphreys SM, Frayn KN.** Secretion of adipokines by human adipose tissue in vivo: partitioning between capillary and lymphatic transport. *Am J Physiol Endocrinol Metab* 301: E659–E667, 2011.
27. **Moré J, Garbow B, Hillström K.** *User Guide for MINPACK-1. Argonne National Laboratiry Report ANL-80-74*. Argonne, IL: Argonne National Laboratory, 1980.
28. **Öberg CM, Rippe B.** Quantification of the electrostatic properties of the glomerular filtration barrier modeled as a charged fiber matrix separating anionic from neutral Ficoll. *Am J Physiol Renal Physiol* 304: F781–F787, 2013.
29. **Pappenheimer J.** Osmotic reflection coefficients in capillary membranes. In: *Capillary Permeability, Second Alfred Benzon Symposium*, edited by Crone c, Lassen NA. Copenhagen: Munksgaard, 1970, p. 278–286.
30. **Patlak CS, Goldstein DA, Hoffman JF.** The flow of solute and solvent across a two-membrane system. *J Theor Biol* 5: 426–442, 1963.
31. **Rippe B, Davies S.** Permeability of peritoneal and glomerular capillaries: what are the differences according to pore theory? *Perit Dial Int* 31: 249–258, 2011.
32. **Rippe B, Haraldsson B.** Fluid and protein fluxes across small and large pores in the microvasculature. Application of two-pore equations. *Acta Physiol Scand* 131: 411–428, 1987.
33. **Rippe B, Haraldsson B.** Transport of macromolecules across microvascular walls: the two-pore theory. *Physiol Rev* 74: 163–219, 1994.
34. **Rippe C, Asgeirsson D, Venturoli D, Rippe A, Rippe B.** Effects of glomerular filtration rate on Ficoll sieving coefficients (theta) in rats. *Kidney Int* 69: 1326–1332, 2006.
35. **Taylor AE, Granger DN.** Exchange of macromolecules across the microcirculation. *Handbook of Physiology. The Cardiovascular System. Microcirculation* Bethesda, MD: Am. Physiol. Soc., 1984, sect. 2, vol. IV, pt. 1, chapt. 11, p. 467–520.
36. **Tencer J, Frick IM, Oquist BW, Alm P, Rippe B.** Size-selectivity of the glomerular barrier to high molecular weight proteins: upper size limitations of shunt pathways. *Kidney Int* 53: 709–715, 1998.
37. **Thomson SC, Blantz RC.** Biophysical basis of glomerular filtration. In: *The Kidney: Physiology and Pathophysiology*, edited by Alpern R and Hebert S. Burlington, VT. Elsevier/Academic, 2007, p. 565–588.
38. **Venturoli D, Rippe B.** Ficoll and dextran vs. globular proteins as probes for testing glomerular permselectivity: effects of molecular size, shape, charge, and deformability. *Am J Physiol Renal Physiol* 288: F605–F613, 2005.
39. **Zemanian AH.** *Distribution Theory and Transform Analysis: an Introduction to Generalized Functions, With Applications*. Mineola, NY: Courier Dover, 1965.
40. **Zydney AL, Aimar P, Meireles M, Pimbley JM, Belfort G.** Use of the log-normal probability density function to analyze membrane pore size distributions: functional forms and discrepancies. *J Membr Sci* 91: 293–298, 1994.

Study III

A distributed solute model: an extended two-pore model with application to the glomerular sieving of Ficoll

Carl M. Öberg[1], Joseph J. Groszek[2], Shuvo Roy[2], William H. Fissell[2] and Bengt Rippe[1]

[1] Department of Nephrology, University Hospital of Lund, Lund University, Lund, Sweden

[2] Nephrology and Hypertension, Vanderbilt University, Nashville, Tennessee, USA

Correspondence: Carl M. Öberg

Department of Nephrology

University Hospital of Lund

S-211 85 Lund, Sweden

Phone: +46-709-221947

E-mail: carl.oberg@med.lu.se

ABSTRACT

One of the many unresolved questions regarding the permeability of the glomerular filtration barrier (GFB) is the reason behind the marked difference in permeability between albumin and polysaccharide probe molecules such as Ficoll and Dextran. The difference in sieving coefficients between albumin and a Ficoll molecule of the same molecular radius (~36 Å) is ~2-3 orders of magnitude. Although this large difference in permeability has been attributed mainly to charge effects, we have previously shown that this would require a supraphysiological amount of charge on the filtration barrier, being about ~10 times more than the charge on the albumin molecule (~0.02 C/m²). The classic heteroporous model by Deen, Bridges, Brenner and Myers (Deen et al, AJP Renal Physiology, 1985) was extended by introducing size distributions on the solute molecules, making them flexible in their conformation. Experimental sieving data for Ficoll, both from the rat glomerulus and from precision-made nanopore membranes, were analyzed using the extended model. The variation in solute size was quantified in terms of the geometric standard deviation (gSD) of the solute size distribution. The barrier was quantified in terms of a small and large pore radii, diffusive area parameter ($A_0/\Delta x$) and fractional conductance through large pores (aL). For the rat glomerulus (n=7) a small pore radius of 36.2 Å ± 0.1 Å and a gSD for the Ficoll size-distribution of 1.16 ± 0.01 was obtained. For the nanopore membranes (n=16), a gSD of 1.24 (± 0.01) and a small-pore radius of 43 ± 2 was found. In the current study, we show, for the first time, that a variation of only ~16% in the size of the polysaccharide molecule is sufficient to explain the marked difference in permeability between albumin and Ficoll. In addition, we show that the effects of applying a size-distribution on the solute molecule are only evident when the molecular size is close to the size of the selective elements of the barrier. This is in line with experimental data both from the human glomerulus and from synthetic membranes. However, it is reasonable to assume that there is at least some variation in the pore radii and, thus, the gSD obtained in the current study is likely an overestimation of the "true" variation in the size of the Ficoll molecule.

KEYWORDS: Heteroporous model, Sieving coefficient

GLOSSARY

$C_i(y)$	Solute (Ficoll) concentration at point y along the GC
$C_{pr}(y)$	Plasma protein concentration at point y along the GC
D	Distributed diffusion coefficient (cm^2/min)
D_∞	Free diffusion coefficient (cm^2/min)
EVF	Erytrocyte volume fraction (Hematocrit)
FC	Fractional clearance (Clearance/GFR)
FF	Filtration fraction (GFR/RPF)
f_L	Fractional large pore volume flow ($1-f_S$)
f_S	Fractional small pore volume flow ($1-f_L$)
G(r)	Solute size distribution (probability density function)
GC	Glomerular capillary
GFB	Glomerular filtration barrier
gSD	Geometrical standard deviation (distribution spread)
HES	Hydroxy ethyl starch
HSA	Human serum albumin
$J_s(y)$	Trans-glomerular solute flux at point y along the GC
$J_v(y)$	Trans-glomerular volume flux at point y along the GC
K_f	Ultrafiltration coefficient (same as LpS)
L	Length of the GC
LpS	Hydraulic conductance of the GFB
MAP	Mean arterial pressure
$\pi(y)$	Oncotic pressure at point y along the GC
P_c	Hydrostatic pressure at the afferent end of the GC (45 mmHg)

$P_{drop}(y)$	Hydrostatic pressure drop at point y along the GC (mmHg)
Pe_L	Solute Péclet number for the large-pore system
Pe_S	Solute Péclet number for the small-pore system
P_i	Hydrostatic pressure in Bowmans' space (10 mmHg)
π_i	Oncotic pressure in Bowman's space (~0 mmHg)
PS_L	Solute diffusion capacity for the large-pore system
PS_S	Solute diffusion capacity for the small-pore system
Q(y)	Renal plasma flow at the point y along the GC
R_A	Afferent glomerular vascular resistance
R_{GFB}	Hydraulic resistance of the GFB = $1/K_f$
RPF	Renal plasma flow (mL/min)
σ_L	Reflection coefficient for the small-pore system
SNGFR	Single nephron GFR
SNKf	Single nephron hydraulic conductance
σ_S	Reflection coefficient for the small-pore system
VEGF	Vascular endothelial growth factor
x	Position across the GFB
y	Non-dimensionalized distance along the GC (Y/L)
Y	Position along GC
Å	1/10 of a nanometre

INTRODUCTION

Much of our knowledge about the permeability of the glomerular filtration barrier (GFB) is derived from experimental studies of the fractional clearance ($FC=Cl_{marker}/GFR$) of polysaccharides such as Dextran [1, 29, 33], Polyvinylpyrrolidone [35], Polyethyleneoxide [1], HES [29], Pullulan [1] and Ficoll [7, 26]. Such studies, along with studies of the FC of endogenous proteins [22, 32], have established

1) the presence of at least two different trans-vascular pathways in the GFB [7, 13, 22, 32] and
2) a seemingly systematic difference in FC between different marker molecules (polysaccharides and plasma proteins) of the same hydrodynamic (Stokes-Einstein) radius [1, 7, 34].

The exact mechanisms behind these observations remain unknown despite decades of research. For example, the difference in FC (usually assumed to be equal to the glomerular sieving coefficient, GSC or θ) between anionic human serum albumin (HSA) and Ficoll of the same hydrodynamic radius (~36 Å) is typically 2-3 orders of magnitude. The difference between Dextran and HSA is even greater [7]. Thus, polysaccharides appear to be hyperpermeable with respect to a protein having the same apparent diffusion coefficient (SE-radius). Furthermore, this hyperpermeability appears to be systematic and correlate with the intrinsic viscosity of the solute [1]. These differences have been ascribed to charge effects [19] as well as an effect of conformation or structure of the molecular species [1, 34].

In the words of Homer Smith: the actual value of the renal clearance of a particular substance reveals nothing about the physiological mechanisms by which it is excreted [30]. Surely, several mechanisms within the kidney can vary the FC to a value between 4-5 (i.e. FF^{-1}, e.g. para-aminohippuric acid), 1 (inulin) and ~10^{-4} (HSA) and even lower. The current view of a highly charge-selective GFB is based on the the pioneering experiments using negatively charged sulfated Dextran to measure charge-selectivity in the GFB [8, 11]. It was later discovered [18, 29] that a portion of the sulfated Dextran

was bound to plasma proteins. Such binding can be expected to be in equilibrium with the surrounding blood plasma concentration and thus, when a small sample is diluted with water or buffer, a large portion of the bound marker will be released into the buffer solution. Notably, even for small Dextran molecules (~18Å) which are not sieved by the GFB, Chang et al [11] found a low FC of ~0.6 which is difficult to reconcile with the traditional concept of charge-selectivity accomplished by adding a few angstroms (a percentage of the Debye length) to the small-pore radius. Conceivably, such a low value indicates that at least a third of the sulfated Dextran marker was bound to proteins in these experiments. It should also however be noted that differently sized Dextran molecules show different degrees of binding [18]. Such protein binding has two effects on the observed FC of a substance. First, a lower FC than that of a neutral (non-bound) solute during normoproteinuric conditions will be observed and, second, during proteinuric conditions, the FC will increase, resulting in an apparent 'loss of charge selectivity'. Such problems are likely dependent on the type of charge modification used. For example, Schaeffer and colleagues found no difference in the FC between fluorescent negatively charged non-sulfated and neutral Dextran in the rat [29]. Similarly, results from our group showed only small differences in FC between anionic and neutral Ficoll [5]. Thus, when using non-sulfated anionic polysaccharides as probe molecules, the charge-selectivity of the GFB is apparently small and cannot explain the observed difference in permeability between proteins and polysaccharides in the GFB.

There seems to be agreement that the glomerular sieving coefficient equals unity ($\theta \approx 1$) for solutes smaller than ~15 Å, i.e. having a radius close to that of Inulin (~13Å). Thus solutes < 15Å are not sieved at all by the glomerular barrier. This implies that any size distribution in the size-selective structures of the GFB would either have to be narrow (so that the number of smaller pores that could sieve smaller molecules is small) or that the distribution is strongly skewed towards higher molecular radii. However, a membrane having a strongly skewed distribution towards higher pore radii could not be highly selective for solutes close to the pore radius. By contrast, many studies using distributed pore models have rather consistently found a narrow distribution for the 'small-pore' population of

pores [13, 24]. In this article we derive a modification of the classical model by Deen, Bridges, Brenner and Myers from 1985 to describe both the bi-selective two-pore nature of the GFB and the behavior of a flexible spherical solute molecule. We introduce a theoretical construction of a distributed solute sphere, having a size that is described by a statistical distribution instead of using a fixed solid sphere radius. Such a size distribution can be expected to be a result both of the conformation and structure of the solute molecule. However, no attempt is made in the current article to distinguish between these two different phenomena. Indeed, for a polydisperse random coil polysaccharide molecule such as Dextran, these two effects may be very difficult to analyze separately in an experimental setting. We show that this model gives almost identical results compared to using a model with a distributed pore size [5] when analyzing experimental sieving data from the rat glomerulus. In addition, Ficoll sieving data from precision-made nanopore membranes were analyzed using the novel model.

MODEL DEVELOPMENT

This section begins with a summary of the model originally developed by Deen, Bridges, Brenner and Myers [13] which has here been extended to include the effects of a 'flexible' solute molecule whose size is described by a statistical distribution rather than, as in previous models, having a fixed solute radius. Several of the differential equations are non-linear and must be evaluated using numerical techniques which, for the sake of clarity, have been moved to an appendix. The entire glomerulus is here represented by an idealized single capillary connected to the circulation via two resistances, an afferent resistance R_A and efferent resistance R_E, such that the effective average filtration pressure along the capillary is 10 mmHg. In other words, it is assumed that the renal autoregulatory mechanisms uphold a constant average filtration pressure under normal conditions and that the hydraulic conductance of the capillary wall is constant along its length and is given by SNKf=SNGFR/10 mmHg. The validity of the model is tested by analyzing the sieving of neutral Ficoll in an experimental rat model [5]. An entire rat kidney is modelled as having ~35000 such ideal capillaries in parallel. The spherical symmetry of the idealized glomerular capillary allows us to reduce the model to the case of two spatial variables: *x* in the direction of solute and volume flow and *y* in the direction of the blood flow. Moreover, the GFB is considered to be a homogenous porous membrane having two different pore-size populations and all transport phenomena are assumed to be in a steady-state (i.e. time-dependent changes are not considered).

Fundamental Equations of Glomerular Transport

Volumetric flux

Conservation of mass is assumed, meaning that the mass (the water and solute matter) that enters the glomerulus must either leave the glomerulus via the efferent capillary or be ultrafiltrated through the

GFB. Thus it is assumed that neither water nor the solutes considered in this article accumulate or degrade within the glomerulus. In other words, the change in renal plasma flow along the idealized glomerular capillary d*Q(y)/dy* must be exactly equal to the loss of volume due to glomerular filtration

$$\frac{dQ}{dy} = -J_v(y) \quad (1)$$

As can be seen, this equation requires knowledge of the volume flux $J_v(y)$ in mL/min at every point *y* along the glomerular capillary. For simplicity, the position along the capillary y has been normalized to the total capillary length, y∈[0,1], so that y=0 represents the afferent end of the capillary and y=1 represents the efferent end. Moreover, $J_v(y)$ can be expected to decrease with increasing y as the pressure drops along the capillary and, also, as the protein content of the plasma remaining inside the glomerular capillary will increase as water is lost to the capsular space. This can be expressed using the a modified version of the Starling equilibrium

$$J_v(y) = K_f\big([P_c - P_{drop}(y) - P_i] - [\pi(y) - \pi_i]\big) \quad (2)$$

According to this equation the volume flux at point y in the capillary is a result of the difference between the capillary pressure P_c, the capsular pressure P_i, the hydrostatic pressure drop along the capillary $P_{drop}(y)$ and the oncotic pressures in the plasma π(y) and in Bowman's space π_i. For all practical purposes π_i can safely be assumed to be zero, even during heavy proteinuria. The oncotic pressure in plasma π(y) can be calculated using the well-known empirical equation by Landis and Pappenheimer from 1963 but first we need to know the protein concentration at any point *y*. Since the glomerular filtrate is virtually a protein-free liquid, the plasma protein *content* $Q(y)\cdot C_{pr}$ is assumed not to change along the capillary and thus

$$\frac{d(QC_{pr})}{dy} = \frac{dQ}{dy}C_{pr} + Q\frac{dC_{pr}}{dy} = 0 \quad (3)$$

or stated differently

$$Q(y)C_{pr}(y) = Q(0)C_{pr}(0) \quad (4)$$

where Q(0) is the RPF and Cpr(0) is the protein concentration at the afferent end of the glomerular capillary. Re-arranging the above equations gives

$$\frac{dQ}{dy} = -\frac{Q(0)C_{pr}(0)}{C_{pr}^2}\frac{dC_{pr}}{dy} \quad (5)$$

Now we can apply the Landis-Pappenheimer equation at each point *y*

$$\pi(y) = a_1 C_{pr}(y) + a_2 C_{pr}^2(y) \quad (6)$$

where a_1 = 0.1629 mmHg/(g/L) and a_2 = 0. 02935 mmHg/(g/L). It is here assumed that the small amounts of Ficoll administered make a negligible contribution to the osmotic pressure. By combining equation 1, 2, 5 and 6 we can now construct a single ordinary differential equation for the protein concentration along the GC

$$\frac{dC_{pr}}{dy} = K_f \frac{C_{pr}^2}{Q(0)C_{pr}(0)}\left([P_c - P_{drop}(y) - P_i] - [a_1 C_{pr} + a_2 C_{pr}^2]\right) \quad (7)$$

The total plasma protein concentration at the afferent end $C_{pr}(0)$ was assumed to be 57 g/L for a healthy Wistar rat, P_c and P_i was assumed to be 55 mmHg and 10 mmHg respectively, and a net pressure drop of 0.7 mmHg along the glomerular capillary was assumed

$$P_{drop}(y) = 0.7y \quad (8)$$

In lack of actual measurements (using for example paraaminohippuric acid), the RPF had to be calculated using equation 7 by fixed point iteration (see appendix). The glomerular vascular resistances can now be calculated as

$$R_A = \frac{MAP - P_c}{RPF}(1 - EVF) \quad (9)$$

$$R_{GFB} = \frac{1}{K_f} \quad (10)$$

Since the post-glomerular pressure is not known, a value for R_E could not be calculated.

Solute flux

Similar to the volume flux, conservation of mass gives us the equation

$$\frac{d(QC_i)}{dy} = \frac{dQ}{dy}C_i + Q\frac{dC_i}{dy} = -J_s(y) \quad (11)$$

where $J_s(y)$ is the solute flux in mmol/min and $C_i(y)$ is the plasma water concentration of the solute i, both at position *y* in the GC. Using equation 1, we can rearrange this equation to

$$\frac{dC_i}{dy} = -\frac{J_s(y) - J_v(y)C_i}{Q(y)} \quad (12)$$

The local solute flux was calculated from two-pore equations

$$J_s(y) = f_S J_v(y)\frac{C_i(1-\sigma_S)}{1-\sigma_S e^{-Pe_S}} + f_L J_v(y)\frac{C_i(1-\sigma_L)}{1-\sigma_L e^{-Pe_L}} \quad (13)$$

where f_S and f_L are the fractional small- and large-pore volume fluxes, respectively. Equation 13 is valid for unidirectional transport only, i.e. when $J_s(y)=J_v \cdot C_b$ where C_b is the downstream Bowman's space solute concentration (c.f. also eq 6 in [24]). However, bi-directional solute transport can be calculated using a bi-directional flux equation (cf. eq 2 in [9]). For example, VEGF produced by podocytes is transported in a 'counter-flow' fashion back to the endothelium demonstrating the relative superiority of diffusive transport over convective transport in GFB. Thus, the flow of the glomerular permeate can be likened to that of a slow flowing river and small substances can diffuse bi-directionally as long as there is a concentration gradient due to the high diffusion capacities of small solutes. However, in the current case of a marker molecule (Ficoll), there is no need for a bi-directional flux equation.

The distributed solute sphere

The free diffusion coefficient of the distributed solute sphere can be calculated from

$$D = \int_0^\infty D_\infty(r)G(r)dr \quad (14)$$

where G is a statistical distribution (a probability density function) of solute-sizes and $D_\infty(R)$ is the free diffusion coefficient calculated from the Einstein relation

$$D_\infty(R) = \frac{kT}{6\pi\eta R} \quad (15)$$

Here k is the Boltzmann constant, T is the body temperature (310°K), R is the solute hydrodynamic radius and η is the viscosity of water (~0.7 mPa·s). In other words it is assumed that the solute molecule has a hydrodynamic radius that can be described by a statistical distribution G(r). A useful distribution is the discrete distribution of n solute sizes

$$G(r) = \sum_{i=1}^{n} w_j \delta(r - R_j) \quad (16)$$

where w_j is the fractional amount ($\sum_{j=1}^{n} w_j = 1$) of the solute size R_j and δ(z) is the Dirac delta function. For example, for a molecule that has a symmetrical discrete size-distribution (w_1,R_1)=(0.2, 25Å), (w_2,R_2)=(0.6, 35Å) (w_3,R_3)=(0.2, 45Å) the diffusion coefficient can be calculated from $D=0.2D_1+0.6D_2+0.2D_3$ – giving a D_2/D-ratio (or 'frictional ratio') of ~0.95. Thus this discretely distributed solute with mean radius 35Å has a slightly higher diffusion coefficient than a 35Å rigid sphere.

In the current article we have chosen to use the log-normal (LN) distribution. This distribution is a nearly symmetrical distribution that is slightly skewed towards higher solute radii and is defined only for positive radii. The LN probability density function is

$$g(R, a_e, gSD) = \frac{e^{-\frac{1}{2}\left(\frac{ln(r)-ln(a_e)}{ln(gSD)}\right)^2}}{R\, ln(gSD)\, \sqrt{2\pi}} \quad (17)$$

Here *u* is the average solute radius and *gSD* is the geometrical standard deviation. Using the analytical solution from [24] (cf. equation 37), the diffusion coefficient for the distributed solute sphere can now be written

$$D = \frac{kT}{6\pi\eta R} e^{\frac{ln^2(gSD)}{2}} \quad (18)$$

Thus, the diffusion coefficient is slightly *larger* for a LN-distributed molecule (s > 1) than that of a solid sphere (s=1) having radius *R*. However, the differences in the free diffusion coefficient between a rigid- and a LN-distributed sphere are small even for high values of *gSD*, being only a few percent. Such small deviations cannot explain why the restricted diffusion of Dextran has been found to greatly exceed the theoretically expected value [9] (i.e. that calculated from the Renkin equation) for a rigid sphere. As we will see, the differences in transport between the rigid and the distributed solute sphere are much larger when considering hindered transport.

Hindered transport

The small- and large-pore reflection coefficients (σ_S and σ_L) were calculated assuming log-normal distributed solute sizes (a_e)

$$\sigma_S(a_e) = \int_0^\infty g(R, a_e, gSD)\sigma_{h,S}(R)dR \quad (19)$$

$$\sigma_L(a_e) = \int_0^\infty g(R, a_e, gSD)\sigma_{h,L}(R)dR \quad (20)$$

and the Péclet numbers (Pe_S and Pe_L) are

$$Pe_S = J_v(y)\frac{1-\sigma_S}{PS_S} \quad (21)$$

$$Pe_L = J_v(y)\frac{1-\sigma_L}{PS_L} \quad (22)$$

where the solute diffusion capacities were calculated from

$$PS_S(a_e) = \int_0^\infty D_\infty(R)g(R, a_e, gSD)\left(\frac{A}{A_0}\right)_{h,S}(R)dr \quad (23)$$

$$PS_L(a_e) = \int_0^\infty D_\infty(R)g(R, a_e, gSD)\left(\frac{A}{A_0}\right)_{h,L}(R)dr \quad (24)$$

In the above equations $\sigma_{h,S}(R)$, $\sigma_{h,L}(R)$, $(A/A0)_{h,S}(R)$, $(A/A0)_{h,L}(R)$ are the homoporous restriction factors as a function of solute radius *R* and were calculated according to equations 20-22 in [24].

The above system of differential equations (Eqn. 1, 7 and 12) were simultaneously solved using a fourth order Runge-Kutta scheme. The sieving coefficient for Ficoll was then calculated as

$$\theta = \frac{Q(0)C(0) - Q(1)C_i(1)}{GFR \cdot C_i(0)} \quad (25)$$

where $C_i(0)$ is the afferent solute (Ficoll) concentration and $C_i(1)$ and $Q(1)$ is the efferent solute concentration and plasma flow ($Q(1)$ =RPF-GFR), respectively.

Non-linear regression

The pore model sieving coefficients were fitted to the same experimental sieving data from rats used in [24] (327 data points) for Ficoll solute radii between 15-80 Å. The non-linear least squares algorithm in the well-known MINPACK library was used with standard settings to calculate the optimal values of rS, rL, gSD, $A_0/\Delta x$ and f_L, by minimizing the weighted objective function

$$\sum_{i=1}^{n} \frac{1}{\theta_{i,data}^2} \left(\theta_{i,model} - \theta_{i,data}\right)^2 \quad (26)$$

Parameter values are presented as means ± SE. There was a tendency for the fit of the model to be dependent on the initial values selected, especially for the large-pore system. Therefore a large number of initial values were tried and the best fit having the lowest χ^2-score was selected, similar to the method in [12, 24].

RESULTS

Analysis of experimental data from the rat glomerulus and from precision-made nanopore membranes

Plotted in Figure 1 is the model fit to the data from the rat glomerulus that were previously analyzed using the distributed two-pore model [24]. As can be seen, the fit is just as good as that obtained previously and thus there is no way of telling, from the analysis of Ficoll sieving coefficients alone, whether it is the pore sizes that are distributed or the solute sizes. Most likely there is variability both in the size of the selective elements of the GFB as well as in the size of the solute molecules. Similar to the previous study [24], a "protein sieving curve" was simulated by reducing the solute size distribution to near unity and lowering the $A_0/\Delta x$ parameter. Surely this latter simulation suggests that the greatest source of variability is in the size of the solute probe molecules in line with that hypothesized in [5] and that the glomerular barrier is a near perfect mechanical filter. The optimized two-pore model parameters for both the rat glomerulus and for the precision-made nanopore membranes are shown in Table 1. The obtained pore-size for the nanopore membranes was ~7Å larger than that in the rat GFB and, also, the obtained gSD was larger, possibly indicating a greater variation in pore sizes in these membranes. There may also be other sources of variation in the data contributing to the obtained gSD. The obtained value for the surface area parameter $A_0/\Delta x$ (29 cm) was smaller than expected from the actual surface area and thickness of the membrane (81 cm).

Simulations of rigid vs. flexible 20Å, 36Å and 60Å molecules

In figure 2, the effects of varying the gSD parameter in the model is shown for three differently sized molecules having radii 20Å, 36Å (cf. albumin) and 60Å. Variation in the flexibility (gSD) of the small and large solute molecules has virtually no effect on their permeability across the GFB. The opposite holds true for the albumin sized 36Å molecule which displays a difference in θ of nearly two orders of

magnitude when increasing the gSD from 1.00 to 1.15. Thus, by assuming a variation of ~15% of the size of the 36Å solute molecule, its permeability across the GFB increases 100-fold.

Simulations of different gSD vs. Dextran data from the rat glomerulus

The effects of altering the gSD of the solute sphere while keeping the other parameters of the model constant (as defined in Table 1) is shown in Figure 3. As expected, the permeability is increasing as the flexibility of the molecule is increased. For comparison, Dextran data from the rat glomerulus [6] was also plotted (dotted line). As seen, the experimental data seem to correlate well with a gSD = 1.37. It is also clear from this simulation that the cut-off between the small- and large pore parts of the sieving curve becomes less well defined the more flexible the solute molecule is. This may explain the finding that Dextran sieving data typically yields a higher estimate for not only the small pore radius but also the large-pore radius when analyzed using the classic 'discrete' two-pore model [1].

Alterations of the glomerular sieving coefficient along the glomerular capillary

The theoretical model in the current article also takes into account the loss of water along the glomerular capillary resulting from glomerular filtration. This causes a relative increase in the concentration of larger molecules along the length of the glomerular capillary (cf. also fig 2 in [13]). In Figure 4, the predicted variation of the plasma solute concentration along the glomerular capillary is plotted. The solute concentration (C_i) is expressed relative to its afferent arteriolar concentration C_{iA} (at y=0). For smaller solutes, the concentration remains nearly constant along the capillary length, reflecting the fact that their glomerular clearance is similar to GFR. For larger solutes, having a clearance lower than GFR, the concentration increases along the capillary. For a 40 Å solute, the concentration at the efferent end of the capillary (at y=1) is ~35% higher than that at the afferent end. This increase is similar for larger solutes (data not shown) having a similar glomerular clearance.

In order to investigate how the transport of small vs. large molecules is affected by this effect, the glomerular sieving coefficients of four differently sized solute molecules was plotted in Figure 5 as a function of the relative position along the glomerular capillary. The model parameters obtained above for the rat glomerulus were assumed. Although the permeability of the glomerular capillary wall is, according to the current theory, the same along its length, the sieving coefficient will increase slightly along the capillary due to the fact that the volume flux is reduced along the capillary length. Especially for larger solutes, the sieving coefficient can increase near the efferent end of the glomerular capillary, corresponding to a factor ~3 for a 40 Å solute (cf. also figure 2 in [22]). This effect is analogous to the changes in transport that occur when the glomerular filtration rate is altered [28]. Again, for small molecules, the GSC does not vary along the glomerular capillary since the clearance is essentially the same as that for water (GFR).

DISCUSSION

In the current study, the classic heteroporous model by Deen, Bridges, Brenner and Myers [13] was extended by introducing size (radius) distributions on the solute molecules, making them flexible in their conformation. By contrast, in the original model, the size-distribution was only applied to the pores while the solute molecules were assumed to be ideal rigid spheres. The extended theoretical model was used to analyze experimental sieving data (θ vs. SE-radius) for Ficoll, both from the rat glomerulus and from precision-made nanopore membranes [15, 16]. Through the years, many other theories and models have been proposed for glomerular filtration. Thus, in the review by Haraldsson, Nystrom and Deen [19], a charged fibrous membrane having a surface charge density of 200 mC/m^2 (equivalent to that of a molecule the size of HSA with a net valence of ~200) is proposed to explain the difference in sieving coefficients between Ficoll and 36 Å anionic albumin. Similar to the current model, the GFB is also a mechanical filter, but with a less size-selective, but highly charged, small-pore pathway. Actually, a more primitive variant of this model can be achieved by simply adjusting the dimensions of the charged solute molecule and charged pore using the Debye screening length as in Munch et al [23]. Using an 'Ogston gel' as a small-pore system, Smithies (re-)discovered that the transport of albumin is almost entirely diffusive [31] and suggested this to be an anti-clogging mechanism (at least for albumin) in the glomerulus along with the constant sweeping of the filter by red blood cells – effectively preventing concentration polarization. Thus, since clogging does not seem to occur in the GFB, the main barrier towards macromolecules is likely close to the luminal end of the GFB. In addition, plasma proteins are, themselves, likely part of the filter as removing them from the perfusate seems to increase permeability [17, 20]. A modification of the pore model was presented by Hausmann and colleagues which suggest that a strong electrical field being ~1600 V/m is generated in the GFB which hinders the transport of anionic species by means of electrophoretic forces [21]. However, some of the assumptions in their model has recently been questioned [27].

The bi-selective nature of the GFB becomes clear when analyzing the permeability for a wider range of solute sizes [18, 32]. The first cut-off occurs at molecular radii between 35-50Å [18, 24]. It is generally assumed that this 'small-pore' pathway is the major renal barrier towards serum albumin [18, 25, 31]. The transport of smaller solutes is entirely filtration flow-limited during normal conditions (e.g. inulin) so most of the transport is by means of convection for these solutes. As the small pore starts to sieve the solute, diffusive transport will start to dominate the transport. Thus, the transport of a molecule the size of albumin (~36Å) is almost entirely diffusive. The small-pore system can easily be replaced by a fiber-matrix giving essentially the same result [31] as using pores. If the small-pore system has a sharp cut-off, then even a relatively small amount of charge-selectivity could possibly have a large impact for molecules that are close to the pore radius and thus a so called 'fringe-effect' has been hypothesized [25]. Loss of charge-selectivity, rather than an increase in large-pore selectivity, could then give rise to isolated albuminuria. The second cut-off is not well characterized but an upper size-limit has been estimated to ~100-120Å [24, 32]. Large pores can be expected to be very rare, accounting only for 1 large pore per 10^7 of the small pores in a healthy glomerulus. Often, when analyzing polysaccharide sieving data, a so called 'shunt' is used as a simplified large-pore pathway [6, 28]. Nevertheless it is this 'large pore' pathway that is affected when the glomeruli are injured by disease [2-4, 18] whereas the small-pore pathway seems to be unaffected. Furthermore, a number of studies from our group show that the increase in permeability for molecules having a hydrodynamic radius > 50Å can occur only minutes after administration of a pharmacological challenge (for example angiotensin II [4] or atrial natriuretic peptide [2]), only to return to baseline in a matter of 30 min. Such rapid and dynamic changes are perhaps more compatible with a transient alteration in the cytoskeleton of the epi- and endothelial cells of the GFB [4] rather than a more permanent structural alteration.

In conclusion, we show, for the first time, that a variation of only ~16 % in the size of an ideal spherical solute molecule is sufficient to explain the observed difference in glomerular permeability between negatively charged human serum albumin and neutral Ficoll36Å. In addition, we show that

the effects of assuming a distribution in the size of the solute molecules are only evident when the molecular mean radius is close to the pore radius. This is in line with experimental observations both from the glomerulus [22] and from synthetic membranes [16]. The modeling proposed here suggests that molecular size and conformation are far more important than electrical charge for the glomerular permeability of macromolecules.

APPENDIX

Calculation of RPF

The glomerular capillary was defined on a partition of equidistant points $i \in [0, N]$. Equation 1 and 7 was then discretized using a fourth order Runge-Kutta scheme as follows

$$J1 = K_f(P_c - P_i - 0.7i\Delta y - [a_1 C_{pr,i} + a_2 C_{pr,i}^2]) \quad (27)$$

$$A1 = -\Delta y \cdot J1 \quad (28)$$

$$B1 = -\Delta y \cdot \frac{C_{pr,i}^2}{Q(0)C_{pr}(0)} A1 \quad (29)$$

$$J2 = K_f(P_c - P_i - 0.7(i\Delta y + \frac{\Delta y}{2}) - [a_1(C_{pr,i} + \frac{B1}{2}) + a_2(C_{pr,i} + \frac{B1}{2})^2]) \quad (30)$$

$$A2 = -\Delta y \cdot J2 \quad (31)$$

$$B2 = -\Delta y \cdot \frac{\left(C_{pr,i} + \frac{B1}{2}\right)^2}{Q(0)C_{pr}(0)} A2 \quad (32)$$

$$J3 = K_f(P_c - P_i - 0.7(i\Delta y + \frac{\Delta y}{2}) - [a_1(C_{pr,i} + \frac{B2}{2}) + a_2(C_{pr,i} + \frac{B2}{2})^2]) \quad (33)$$

$$A3 = -\Delta y \cdot J3 \quad (34)$$

$$B3 = -\Delta y \cdot \frac{\left(C_{pr,i} + \frac{B2}{2}\right)^2}{Q(0)C_{pr}(0)} A3 \quad (35)$$

$$J4 = K_f(P_c - P_i - 0.7(i+1)\Delta y - [a_1(C_{pr,i} + B3) + a_2(C_{pr,i} + B3)^2]) \quad (36)$$

$$A4 = -\Delta y \cdot J4 \quad (37)$$

$$B4 = -\Delta y \cdot \frac{\left(C_{pr,i} + \frac{B3}{2}\right)^2}{Q(0)C_{pr}(0)} A4 \quad (38)$$

The initial points (i=0) were Q_0 = RPF and $C_{pr,0}$=57 g/L. The next points on the grid was calculated from

$$Q_{i+1} = Q_i + \frac{A1}{6} + \frac{A2}{3} + \frac{A3}{3} + \frac{A4}{6} \quad (39)$$

$$C_{pr,i+1} = C_{pr,i} + \frac{B1}{6} + \frac{B2}{3} + \frac{B3}{3} + \frac{B4}{6} \quad (40)$$

The difference in the modeled glomerular filtration rate (Q_0-Q_N) and the measured GFR can be written as

$$F(RPF) = Q_0 - Q_N - GFR \quad (41)$$

To find RPF, the minimum of this equation was approximated using the gradient descent method.

Numerical solution of the differential equations for Glomerular Transport

After the calculation of the RPF, Equation 12 was also discretized according to

$$C1 = -\Delta y \left(f_S J1 \frac{C_i(1-\sigma_S)}{1-\sigma_S e^{-Pe_S}} + f_L J1 \frac{C_i(1-\sigma_L)}{1-\sigma_L e^{-Pe_L}} \right) \quad (42)$$

$$C2 = -\Delta y \left(f_S J2 \frac{(C_i+\frac{C_1}{2})(1-\sigma_S)}{1-\sigma_S e^{-Pe_S}} + f_L J2 \frac{(C_i+\frac{C_1}{2})(1-\sigma_L)}{1-\sigma_L e^{-Pe_L}} \right) \quad (43)$$

$$C3 = -\Delta y \left(f_S J3 \frac{(C_i+\frac{C_2}{2})(1-\sigma_S)}{1-\sigma_S e^{-Pe_S}} + f_L J3 \frac{(C_i+\frac{C_2}{2})(1-\sigma_L)}{1-\sigma_L e^{-Pe_L}} \right) \quad (44)$$

$$C4 = -\Delta y \left(f_S J3 \frac{(C_i+C3)(1-\sigma_S)}{1-\sigma_S e^{-Pe_S}} + f_L J3 \frac{(C_i+C3)(1-\sigma_L)}{1-\sigma_L e^{-Pe_L}} \right) \quad (45)$$

$$C_{i+1} = C_{pr,i} + \frac{C1}{6} + \frac{C2}{3} + \frac{C3}{3} + \frac{C4}{6} \quad (46)$$

For simplicity, the initial concentration C_0 was assumed to be unity.

REFERENCES

1. **Asgeirsson D, Venturoli D, Fries E, Rippe B, and Rippe C**. Glomerular sieving of three neutral polysaccharides, polyethylene oxide and bikunin in rat. Effects of molecular size and conformation. *Acta Physiol (Oxf)* 191: 237-246, 2007.

2. **Axelsson J, Rippe A, and Rippe B**. Transient and sustained increases in glomerular permeability following ANP infusion in rats. *American journal of physiology Renal physiology* 300: F24-30, 2011.

3. **Axelsson J, Rippe A, Venturoli D, Sward P, and Rippe B**. Effects of early endotoxemia and dextran-induced anaphylaxis on the size selectivity of the glomerular filtration barrier in rats. *American journal of physiology Renal physiology* 296: F242-248, 2009.

4. **Axelsson J, Rippe A, Öberg CM, and Rippe B**. Rapid, dynamic changes in glomerular permeability to macromolecules during systemic Angiotensin II (AngII) infusion in rats. *American journal of physiology Renal physiology* 303: F790-F799, 2012.

5. **Axelsson J, Sverrisson K, Rippe A, Fissell W, and Rippe B**. Reduced diffusion of charge-modified, conformationally intact anionic Ficoll relative to neutral Ficoll across the rat glomerular filtration barrier in vivo. *American journal of physiology Renal physiology* 301: F708-712, 2011.

6. **Axelsson J, Öberg CM, Rippe A, Krause B, and Rippe B**. Size-selectivity of a synthetic high-flux and a high cut-off dialyzing membrane compared to that of the rat glomerular filtration barrier. *J Membrane Sci* 2012.

7. **Blouch K, Deen WM, Fauvel JP, Bialek J, Derby G, and Myers BD**. Molecular configuration and glomerular size selectivity in healthy and nephrotic humans. *The American journal of physiology* 273: F430-437, 1997.

8. **Bohrer MP, Baylis C, Humes HD, Glassock RJ, Robertson CR, and Brenner BM**. Permselectivity of the glomerular capillary wall. Facilitated filtration of circulating polycations. *The Journal of clinical investigation* 61: 72-78, 1978.

9. **Bohrer MP, Patterson GD, and Carroll PJ**. Hindered Diffusion of Dextran and Ficoll in Microporous Membranes. *Macromolecules* 17: 1170-1173, 1984.

10. **Brenner BM, Troy JL, and Daugharty TM**. The dynamics of glomerular ultrafiltration in the rat. *The Journal of clinical investigation* 50: 1776-1780, 1971.

11. **Chang RL, Deen WM, Robertson CR, and Brenner BM**. Permselectivity of the glomerular capillary wall: III. Restricted transport of polyanions. *Kidney international* 8: 212-218, 1975.

12. **Deen WM**. Hindered Transport of Large Molecules in Liquid-Filled Pores. *Aiche J* 33: 1409-1425, 1987.

13. **Deen WM, Bridges CR, Brenner BM, and Myers BD**. Heteroporous model of glomerular size selectivity: application to normal and nephrotic humans. *The American journal of physiology* 249: F374-389, 1985.

14. **Deen WM, Robertson CR, and Brenner BM**. A model of glomerular ultrafiltration in the rat. *The American journal of physiology* 223: 1178-1183, 1972.

15. **Fissell WH, Dubnisheva A, Eldridge AN, Fleischman AJ, Zydney AL, and Roy S**. High-Performance Silicon Nanopore Hemofiltration Membranes. *J Memb Sci* 326: 58-63, 2009.

16. **Fissell WH, Manley S, Dubnisheva A, Glass J, Magistrelli J, Eldridge AN, Fleischman AJ, Zydney AL, and Roy S**. Ficoll is not a rigid sphere. *American journal of physiology Renal physiology* 293: F1209-1213, 2007.

17. **Fried TA, McCoy RN, Osgood RW, and Stein JH**. Effect of albumin on glomerular ultrafiltration coefficient in isolated perfused dog glomerulus. *The American journal of physiology* 250: F901-906, 1986.

18. **Guasch A, Deen WM, and Myers BD**. Charge selectivity of the glomerular filtration barrier in healthy and nephrotic humans. *Journal of Clinical Investigation* 92: 2274-2274, 1993.

19. **Haraldsson B, Nystrom J, and Deen WM**. Properties of the glomerular barrier and mechanisms of proteinuria. *Physiological reviews* 88: 451-487, 2008.

20. **Haraldsson BS, Johnsson EK, and Rippe B**. Glomerular permselectivity is dependent on adequate serum concentrations of orosomucoid. *Kidney international* 41: 310-316, 1992.

21. **Hausmann R, Kuppe C, Egger H, Schweda F, Knecht V, Elger M, Menzel S, Somers D, Braun G, Fuss A, Uhlig S, Kriz W, Tanner G, Floege J, and Moeller MJ**. Electrical forces determine glomerular permeability. *Journal of the American Society of Nephrology : JASN* 21: 2053-2058, 2010.

22. **Lund U, Rippe A, Venturoli D, Tenstad O, Grubb A, and Rippe B**. Glomerular filtration rate dependence of sieving of albumin and some neutral proteins in rat kidneys. *Am J Physiol-Renal* 284: F1226-F1234, 2003.

23. **Munch WD, Zestar LP, and Anderson JL**. Rejection of Polyelectrolytes from Microporous Membranes. *J Membrane Sci* 5: 77-102, 1979.

24. **Oberg CM, and Rippe B**. A distributed two-pore model: theoretical implications and practical application to the glomerular sieving of Ficoll. *American journal of physiology Renal physiology* 306: F844-854, 2014.

25. **Oberg CM, and Rippe B**. Quantification of the electrostatic properties of the glomerular filtration barrier modeled as a charged fiber matrix separating anionic from neutral Ficoll. *American journal of physiology Renal physiology* 304: F781-787, 2013.

26. **Oliver JD, 3rd, Anderson S, Troy JL, Brenner BM, and Deen WH**. Determination of glomerular size-selectivity in the normal rat with Ficoll. *Journal of the American Society of Nephrology : JASN* 3: 214-228, 1992.

27. **Rippe B, and Oberg CM**. Counterpoint: Defending pore theory. *Peritoneal dialysis international : journal of the International Society for Peritoneal Dialysis* 35: 9-13, 2015.

28. **Rippe C, Asgeirsson D, Venturoli D, Rippe A, and Rippe B**. Effects of glomerular filtration rate on Ficoll sieving coefficients (theta) in rats. *Kidney international* 69: 1326-1332, 2006.

29. **Schaeffer Jr RC, Gratrix M, Mucha D, and Carbajal J**. The Rat Glomerular Filtration Barrier Does Not Show Negative Charge Selectivity. *Microcirculation* 9: 329-342, 2002.

30. **Smith HW**. *The kidney: structure and function in health and disease*. Oxford University Press, USA, 1951.

31. **Smithies O**. Why the kidney glomerulus does not clog: a gel permeation/diffusion hypothesis of renal function. *Proceedings of the National Academy of Sciences* 100: 4108-4113, 2003.

32. **Tencer J, Frick IM, Oquist BW, Alm P, and Rippe B**. Size-selectivity of the glomerular barrier to high molecular weight proteins: upper size limitations of shunt pathways. *Kidney international* 53: 709-715, 1998.

33. **Wallenius G**. [Renal clearance of dextran as a measure of glomerular permeability]. *Acta Societatis Medicorum Upsaliensis Supplementum* 59: 1-91, 1954.

34. **Venturoli D, and Rippe B**. Ficoll and dextran vs. globular proteins as probes for testing glomerular permselectivity: effects of molecular size, shape, charge, and deformability. *American journal of physiology Renal physiology* 288: F605-613, 2005.

35. **Verniory A, Du Bois R, Decoodt P, Gassee JP, and Lambert PP**. Measurement of the permeability of biological membranes. Application to the glomerular wall. *The Journal of general physiology* 62: 489-507, 1973.

LEGENDS

Figure 1

Glomerular sieving coefficient (θ) vs. Hydrodynamic radius for the best-fit of the theoretical model (solid line) to the experimental data (dashed line). A simulated scenario is also shown (dotted line) where the gSD of the solute molecule and $A_0/\Delta x$ has been reduced to match the GSC of five different plasma proteins (from Lund et al [22]): myoglobin (myo: 19.4 Å), human myeloma dimeric κ-chain (κ-dimer; 28.4 Å), neutral horse-radish peroxidase (nHRP; 30.4 Å), neutral HSA (nHSA; 35.0Å), and HSA (35.5 Å).

Figure 2

Effects of varying the gSD parameter for three differently sized molecules having radii 20Å, 36Å (cf. albumin) and 60Å. Variation in the flexibility (gSD) of the smaller 20 Å and the larger 60 Å solute molecules has virtually no effect on their permeability across the GFB. The opposite holds true for the 36Å molecule which has a radius close to the pore radius.

Figure 3

Effects of altering the 'softness' (gSD) of the solute while keeping the other parameters of the model constant (as defined in Table 1). For comparison, Dextran sieving data from the rat glomerulus (from [6]) is also shown (dotted line). The experimental data seem to correlate well with a gSD = 1.37.

Figure 4

Theoretical increase in the concentration of differently sized Ficolls along a glomerular capillary. Solute concentration is expressed relative to that in the afferent end of the capillary. The concentration of larger Ficolls are increasing as the water content of the glomerular capillary blood plasma escapes due to glomerular filtration. The protein concentration at the afferent end of the capillary was assumed to be 57 g/L which in the current simulation lead to a concentration of ~77 g/L at the efferent end (cf. also [10]).

Figure 5

Theoretical variation in glomerular sieving coefficients of differently sized Ficolls with position (y) along a glomerular capillary. The differences observed for the larger Ficolls are caused by the increase in their concentration as is shown in Fig 4.

Figure 6

Theoretical pressure profile along the length of the glomerular capillary. A pressure drop of 0.7 mmHg across the entire length of the capillary was assumed [14]. The pressure was assumed to be 45 mmHg at the afferent end of the capillary and 10 mmHg in Bowman's space, similar to that found experimentally [10].

Figure 1

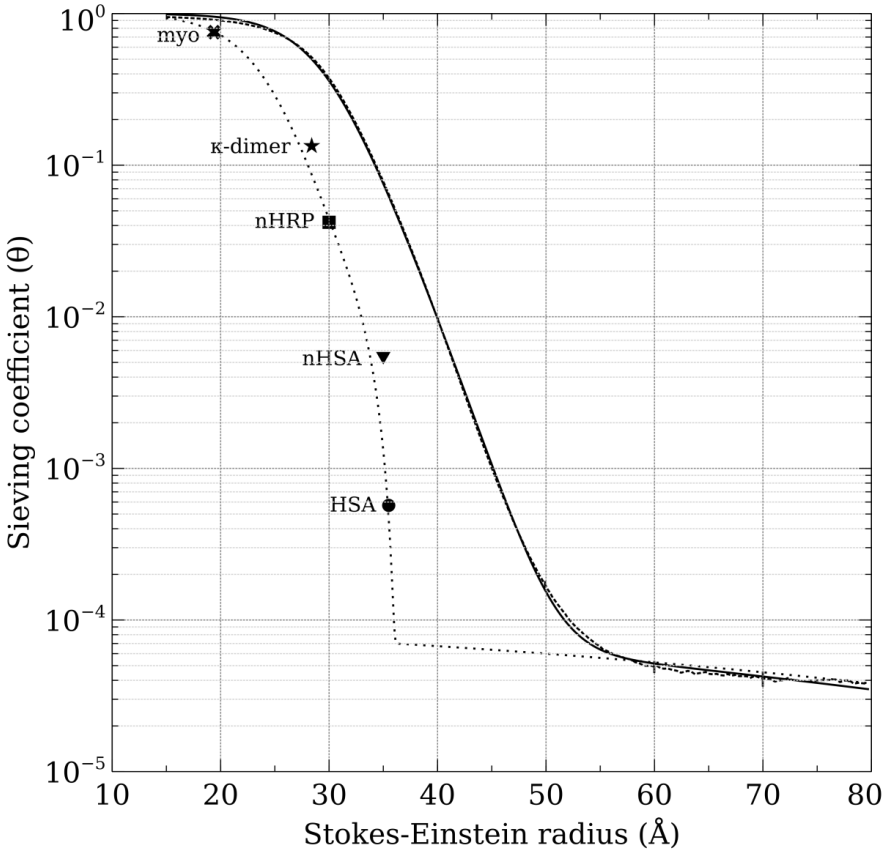
myo
κ-dimer
nHRP
nHSA
HSA
Sieving coefficient (θ)
Stokes-Einstein radius (Å)
10^0
10^{-1}
10^{-2}
10^{-3}
10^{-4}
10^{-5}
10
20
30
40
50
60
70
80

Figure 2

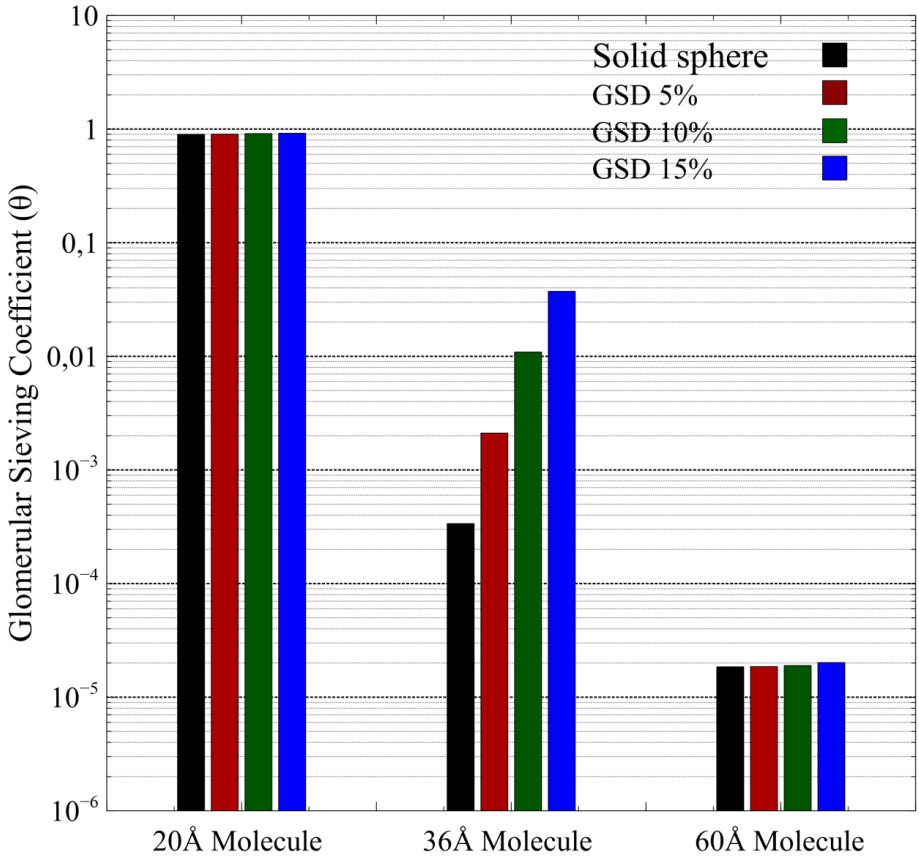
10
1
0,1
0,01
10^{-3}
10^{-4}
10^{-5}
10^{-6}
Glomerular Sieving Coefficient (θ)
Solid sphere
GSD 5%
GSD 10%
GSD 15%
20Å Molecule
36Å Molecule
60Å Molecule

Figure 3

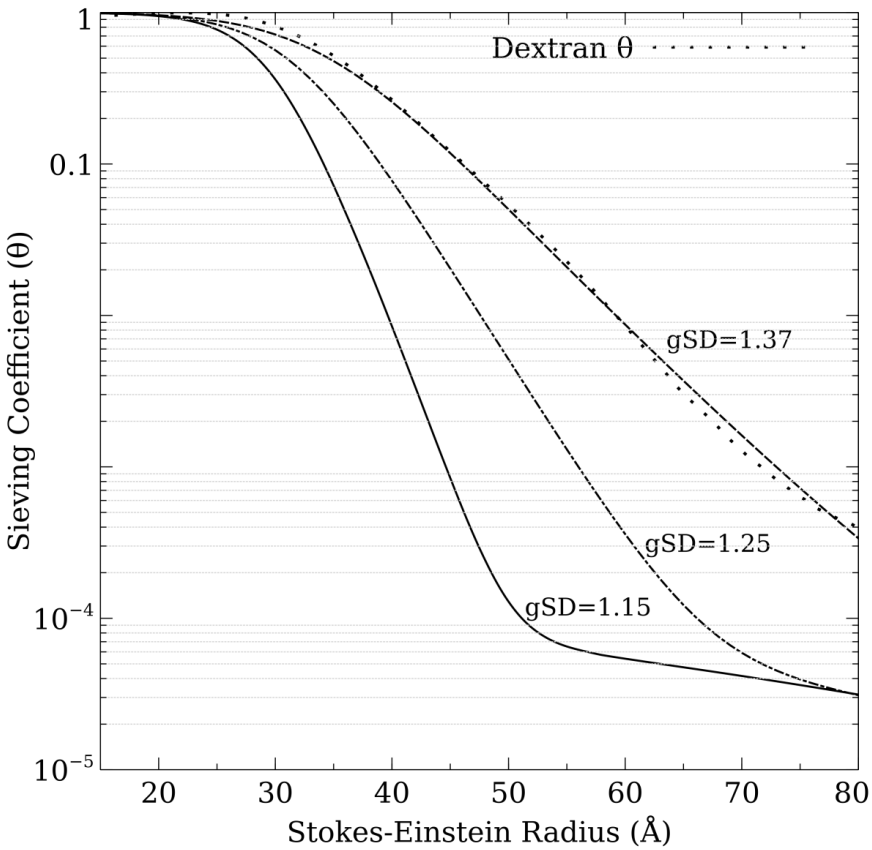
Dextran θ
gSD=1.37
gSD=1.25
gSD=1.15
Sieving Coefficient (θ)
Stokes-Einstein Radius (Å)
1
0.1
10^{-4}
10^{-5}
20
30
40
50
60
70
80

Figure 4

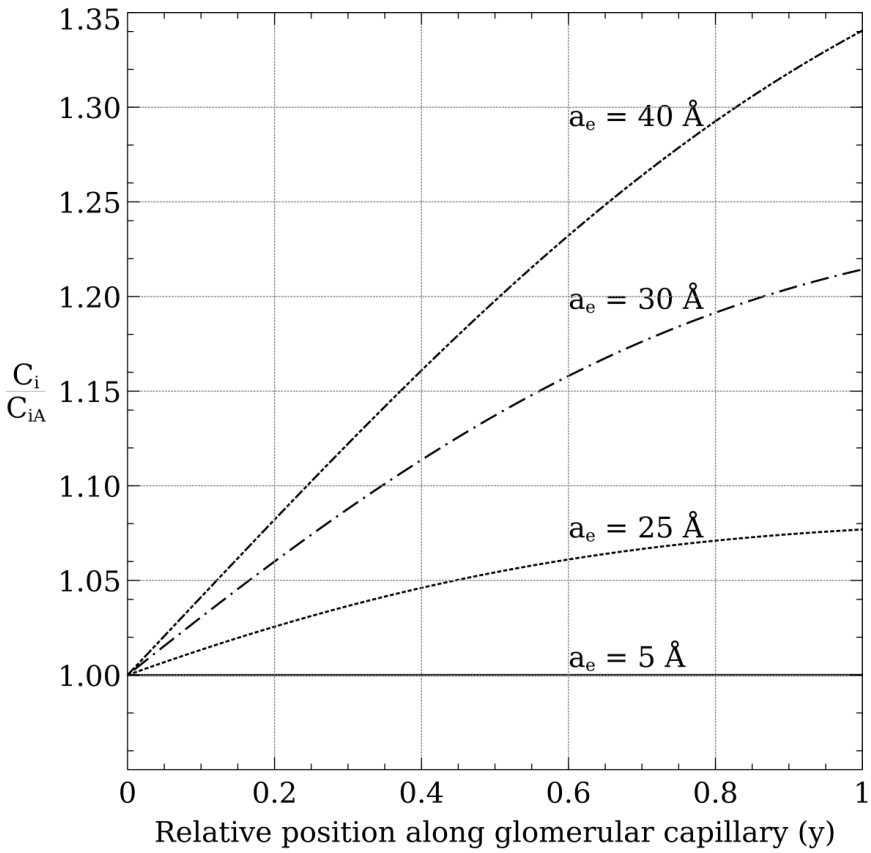
1.35
1.30
1.25
1.20
1.15
1.10
1.05
1.00
$\frac{C_i}{C_{iA}}$
a_e = 40 Å
a_e = 30 Å
a_e = 25 Å
a_e = 5 Å
0
0.2
0.4
0.6
0.8
1
Relative position along glomerular capillary (y)

Figure 5

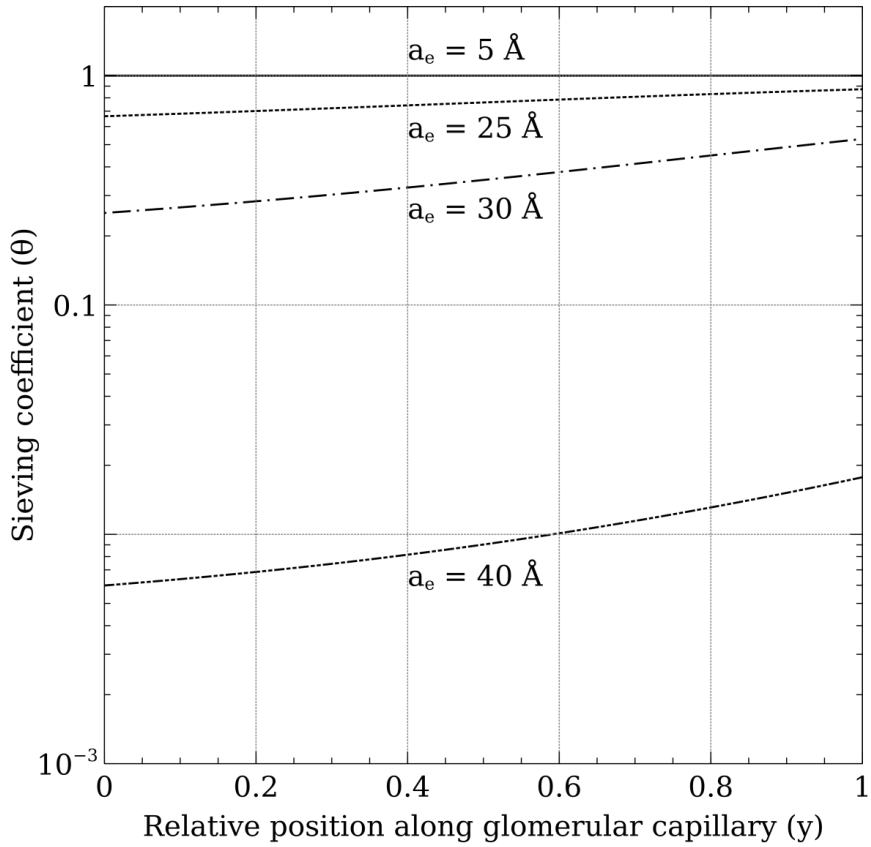
a_e = 5 Å
a_e = 25 Å
a_e = 30 Å
a_e = 40 Å
Sieving coefficient (θ)
1
0.1
10^{-3}
0
0.2
0.4
0.6
0.8
1
Relative position along glomerular capillary (y)

Figure 6

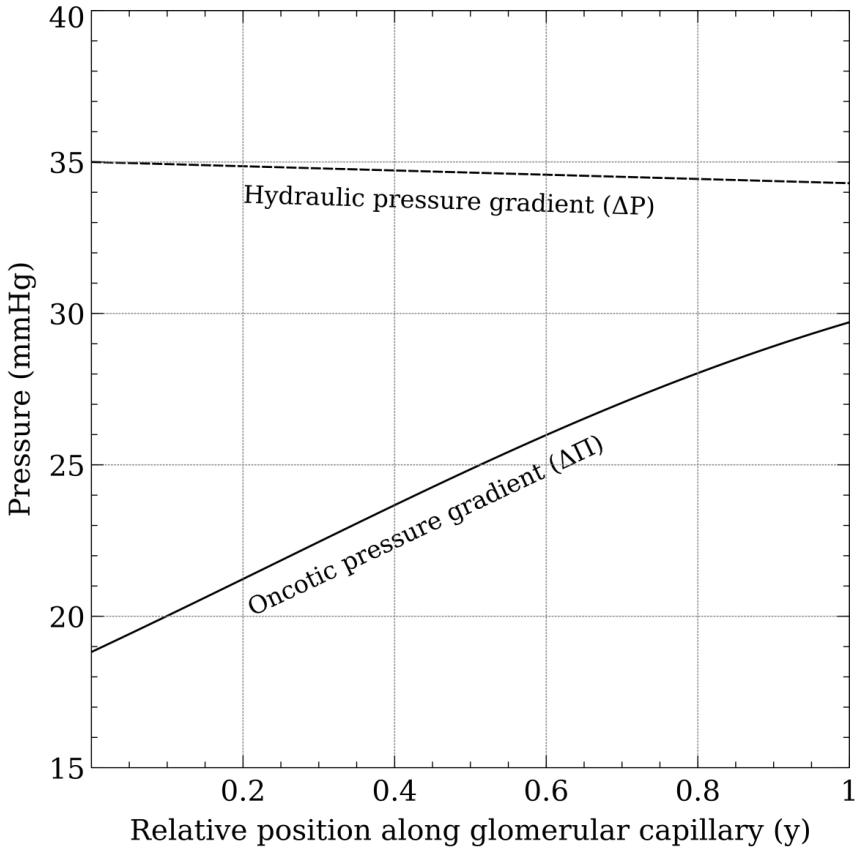
40
35
30
25
20
15
Pressure (mmHg)
Hydraulic pressure gradient (ΔP)
Oncotic pressure gradient (ΔΠ)
0.2
0.4
0.6
0.8
1
Relative position along glomerular capillary (y)

Table 1 – Two-pore model parameters

Model parameter	Rat Glomerulus	Nanopore Membrane
Small pore radius (r_S), Å	36.2 ± 0.5	43 ± 2
Geometric S.D. (gSD)	1.16 ± 0.01	1.24 ± 0.01
$A_0/\Delta x$, cm	$24 \cdot 10^5 \pm 7 \cdot 10^5$ †	29 ± 7
L_pS, mL min^{-1} mmHg^{-1} †	0.065 ± 0.04 †	$2.2 \cdot 10^{-5} \pm 0.2 \cdot 10^{-5}$
Large pore radius (r_L), Å	152 ± 7	-
$J_{vL}/GFR \times 10^5$	9 ± 1	-
RPF, mL min^{-1}	2.6 ± 0.2 †[a]	-
J_v, mL min^{-1} †	0.65 ± 0.4 †	$2.3 \cdot 10^{-3} \pm 0.2 \cdot 10^{-3}$
Goodness of fit, χ^2	0.15 ± 0.02	0.24 ± 0.06

See *Glossary* for abbreviations. † refers to g kidney. [a] Theoretical estimation (see appendix).

Study IV

Optimizing automated peritoneal dialysis (APD) using an extended three-pore model

Carl M. Öberg, Bengt Rippe

Lund University, Skåne University Hospital, Clinical Sciences Lund, Department of Nephrology, Lund, Sweden

Correspondence: Carl M. Öberg

Department of Nephrology

Skåne University Hospital

S-211 85 Lund, Sweden

Phone: +46-709-221947

E-mail: carl.oberg@med.lu.se

Running title: Optimizing APD

ABSTRACT

In the current study, an extended three pore model (TPM) is presented and applied to the problem of optimizing APD with regard to osmotic water transport (UF), small/middle-molecule clearance and glucose absorption. Simulations were performed for either intermittent APD (IPD) or tidal APD (TPD). IPD was simulated for fill and drain volumes of 2 L, while TPD was simulated using a tidal volumes of 0.5L, 1 L, or 1.5L with full drains and subsequent fills (2 L) occurring after every fifth dwell. A total of 25 cycles for a large number of different dialysate flow rates (DFR) were simulated using 3 different glucose concentrations (1.5%, 2.27% and 3.86%) and 3 different peritoneal transport types: slow (PET $D/P_{crea} < 0.6$), fast (PET $D/P_{crea} > 0.8$) and average. Solute clearance and UF were simulated to occur during the entire dwell including both fill and drain periods. It is demonstrated that DFRs exceeding ~3L/h are of little benefit both for UF and small-solute transport while middle-molecule clearance is actually enhanced at higher DFRs. The extended model is compared with clinical data with good agreement. The simulations predict that large reductions (>20%) in glucose absorption are possible by using moderately higher DFRs than a standard 6x2L prescription and by using shorter optimized 'bi-modal' APD regimes that alternate between a glucose-free solution and a glucose containing solution. Further research should assess whether such optimized regimes are feasible and safe, since the possible reductions in glucose absorption appear to be significant.

KEYWORDS: Dialysis efficiency, Automated peritoneal dialysis, Transport, Urea kinetics, Water transport

INTRODUCTION

Automated peritoneal dialysis (APD) is peritoneal dialysis performed with the aid of a mechanical device (a cycler), freeing the patient or caregiver from the repetitive and tedious labor of replacing spent dialysis fluid manually. APD is usually performed during the night when the patient is asleep, followed by a 'dry day' or a single long daytime dwell ('wet day'). Compared to conventional techniques, such as continuous ambulatory peritoneal dialysis (CAPD), APD offers the possibility to use increased dialysate flow rates (DFR) which would either be impractical or impossible to accomplish manually. Increasing the dialysate flow rate (DFR) by using more frequent exchanges will typically improve the efficiency of APD [14]. However, an increased DFR will increase the time spent filling and draining the peritoneal cavity, reducing the efficiency of the dialysis at higher DFRs [6, 25]. Thus, too frequent exchanges will reduce the efficiency of the dialysis and lead to a reduced cost-efficiency due to the increased consumption of dialysis fluid.

There are three exchange techniques of peritoneal dialysis, intermittent (IPD), tidal (TPD) and continuous (CPD) technique [19]. The latter requires the use of dual catheters and has only rarely been used. In IPD, each dwell is followed by a complete drain after which the peritoneal cavity is filled again with fresh dialysate. The outflow of drained fluid is bi-phasic, having a 'fast-phase' with flows ~350 mL/min and a 'slow-phase' with significantly lower flows, being only 30-40 mL/min. The separation between the fast and slow outflow phase is called the transition or break point which usually occurs after ~5 min after a 2L dwell [19]. In TPD, after an initial fill volume (of usually 2L), only a portion of the initial fill volume is drained and replaced by fresh dialysis fluid during each cycle. Thus, there is always a certain minimal amount of dialysate (the 'reservoir volume') that stays in contact with the peritoneal membrane throughout the dialysis session, after which the peritoneal cavity is drained completely. A prescription of TPD is usually defined by the percentage of the initial fill volume drained from the patient, e.g. 50% Tidal APD for a 2L initial volume means that 1L is cycled with 1L reserve volume remaining in the peritoneal cavity. In addition to draining the tidal volume, cyclers usually allow the prescriber to drain a surplus amount of fluid to compensate for the expected

ultrafiltration (UF) in order to avoid overfilling the peritoneal cavity with the accumulated ultrafiltrated volume. Thus, the tidal drain volume (TDV) is usually larger than the tidal fill volume (TFV). However, in clinical practice, it is nearly impossible to exactly match the predicted UF with the actual UF and, thus, a certain amount of "overdrain" or overfill is unavoidable.

The TPM was originally derived directly from patient data, some of which were published in 1990 [20], focusing on the most difficult task of PD modeling, namely to model UF volume as a function of time. The first head-to-head comparison of the TPM in its original version vs. conventional models (the Pyle & Popovich model) was done by Vonesh & Rippe [24], fitting the two fundamentally different models to rather detailed patient data. It was shown that the two models' ability to predict UF volume curves for 360 min were identical. The P&P model operated with high reflection coefficients to small solutes. It also utilized an albumin oncotic pressure term, contributing to the total fluid loss from the peritoneal cavity, whereby the lymph flow (parameter) became 0.54 ml/min in the P&P model (compared to 0.3 ml/min in the TPM). Although mathematical predictability was excellent, using non-TPM reflection coefficients and an inflated lymph flow parameter, problems with the P&P model turned up when simulating drained volume vs. times curves for Icodextrin. Furthermore, in dwells lasting longer than 6 hrs, the rate of final reabsorption became too large. This was the reason why the P&P model was abandoned for the purpose of UF simulations in favor of the TPM in Vonesh's later models (cf. PD-Adequest) [23]. A slightly extended version of the TPM has been very extensively validated by Haraldsson in 1995 [7], and later by its use in the computer software PDC®. The Haraldsson modification of the TPM included an initial inflation parameter for small solute PS values, essentially operating during the first hour of the dwell. Since PS to glucose was not inflated during the entire dwell, the term "final reabsorption rate" had to be increased from ~1.1 to ~1.5 ml/min to fit measured UF data (cf. [20, 24]). Haraldsson also increased the PS for urea by 20% from the theoretical value, but a further inflation actually seems appropriate. Furthermore, there was essentially an uncoupling between the hydraulic conductance (LpS) and the diffusive parameter, $A_0/\Delta x$ (if there was more than a 5% deviation of calculated UF volume vs. measured UF volume, which regularly occurred). The TPM is thus very well validated, and especially suitable for modeling of Icodextrin [6]

and long (>6 hrs) dwells, which is problematic with most other models. Validation is itself very problematic because of the high scatter in input data, especially in UF data. Vonesh et al [4] noted that the level of precision (standard deviation) in differences between two measured values was 707 ml/day for UF. Given such variability in input data, actually most models can be made to fit experimental data.

The classic TPM does not describe the inflow or outflow phase of the dwell. However, at higher dialysate flows, a significant part of the exchange time is spent either filling or draining the peritoneal cavity. In the current study, we present an extended 3PM having an additional compartment, allowing simulation also of the drain and fill phases of the dwell. The extended model is used to optimize the treatment with APD with regard to osmotic water transport (UF), small/middle-molecule clearance and glucose absorption. The results demonstrate that the 'metabolic cost' in terms of glucose absorption can be significantly reduced by using slightly higher DFRs than usually prescribed and a 'bi-modal' regime where relatively short dwells containing a high glucose concentration are combined with longer dwells containing no or a low glucose concentration. In addition, it is demonstrated that these regimes make it possible to shorten the total treatment time while achieving the same or better small-solute transport and UF. However, this will of course occur at a higher cost of treatment.

RESULTS

Urea clearance

In Figure 1, the simulated urea clearance as a function of DFR is plotted for the different techniques (IPD,TPD75/50/25) and different transport types: Fast (red line), Average (black line), Slow (blue line) for three different glucose concentrations:1.5% (dotted line), 2.27% (solid line) and 3.86% (dashed line). At low to moderate dialysate flow rates (< 2-3L/h) the intermittent technique provides slightly higher clearances than the tidal technique. For slow transporters, higher volume flows become ineffective (reach a plateau) at lower DFRs compared to average and fast transport types. Thus, for small solute transport, there is little benefit in exceeding 2L/h for a slow transporter. For the lower tidal volumes (TPD50 and TPD25), the urea clearance is lower in the leftmost part of the curve compared to the other modalities, demonstrating a relative inefficiency of low tidal volumes at lower DFRs. The right-most value for each curve represents the maximal flow rate possible at the chosen fill and drain flow rates (i.e. all time is spent either filling or draining the peritoneal cavity) and is, expectedly, higher for the tidal technique. The results for the other small solutes, creatinine, sodium and phosphate are very similar to the urea results (data not shown) although the transport of sodium more closely follow the UF curve (as is expected since ~80% of sodium is transported via convection).

Osmotic water transport (UF)

In Figure 2, the osmotic water transport, or "UF", per session hour is shown as a function of DFR. Expectedly, in absolute terms, the UF is higher for the slow transporters due to the slower dissipation of glucose, improving the average osmotic pressure gradient. The peak values occur at similar DFRs compared to the urea clearance vs. DFR curves in Fig. 1. At first glance, this might seem a bit surprising, since it is at these DFRs that the glucose absorption is at its greatest. However, the increased glucose dissipation at these high DFRs will be more than well compensated by the influx of

fresh dialysis fluid. Thus the glucose gradient will be maintained despite increasing absorption. Thus, it is the addition of fresh dialysis fluid that will increase both UF and clearance of small solutes at higher DFRs. The inefficiency at higher flows is due to the fact that, in relative terms, more time is spent filling and draining the peritoneal cavity, leading to a decrease in both UF and small solute clearance. Again, fast transporters will benefit from slightly higher DFRs while there is no benefit for slow transporters usinf DFRs > 2L/h.

Osmotic water transport ("UF") efficiency

The osmotic transport of water ("UF") during PD occurs at a "metabolic cost", in terms of glucose absorption. In Figure 3 the UF in mL per gram glucose absorbed (or "UF efficiency" [2]) is plotted as a function of DFR. The UF efficiency is markedly improved by increasing the DFR up to about 2L/h after which a plateau is reached and small or no further improvements are attained. For DFRs lower than 1L/h, the UF efficiency drops rapidly. The higher glucose concentrations are far more efficient in achieving UF. Thus, at a DFR of 2L/h, the patient will absorb more than twice the amount of glucose for the same amount of UF using the 1.5% solution compared to the 3.86% solution.

Small-solute transport efficiency (mmol UreaR per g glucose absorbed)

In Figure 4, the small solute transport efficiency (in mmol urea removed per g glucose absorbed) as a function of DFR is plotted. Similar to the osmotic efficiency above, the removal reaches an early plateau at DFRs higher than 2L/h. However, concerning the glucose strength, the situation here is the opposite compared to the UF efficiency curves. The higher glucose concentrations are much less efficient in achieving urea transport. Thus, the patient will absorb almost twice the amount of glucose per mmol of urea removed using a 3.86% solution instead of a 1.5% solution. Apparently, for both UF- and transport efficiency, there seems to be little benefit in increasing the DFR over 2L/h.

Middle molecule transport vs. DFR

In Figure 5, the clearance of β_2-microglobulin as a function of DFR is shown. In comparison to the results for the small-solute transport, no peak or decrease in clearance was observed at higher DFRs for the tidal techniques. Furthermore, the smaller tidal volumes are clearly beneficial for middle-molecule transport.

Comparison with clinical studies

In Table 2, the extended 3PM is compared with the study by Aasaröd and colleagues [1]. There is good agreement between the model and the clinical measurements, although there seems to be a tendency for the model to underestimate the clearances at higher DFRs.

Osmotic efficiency

The osmotic efficiency expressed in terms of UF per liter dialysis fluid ”consumed” as a function of DFR is shown in Figure 6 for the different techniques, transport types and different glucose concentrations. The extreme points to the left in the curves represent the lowest DFR at which the dialysis fluid will be efficient at removing water from the patient. Similarly, increasing the DFR to very high values means that a lot of dialysis fluid is spent for very little UF. Thus, from an economical point of view, the highest osmotically efficient DFR should be the extreme points in Figure 2. Intervals for these extreme points are ‘osmotically efficient’ and have been compiled Table 3.

Optimization Examples

The simulation results for UF efficiency and transport efficiency suggest that the overall glucose absorption can be decreased by alternating between short “UF dwells” and longer “Removal dwells”. In Figure 7, a standard prescription of 6x2L 1.36% glucose with a duration of 9 hours is compared

with scenarios were each dwell is optimized for either UF (using 3.86% glucose) or small-solute transport (using 0% glucose) keeping the glucose absorption low. The treatment time for the two latter scenarios was chosen to fit the UF and urea transport of the “standard prescription”. The corresponding transport parameters are shown in Table 4.

DISCUSSION

We have here presented an extended 3-pore model and applied it to a clinical problem: how to optimize APD with regard to maximizing UF and small-solute transport and, at the same time, minimizing the metabolic cost in terms of glucose absorption. The computer simulations were performed for different techniques (IPD, TPD25/50/75), different transport types (Slow, Average, Fast) and three different glucose concentrations (1.5%, 2.27% and 3.86%). To the best of our knowledge, these are the first simulations of this kind. We have demonstrated that the ”metabolic cost” in terms of both urea removal and UF per gram glucose absorbed is improved at somewhat higher DFRs (>2L/h) than is usually prescribed. The relative inefficiency of increasing DFR above 3L/h is demonstrated in these simulations with the only exception being middle-molecular transport, which, according to the current results, is actually improved at higher DFRs and lower tidal volumes. It is also clear, from these simulations that the metabolic efficiency, in terms of removal of small solutes per g glucose absorbed, is higher for lower glucose concentrations. The opposite holds true for UF in mL per g glucose absorbed which is higher for higher glucose concentrations. These properties can be expected á priori simply on the basis of the difference in the clearance of glucose from the PC and the osmotic flux of water to the PC and are not consequences of the TPM per se. Thus, relatively short ‘fluid removal dwells’ containing a high glucose concentration take advantage of the fact that ultrafiltration is much larger in the initial part of the dwell while longer 'diffusion' dwells containing no glucose can be used to obtain sufficient small-solute removal using the fact that the reabsorption rate is far lower than the initial flow rates in a glucose containing dwell. Also, the higher DFR used in these dwells seems to facilitate middle-molecule removal.

Glucose sparing optimization techniques

In light of the increasing number of type II diabetic patients on PD treatment, the systemic glucose absorption associated with PD has become a growing concern. However, while glucose sparing

techniques improves the metabolic control in diabetic patients, low-glucose regimes may apparently lead to an increased risk of extracellular fluid volume expansion [12], presumably due to the lower amount of UF associated with these regimes. Optimizing a single PD dwell will typically mean finding a balance between UF and small solute removal. However, since APD is based on several subsequent dwells, this allows for optimizing single dwells for either solute transport (low or, preferably, no glucose) or UF (high glucose) keeping the glucose absorption as low as possible during each dwell. Thus, the fact that weak glucose solutions provide more solute removal per g glucose absorbed and strong glucose solutions provide more UF per g glucose absorbed [2] can be used to optimize APD with regard to minimizing glucose absorption. Of course, such a strategy will lead to higher glucose concentrations for the ”UF-dwells” than would be used in a ”balanced” approach and exposing the peritoneal tissues to higher glucose concentrations may have undesired effects. On the other hand, the systemic glucose exposure can be far lower (see table 3) and the contact time with the stronger glucose solution can be kept relatively short (see figure 7).

The 3-pore model of peritoneal dialysis

A number of different variants of the TPM have been in use over the years. The three-pore concept was early included into the PD-Adequest model to be able to properly model UF [23, 24], especially for Icodextrin [17]. Common modifications of the model is to employ the old Pyle & Popovich (P&P) concept, namely that of a high lymphatic reabsorption term, low values for LpS and high values for the small solute reflection coefficients. The apparent advantage of such models is that the PS for glucose can be kept at a low value throughout the dwell. However, since the disappearance rate of the crystalloid osmotic gradient is about twice that of the intraperitoneal glucose concentration (rate constants 0.01 vs. 0.005, respectively) [8, 24], the original TPM uses a constantly inflated PS value for glucose during the entire dwell exclusively for UF simulations. Because small solute reflection coefficients can be kept low in the TPM, it is possible to model the osmotic behavior of Icodextrin and to have a fully operating Starling balance in this model [17]. As already discussed above, for short

dwells the old P&P concept or the KI modification of the TPM (KI-TPM) [22] work mathematically in an excellent way as compared to the original TPM. However, for longer dwells, this model, as well as the KI-TPM, will not work properly. The final reabsorption rate from the peritoneal cavity will be much too high (~3 ml/min). For short dwells, simulated during APD, the difference among the various versions of the TPM will be small.

Conclusions

The current simulations using an extended TPM indicate that the glucose absorption of APD-prescriptions can be greatly reduced by using moderately higher dialysate flows and utilizing a bi-modal treatment regime. The side-effects of such a treatment regime compared to standard regimes with higher glucose absorption are, however, not known. Further research should assess whether such optimized bi-modal regimes are feasible and safe, since the possible reduction in glucose absorption appear to be significant. By using DFRs higher than standard prescriptions (~1.5-2L/h), improvements in small-solute clearance and UF are also possible, although the relative benefits in UF and Kt/V seem to be relatively small compared to the increased cost of the treatment. It would, however, appear that the current model slightly underestimates the urea clearance at higher DFRs. Of course, higher DFRs will achieve the same UF and urea removal in a shorter period of time compared to standard treatments, although at a higher consumption of dialysis fluid. By contrast, using DFRs lower than 1L/h would appear to increase the glucose absorption in relation to the achieved UF and small-solute removal. Thus, according to the current results, considering both the metabolic cost in terms of glucose absorption per mL UF and the efficiency of the treatment in terms of small solute transport and UF: a “UF efficient” and economical DFR for most patients should lie between 1-3 L/h.

METHODS

During peritoneal dialysis, the net volume flow across the peritoneal membrane, at any time *t* from the start of the filling phase, is assumed to be the sum of 6 different volume flows

$$\frac{dV_D}{dt} = J_{v,C} + J_{v,S} + J_{v,L} - L + J_{fill} - J_{drain} \quad (1)$$

In this equation, $J_{v,C}$, $J_{v,S}$, and $J_{v,L}$ represent the net flow of water (in mL/min) across the aquaporines, the highly selective pathways ("small pores") and the weakly selective pathways ("large pores"), respectively. In the 3-pore model, the flows in equation 1 are assumed to vary only as a function of time and are directed into the peritoneal cavity when positive. The net lymphatic clearance from the peritoneal cavity to the circulation is denoted L (in mL/min) and is typically on the order of 0.2-0.3 mL/min when measured as a clearance to the circulation [18]. The clearance of an intraperitoneal volume marker is, however, larger than this value, which has been the source of much discussion [15]. The value of L is coupled to the reflection coefficient of glucose (and thus α_c) and to Kf, which can be used to estimate a plausible range for these parameters [20].

The model in the present work has been extended to include also the fill and drain phases of the dwell. Thus, J_{drain} and J_{fill} represent the flows of volume (in mL/min) to and from the source of dialysis fluid, respectively. The change in the intra-peritoneal concentration of a solute *i* (denoted $dC_{D,i}/dt$ in mmol/mL/min) at any time *t* is dependent on three separate terms

$$\frac{dC_{D,i}}{dt} = \frac{J_{s,S,i}+J_{s,L,i}}{V_D} - C_{D,i}\frac{J_{v,C}+J_{v,S}+J_{v,L}+J_{fill}}{V_D} + \frac{C_{B,i}J_{fill}}{V_D} \quad (2)$$

The first term is the change in intra-peritoneal concentration caused by the flow of solutes (through small and large pores, $J_{s,S,i}$ and $J_{s,L,i}$ in mmol/min) in and out of the peritoneal cavity. As can be seen, a positive solute flow is directed into the peritoneal cavity, increasing the concentration in the dialysate. The second term represents the dilution/concentration due to volume flux in and out of the peritoneum. Only water flows that affect the dialysate concentration are included in this term (i.e. L and J_{drain} are

not included). The last term is the change in concentration due to the inflow of fresh dialysate J_{fill} having a concentration $C_{B,i}$ (in mmol/mL). The change in concentration in the drain resevoir of solute i ($dC_{B,i}(t)/dt$ in mmol/mL/min) is given by

$$\frac{dC_{B,i}}{dt} = \frac{J_{drain}C_{D,i} - J_{fill}C_{B,i}}{V_B} - \frac{C_{B,i}}{V_B}\frac{dV_B}{dt} \quad (3)$$

The change in reservoir "bag" volume V_B is simply

$$\frac{dV_B}{dt} = -J_{fill} + J_{drain} \quad (4)$$

Thus, the concentration in the reservoir does not change during the fill phase ($dC_{B,i}/dt = 0$). This equation implies that the drain compartment is identical to the compartment with fresh dialysis fluid which is not the case in actual practice. However, since drain fluid and fresh dialysate are never mixed, there is no need for more than one "reservoir" compartment in the model. Hence, the compartment V_B acts as a source during the fill phase and as a collector of drain fluid during the drain phase. The initial conditions for the simulations are

$$V_D(0) = V_r \quad (5)$$

$$C_{D,i}(0) = C_{p,i} \quad (6)$$

$$C_{B,i}(0) = C_{I,i} \quad (7)$$

$$V_B(0) = V_I \quad (8)$$

where V_r is the residual volume, V_I the fill/instilled volume (at the start of the fill phase) or 0 at the start of the drain phase), $C_{I,i}$ is the dialysis fluid concentration of solute i, $C_{p,i}$ is the plasma concentration of solute *i* which is assumed to be constant during the dwell. The ordinary differential equations (ODE) 1-4 above, along with the initial conditions, represent the initial value problem (IVP) to be solved in order to obtain the unknown functions $V_D(t)$, $C_{D,i}(t)$, $V_B(i)$ and $C_{B,i}(t)$.

Volume and solute flow in the 3PM

The solute flow (in mmol/min) over each pathway is calculated according to the Patlak equation

$$J_{s,S,i} = J_{v,S}\left(1-\sigma_{s,i}\right)\frac{C_{P,i}-C_{D,i}e^{-Pe_{S,i}}}{1-e^{-Pe_{S,i}}} \quad (8)$$

$$J_{s,L,i} = J_{v,L}(1-\sigma_{L,i})\frac{C_{P,i}-C_{D,i}e^{-Pe_{L,i}}}{1-e^{-Pe_{L,i}}} \quad (9)$$

where $Pe_{S,i}=J_{vS}(1-\sigma_{S,i})/PS_{S,i}$ an $Pe_{L,i}=J_{vL}(1-\sigma_{L,i})/PS_{L,i}$ are the Péclet numbers (the ratio between the maximum convective and diffusive clearance for solute *i*) for the small and large pore pathway, respectively. The mass transfer area coefficients, $PS_{S,i}$ and $PS_{L,i}$ (in mL/min), are either set according to Table 1 or calculated according to pore theory $PS=D\cdot A_0/\Delta x\cdot A/A_0$ where A/A_0 is the diffusive restriction factor (cf. also [13]) and D is the free diffusion coefficient. The reflection coefficients are calculated according to theory [17]. The volume flow (mL/min) is calculated using Starling equilibria over each parallel pathway

$$J_{vC} = \alpha_C L_p S\left(\Delta P - RT\sum_{i=1}^{N}\left(C_{p,i}-C_{D,i}\right)\right) \quad (10)$$

$$J_{vS} = \alpha_S L_p S\left(\Delta P - RT\sum_{i=1}^{N}\sigma_{S,i}\left(C_{p,i}-C_{D,i}\right)\right) \quad (11)$$

$$J_{vL} = \alpha_L L_p S\left(\Delta P - RT\sum_{i=1}^{N}\sigma_{L,i}\left(C_{p,i}-C_{D,i}\right)\right) \quad (12)$$

where α_C, α_S and α_L are the fractional hydraulic conductances for the different pathways (see Table 1), R is the gas constant and T is the body temperature (310°K). Thus, the osmotic reflection coefficients are assumed to be the same for osmosis and solute transport (cf. also [5, 10]). In this publication a filtration coefficient (LpS) of 0.074 mL/min/mmHg was assumed for a patient $A_0/\Delta x$ of 25000 centimeters. For different peritoneal transport types LpS was scaled accordingly. To account for the recruitment/loss of peritoneal surface area due to a high/low IPV, an area factor was multiplied to all PS-values and LpS according to Keshavia et al [11].

$$af = 16.18\left(1-e^{-0.00077\cdot V_D(t)}\right)/13.3187 \quad (13)$$

Thus, the mass transfer area coefficients and the filtration coefficient were inflated for volumes > 2250 mL and vice versa.

Pressure dynamics in the 3-pore model

The average capillary hydrostatic pressure was calculated according to a pre-to-post-capillary resistance ratio (PTP=R_a/R_v) of 8:1. This ratio may be a bit low, but in the current simulations this will matter very little. Thus, given the mean arterial pressure (MAP) and the large-vein pressure (P_v) of the patient, the capillary pressure is calculated according to the well-known equation

$$P_c = fR_v \cdot MAP + fR_a \cdot P_v \quad (14)$$

where fR_a = 1-fR_v and fR_a = PTP/(PTP+1) are the fractional pre-capillary and post-capillary resistances, respectively. The net hydrostatic pressure gradient is simply

$$\Delta P = P_c - IPP \quad (15)$$

where the intra-peritoneal pressure (IPP) was assumed to be dependent only on the intraperitoneal volume (IPV). Here we used a modified equation by Twardowski et al [21] for the supine position.

$$IPP = 4.7 + \frac{V_D(t)}{690} \quad (16)$$

Note that the intercept used here is higher than that obtained in the study by Twardowski et al since the IPP for a total IPV of 2250 mL is here assumed to be 8 mmHg [9] in the supine position. However, in a patient naïve to peritoneal dialysis, a lower (negative) intercept can be expected. Furthermore, IPP might not be a completely linear function of IPV especially in the lower and higher ranges. In the current article, a MAP of 90 mmHg was used and, further, it is assumed that the large-vein pressure is equal to the intra-peritoneal pressure (P_v = IPP). This last assumption has been the subject of some controversy [16] since the net effect of this assumption is that variations in IPP has an almost negligible effect on trans-peritoneal volume flux.

Temporal discretization and numerical solution of the 3-pore IVP

To solve equations (1-4) numerically, we implement a fourth order Runge-Kutta scheme. If N represents the total number of solutes included in the simulation, the scystem of equations (1-4) can be re-written

$$\frac{dV_D}{dt} = \mathcal{F}(t, C_{D,1}, C_{D,2}, \dots, C_{D,N})$$

$$\frac{dC_{D,i}}{dt} = \mathcal{G}\left(t, C_{D,i}, C_{B,i}, V_D\right)$$

$$\frac{dC_{B,i}}{dt} = \mathcal{H}\left(t, C_{D,i}, C_{B,i}, V_B\right)$$

where F, G and H are functionals ("functions of functions") corresponding to the right-hand side of equations 1-3 and i = 0,1, … , N. We proceed by defining all functions of interest ($V_D(t)$, $C_{D,i}(t)$, $V_B(i)$ and $C_{B,i}(t)$) on Q+1 equally spaced grid points over the total simulation time $[0,\tau]$ with a time-step $\Delta t = \tau/Q$. The grid points are labeled k=0,1,2 … Q with k=0 representing the initial values. The functions are then calculated on the grid points $C_{D,i,k}=C_{D,i}(k\Delta t)$, $C_{B,i,k}=C_{B,i}(k\Delta t)$ and $V_{D,i,k}= V_{D,i}(k\Delta t)$. Starting with the initial value (k=0) the next grid point (k+1) is calculated according to

$$K_1 = \Delta t \cdot \mathcal{F}\left(k\Delta t, C_{D,1,k}, C_{D,2,k}, \dots, C_{D,N,k}\right)$$

$$L_{1,i} = \Delta t \cdot \mathcal{G}(k\Delta t, C_{D,i,k}, C_{B,i,k}, V_{D,k})$$

$$M_{1,i} = \Delta t \cdot \mathcal{H}(k\Delta t, C_{D,i,k}, C_{B,i,k}, V_{D,k})$$

$$K_2 = \Delta t \cdot \mathcal{F}\left(k\Delta t + \frac{\Delta t}{2}, C_{D,1,k} + \frac{L_{1,1}}{2}, C_{D,2,k} + \frac{L_{1,2}}{2}, \dots, C_{D,N,k} + \frac{L_{1,N}}{2}\right)$$

$$L_{2,i} = \Delta t \cdot \mathcal{G}(k\Delta t + \frac{\Delta t}{2}, C_{D,i,k} + \frac{L_{1,i}}{2}, C_{B,i,k} + \frac{M_{1,i}}{2}, V_{D,k} + \frac{K_1}{2})$$

$$M_{2,i} = \Delta t \cdot \mathcal{H}(k\Delta t + \frac{\Delta t}{2}, C_{D,i,k} + \frac{L_{1,i}}{2}, C_{B,i,k} + \frac{M_{1,i}}{2}, V_{D,k} + \frac{K_1}{2})$$

$$K_3 = \Delta t \cdot \mathcal{F}\left(k\Delta t + \frac{\Delta t}{2}, C_{D,1,k} + \frac{L_{2,1}}{2}, C_{D,2,k} + \frac{L_{2,2}}{2}, \dots, C_{D,N,k} + \frac{L_{2,N}}{2}\right)$$

$$L_{3,i} = \Delta t \cdot \mathcal{G}(k\Delta t + \frac{\Delta t}{2}, C_{D,i,k} + \frac{L_{2,i}}{2}, C_{B,i,k} + \frac{M_{2,i}}{2}, V_{D,k} + \frac{K_2}{2})$$

$$M_{3,i} = \Delta t \cdot \mathcal{H}(k\Delta t + \frac{\Delta t}{2}, C_{D,i,k} + \frac{L_{2,i}}{2}, C_{B,i,k} + \frac{M_{2,i}}{2}, V_{D,k} + \frac{K_2}{2})$$

$$K_4 = \Delta t \cdot \mathcal{F}\left(k\Delta t + \Delta t, C_{D,1,k} + L_{3,1}, C_{D,2,k} + L_{3,2}, \dots, C_{D,N,k} + L_{3,N}\right)$$

$$L_{4,i} = \Delta t \cdot \mathcal{G}\left(k\Delta t + \Delta t, C_{D,i,k} + L_{3,i}, C_{B,i,k} + M_{3,i}, V_{D,k} + K_3\right)$$

$$M_{4,i} = \Delta t \cdot \mathcal{H}(k\Delta t + \Delta t, C_{D,i,k} + L_{3,i}, C_{B,i,k} + M_{3,i}, V_{D,k} + K_3)$$

$$V_{D,k+1} = V_{D,k} + \frac{K_1 + 2K_2 + 2K_3 + K_4}{6}$$

$$C_{D,i,k+1} = C_{D,i,k} + \frac{L_{1,i} + 2L_{2,i} + 2L_{3,i} + L_{4,i}}{6}$$

$$C_{B,i,k+1} = C_{B,i,k} + \frac{M_{1,i} + 2M_{2,i} + 2M_{3,i} + M_{4,i}}{6}$$

$$V_{B,i,k+1} = V_{B,i,k} + \Delta t\left(J_{drain} - J_{fill}\right)$$

The total simulation time (τ) was chosen so that a total of 25 subsequent dwells was simulated with a timestep of 0.001 min. This short timestep was chosen so that the error in fill/drained volume would be less than 0.1 mL per dwell.

Regulation of fill/drain cycles

In the current simulations, a fill flow rate of 200 mL/min was used. For the drain phase, drain flow rates of 350 mL/min (fast-phase) and 36 mL/min (slow-phase) were implemented with a transition point (break point) at an intraperitoneal volume of 381 mL [3, 4]. Each cycle starts with a fill phase followed by a dwell phase which lasts for a pre-determined dwell time (DT) after which the drain

phase starts. The whole duration of the cycle, consisting of the fill-, dwell- and drain-time is referred to as the exchange time (ET). For IPD, the drain phase ends when the calculated intra-peritoneal volume for the next grid point is less than the residual volume ($V_{D,k+1} < V_r$) after which either a new cycle starts or the simulation ends. Depending on the time-step chosen, this leads to a small error since the actual volume left in the peritoneal cavity after a cycle will always be larger than (or equal to) V_r. The drain phase terminates when the calculated volume for the next grid point is less than the sum of the residual volume and the tidal reserve volume ($V_{D,k+1} < V_r + TRV$).

ACKNOWLEDGEMENTS

Presented in part at EuroPD in Krakow 2-5 October 2015. This study was supported by the Swedish Research Council (Grant 08285), the Swedish Heart and Lung Foundation, the Medical Faculty at Lund University, and a grant from Baxter Healthcare Corporation.

DISCLOSURE

Carl M. Öberg is the inventor of a pending patent filed by Gambro Lundia AB based on the content in the current article, and has also worked as a consultant for Baxter Healthcare Corporation. Bengt Rippe is participating in a clinical trial with Fresenius Medical Care, and has received speaker's honoraria from Fresenius Medical Care and Baxter Gambro Healthcare at Lund.

References

1. **Aasarod K, Wideroe TE, and Flakne SC**. A comparison of solute clearance and ultrafiltration volume in peritoneal dialysis with total or fractional (50%) intraperitoneal volume exchange with the same dialysate flow rate. *Nephrology, dialysis, transplantation : official publication of the European Dialysis and Transplant Association - European Renal Association* 12: 2128-2132, 1997.
2. **Akonur A, Holmes CJ, and Leypoldt JK**. Ultrafiltration efficiency during automated peritoneal dialysis using glucose-based solutions. *Advances in peritoneal dialysis Conference on Peritoneal Dialysis* 24: 69-74, 2008.
3. **Amici G, and Thomaseth K**. Role of drain and fill profile in automated peritoneal dialysis. *Contrib Nephrol* 129: 44-53, 1999.
4. **Brandes JC, Packard WJ, Watters SK, and Fritsche C**. Optimization of dialysate flow and mass transfer during automated peritoneal dialysis. *Am J Kidney Dis* 25: 603-610, 1995.
5. **Deen WM**. Hindered Transport of Large Molecules in Liquid-Filled Pores. *Aiche J* 33: 1409-1425, 1987.
6. **Durand PY, Freida P, Issad B, and Chanliau J**. How to reach optimal creatinine clearances in automated peritoneal dialysis. *Peritoneal dialysis international : journal of the International Society for Peritoneal Dialysis* 16 Suppl 1: S167-170, 1996.
7. **Haraldsson B**. Assessing the peritoneal dialysis capacities of individual patients. *Kidney international* 47: 1187-1198, 1995.
8. **Heimburger O, Waniewski J, Werynski A, and Lindholm B**. A quantitative description of solute and fluid transport during peritoneal dialysis. *Kidney international* 41: 1320-1332, 1992.
9. **Imholz AL, Koomen GC, Struijk DG, Arisz L, and Krediet RT**. Effect of an increased intraperitoneal pressure on fluid and solute transport during CAPD. *Kidney international* 44: 1078-1085, 1993.
10. **Katz MA, Schaeffer RC, Gratrix M, Mucha D, and Carbajal J**. The glomerular barrier fits a two-pore-and-fiber-matrix model: Derivation and physiologic test. *Microvasc Res* 57: 227-243, 1999.
11. **Keshaviah P, Emerson PF, Vonesh EF, and Brandes JC**. Relationship between body size, fill volume, and mass transfer area coefficient in peritoneal dialysis. *J Am Soc Nephrol* 4: 1820-1826, 1994.
12. **Li PK, Culleton BF, Ariza A, Do JY, Johnson DW, Sanabria M, Shockley TR, Story K, Vatazin A, Verrelli M, Yu AW, and Bargman JM**. Randomized, controlled trial of glucose-sparing peritoneal dialysis in diabetic patients. *Journal of the American Society of Nephrology : JASN* 24: 1889-1900, 2013.
13. **Oberg CM, and Rippe B**. A distributed two-pore model: theoretical implications and practical application to the glomerular sieving of Ficoll. *American journal of physiology Renal physiology* 306: F844-854, 2014.
14. **Perez RA, Blake PG, McMurray S, Mupas L, and Oreopoulos DG**. What is the optimal frequency of cycling in automated peritoneal dialysis? *Periton Dialysis Int* 20: 548-556, 2000.
15. **Rippe B**. Free water transport, small pore transport and the osmotic pressure gradient three-pore model of peritoneal transport. *Nephrology, dialysis, transplantation : official publication of the European Dialysis and Transplant Association - European Renal Association* 23: 2147-2153, 2008.
16. **Rippe B**. Is intraperitoneal pressure important? *Perit Dial Int* 26: 317-319; discussion 411, 2006.
17. **Rippe B, and Levin L**. Computer simulations of ultrafiltration profiles for an icodextrin-based peritoneal fluid in CAPD. *Kidney international* 57: 2546-2556, 2000.
18. **Rippe B, Stelin G, and Ahlmen J**. Lymph flow from the peritoneal cavity in CAPD patients. In: *Frontiers in Peritoneal Dialysis*Springer, 1986, p. 24-30.
19. **Ronco C**. *Automated peritoneal dialysis*. Karger Medical and Scientific Publishers, 1999.

20. **Stelin G, and Rippe B**. A phenomenological interpretation of the variation in dialysate volume with dwell time in CAPD. *Kidney international* 38: 465-472, 1990.
21. **Twardowski ZJ, Prowant BF, Nolph KD, Martinez AJ, and Lampton LM**. High volume, low frequency continuous ambulatory peritoneal dialysis. *Kidney Int* 23: 64-70, 1983.
22. **Waniewski J, Debowska M, and Lindholm B**. How accurate is the description of transport kinetics in peritoneal dialysis according to different versions of the three-pore model? *Periton Dialysis Int* 28: 53-60, 2008.
23. **Vonesh EF, Burkart J, McMurray SD, and Williams PF**. Peritoneal dialysis kinetic modeling: validation in a multicenter clinical study. *Peritoneal dialysis international : journal of the International Society for Peritoneal Dialysis* 16: 471-481, 1996.
24. **Vonesh EF, and Rippe B**. Net fluid absorption under membrane transport models of peritoneal dialysis. *Blood purification* 10: 209-226, 1992.
25. **Vychytil A, and Horl WH**. The role of tidal peritoneal dialysis in modern practice: A European perspective. *Kidney international Supplement* S96-S103, 2006.

LEGENDS

Figure 1

Simulated urea clearances as a function of DFR for the different techniques (IPD,TPD75/50/25), different transport types: Fast (red line), Average (black line), Slow (blue line) and three different glucose concentrations:1.5% (dotted line), 2.27% (solid line) and 3.86% (dashed line).

Figure 2

Osmotic water transport (UF) per session hour as a function of DFR for the different techniques (IPD,TPD75/50/25), different transport types: Fast (red line), Average (black line), Slow (blue line) and three different glucose concentrations:1.5% (dotted line), 2.27% (solid line) and 3.86% (dashed line).

Figure 3

Osmotic water transport (UF) in mL per gram glucose absorbed (or "UF efficiency") plotted as a function of DFR for the different techniques (IPD,TPD75/50/25), different transport types: Fast (red line), Average (black line), Slow (blue line) and three different glucose concentrations:1.5% (dotted line), 2.27% (solid line) and 3.86% (dashed line).

Figure 4

The small solute transport efficiency (in mmol urea removed per g glucose absorbed) as a function of DFR for the different techniques (IPD,TPD75/50/25), different transport types: Fast (red line),

Average (black line), Slow (blue line) and three different glucose concentrations:1.5% (dotted line), 2.27% (solid line) and 3.86% (dashed line).

Figure 5

The clearance of β_2-microglobulin as a function of DFR for the different techniques (IPD,TPD75/50/25), different transport types: Fast (red line), Average (black line), Slow (blue line) and three different glucose concentrations:1.5% (dotted line), 2.27% (solid line) and 3.86% (dashed line).

Figure 6

Osmotic water transport (UF) in mL per liter dialysis fluid ”consumed” as a function of DFR for the different techniques, transport types and different glucose concentrations.

Figure 7

Simulated scenarios were each dwell is optimized for either UF (using 3.86% glucose) or small-solute transport (using 0% glucose) keeping the glucose absorption low. The corresponding transport parameters are shown in Table 3.

Figure 1

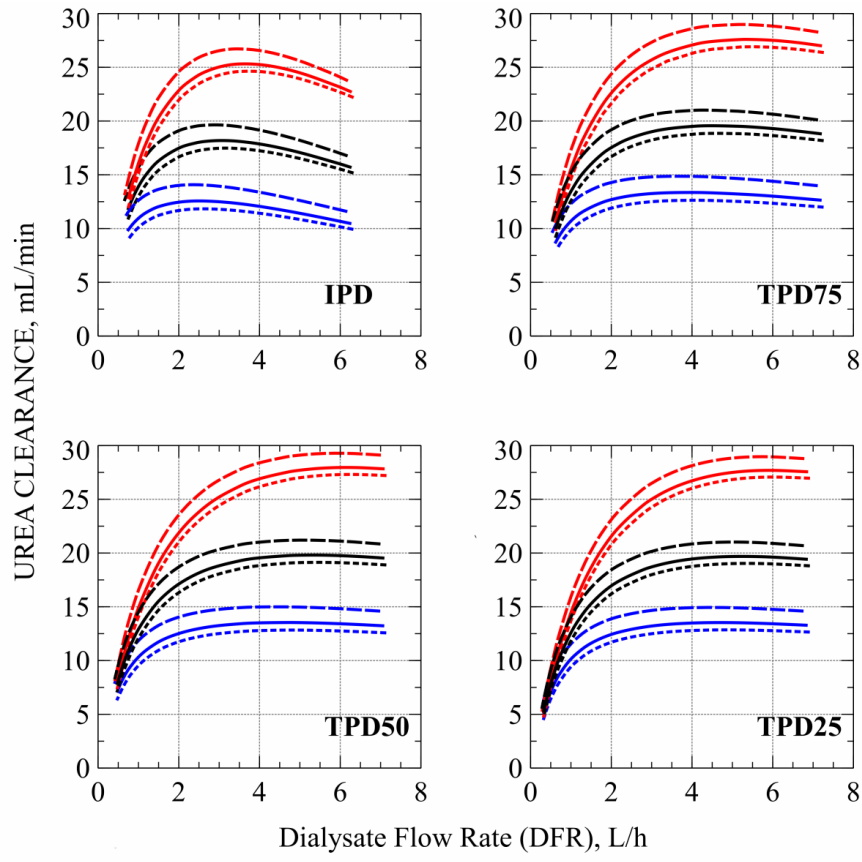
UREA CLEARANCE, mL/min
Dialysate Flow Rate (DFR), L/h
IPD
TPD75
TPD50
TPD25
0
5
10
15
20
25
30
0
2
4
6
8

Figure 2

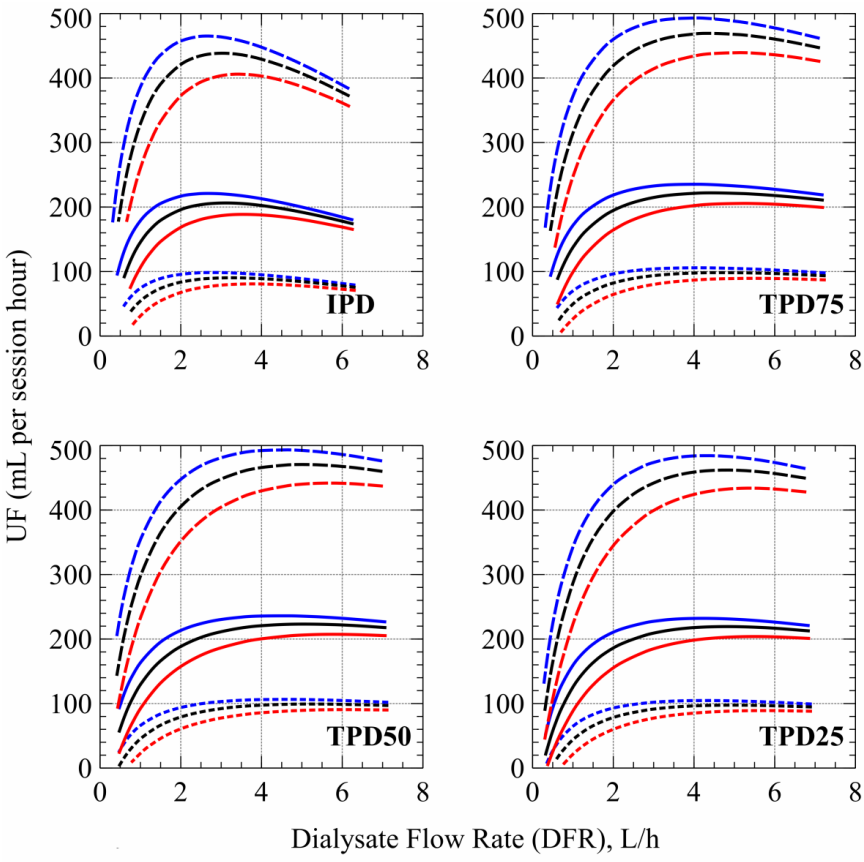
UF (mL per session hour)
Dialysate Flow Rate (DFR), L/h
IPD
TPD75
TPD50
TPD25
0
100
200
300
400
500
0
2
4
6
8

Figure 3

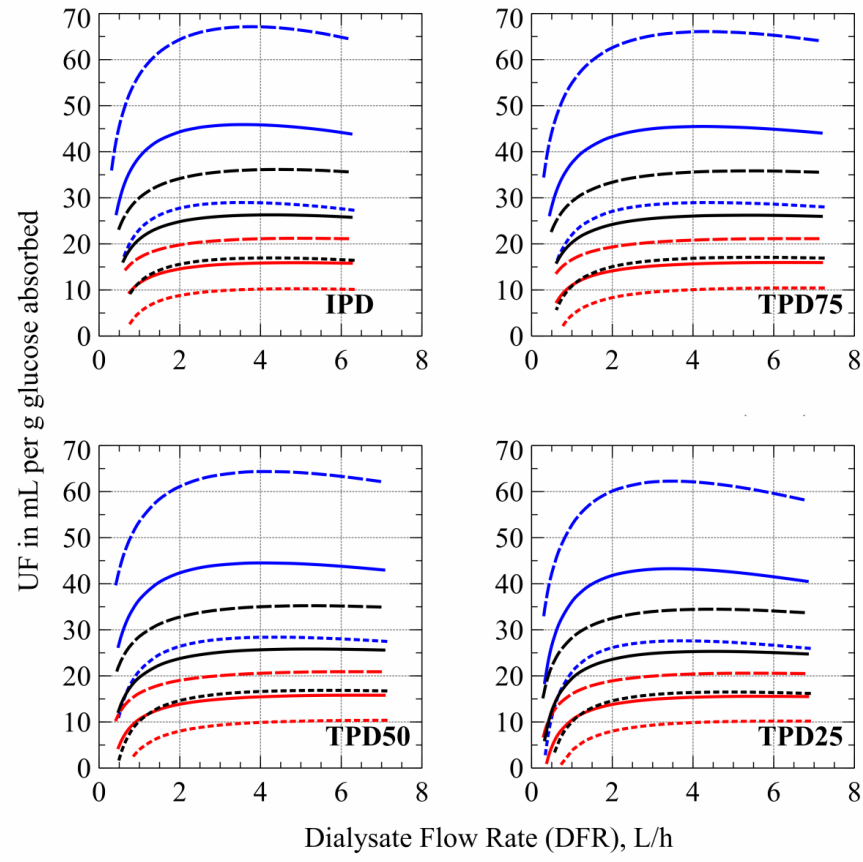
IPD
TPD75
TPD50
TPD25
UF in mL per g glucose absorbed
Dialysate Flow Rate (DFR), L/h

Figure 4

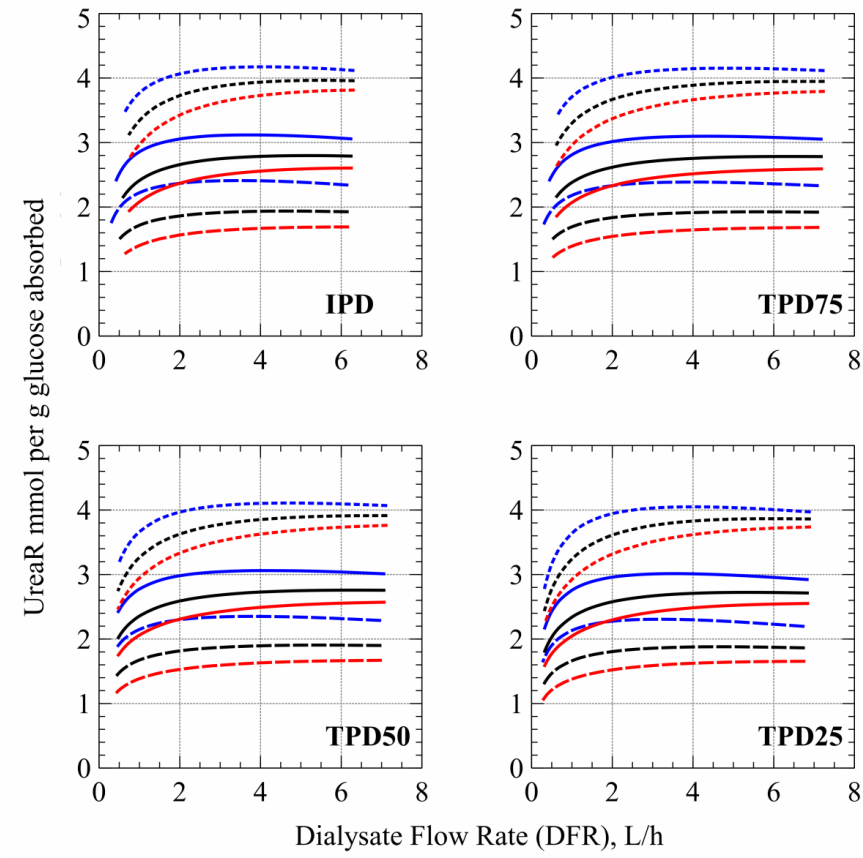
UreaR mmol per g glucose absorbed
IPD
TPD75
TPD50
TPD25
Dialysate Flow Rate (DFR), L/h

Figure 5

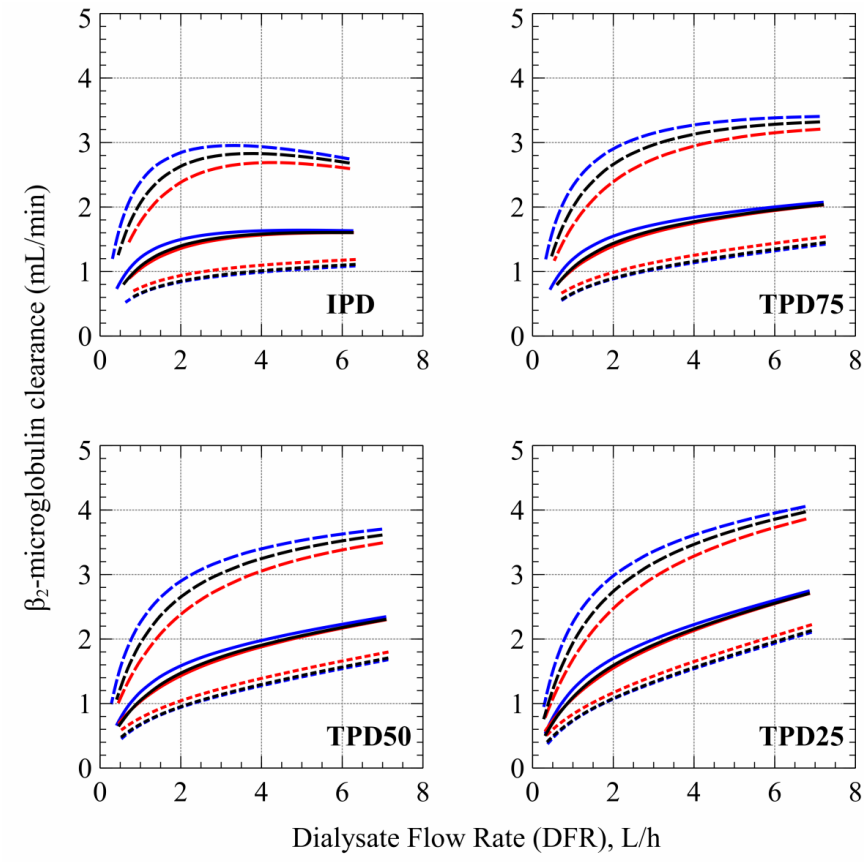
β2-microglobulin clearance (mL/min)
IPD
TPD75
TPD50
TPD25
Dialysate Flow Rate (DFR), L/h

Figure 6

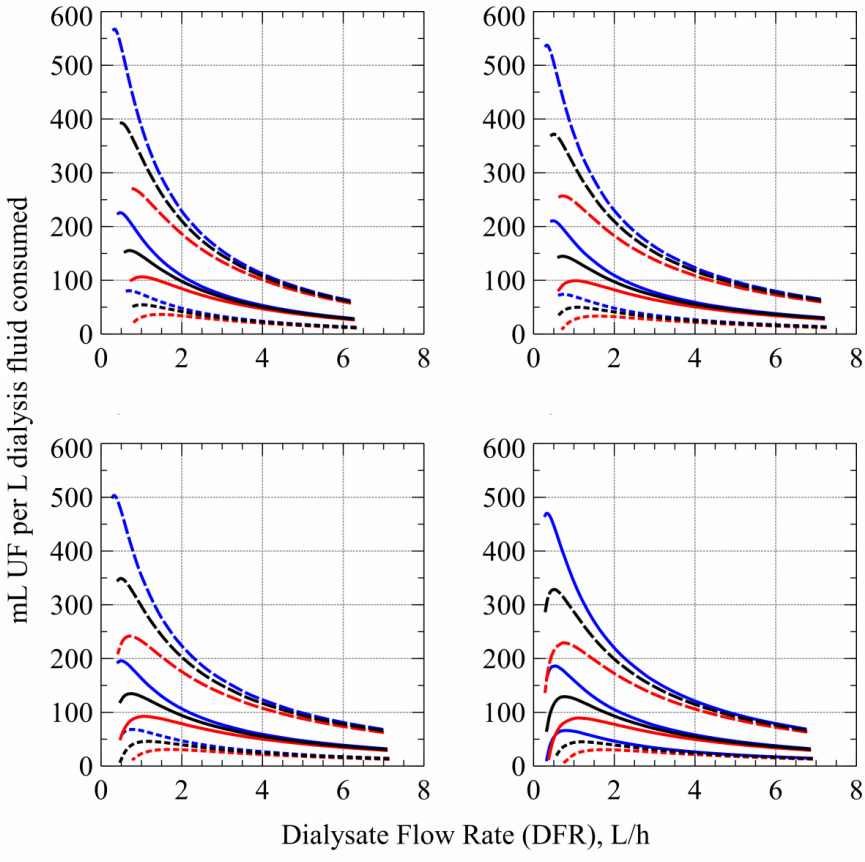
mL UF per L dialysis fluid consumed
Dialysate Flow Rate (DFR), L/h
0
100
200
300
400
500
600
0
2
4
6
8

Figure 7

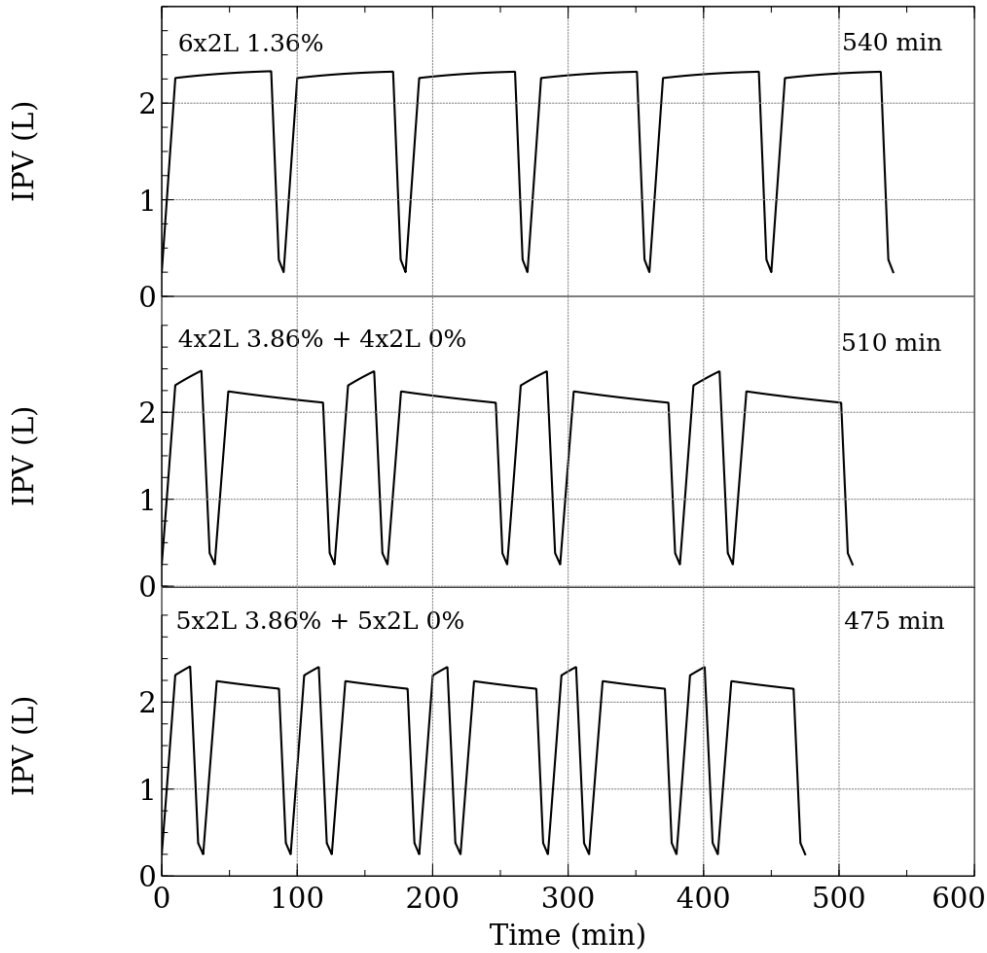
6x2L 1.36%
540 min
4x2L 3.86% + 4x2L 0%
510 min
5x2L 3.86% + 5x2L 0%
475 min
IPV (L)
IPV (L)
IPV (L)
0
1
2
0
100
200
300
400
500
600
Time (min)

Table 1. Three-pore model parameters

Parameters used for computer simulations of intraperitoneal volume *vs.* time V(t) curves according to a three-pore model of membrane selectivity	
Small pore radius (r_s) (Å)	43
Large pore radius (r_L) (Å)	250
Fractional small pore UF-coeff. (α_s)	0.900
Fractional transcellular UF-coeff. (α_c)	0.020
Fractional large pore UF-coeff. (α_L)	0.080
Ultrafiltration coefficient (L_pS) (mL/min/mmHg)	0.074
Osmotic conductance to glucose ($L_pS\ \sigma_g$) (μL/min/mmHg)	3.6
”Unrestricted” pore area over unit diffusion distance for small pores $(A_0/\Delta X)_s$ (cm)	25,000*
PS for glucose (mL/min)	15.4
PS for urea (mL/min)	26.0
PS for "Na" and "anion" (mL/min)	4.5
PS for phosphate (mL/min)	10.2
Peritoneal lymph flow (L) (mL/min)	0.3
Transperitoneal oncotic pressure gradient ($\Delta\pi_{prot}$) (mmHg)	22
Peritoneal residual volume (V_r) (mL)	250
Serum urea conc. (mmol/L)	20
Serum creatinine conc. (μmol/l)	660
Dialysis fluid sodium conc. (mmol/L)	132
Serum sodium (and sodium associated ”anion” conc.) (mmol/L)	140
Serum glucose conc. (mmol/L)	6.5
Dissociation factor for “Na^+” and “anions”	0.93

***)** 25,000 cm was used for an average peritoneal transport type, 40,000 cm for high transporters and 15,000 cm for low transporters.

Table 2. Comparison with clinical data

DFR	**IPD Cl_{urea}**	**TPD 50% Cl_{urea}**
1.1 L/h	14.3* mL/min (14.9)	13.3 mL/min (13.9)
1.6 L/h	16.9 mL/min (17.0)	15.9 mL/min (16.2)
2.7 L/h	20.9 mL/min (18.8)	19.9 mL/min (19.1)

Results from the clinical study by Aasaröd et al, 1994 (Average PET D/P_{crea} = 0.77) for IPD and TPD50 compared with the values predicted by the extended 3PM (within parenthesis). *) The Cl_{urea} was significantly higher for IPD in the clinical study. There were no significant differences for the two higher DFRs.

Table 3. Effective DFR intervals

Intermittent technique	**Slow**	**Average**	**Fast**
1.5 %	0.7 L/h – 2.7 L/h	1.0 L/h – 3.0 L/h	1.5 L/h – 3.5 L/h
2.27%	0.5 L/h – 2.7 L/h	0.7 L/h – 3.0 L/h	1.0 L/h – 3.5 L/h
3.86 %	0.3 L/h – 2.7 L/h	0.5 L/h – 3.0 L/h	0.7 L/h – 3.5 L/h
75% tidal technique	**Slow**	**Average**	**Fast**
1.5 %	0.7 L/h – 4.1 L/h	1.0 L/h – 4.5 L/h	1.8 L/h – 5.5 L/h
2.27%	0.5 L/h – 4.1 L/h	0.9 L/h – 4.5 L/h	1.0 L/h – 5.2 L/h
3.86 %	0.3 L/h – 4.0 L/h	0.5 L/h – 4.4 L/h	0.7 L/h – 5.1 L/h
50% tidal technique	**Slow**	**Average**	**Fast**
1.5 %	0.8 L/h – 4.7 L/h	1.0 L/h – 5.1 L/h	1.8 L/h – 5.9 L/h
2.27%	0.5 L/h – 4.7 L/h	0.8 L/h – 5.1 L/h	1.0 L/h – 5.9 L/h
3.86 %	0.3 L/h – 4.7 L/h	0.5 L/h – 5.0 L/h	0.8 L/h – 5.8 L/h
25% tidal technique	**Slow**	**Average**	**Fast**
1.5 %	0.7 L/h – 4.4 L/h	1.3 L/h – 4.8 L/h	1.8 L/h – 6.0 L/h
2.27%	0.5 L/h – 4.3 L/h	0.7 L/h – 4.8 L/h	1.0 L/h – 5.3 L/h
3.86 %	0.3 L/h – 4.3 L/h	0.5 L/h – 4.7 L/h	0.7 L/h – 5.2 L/h

The lower limit represents the DFR at which a maximum UF per L dialysis fluid used is attained (see Fig. 6). Using a lower DFR than this value will be lead to less UF per L/dialysis fluid spent. Also, DFRs lower than 1L/h will increase the glucose absorption in relation to the achieved UF (see fig. 3). The high part of the interval is the DFR at which a maximum UF as a function of DFR is reached. Using a higher DFR will give less UF while spending more dialysis fluid. Note also that the peak values of the urea vs. DFR curves (Fig. 1) are very similar to the maximas of the UF vs. DFR curves (fig. 2).

Table 4. Bi-modal regimes compared with a standard 6x2L regime

Regime	**UreaR**	**UF**	**Glucose abs.**	**Decrease**	**Total time**
6x2L 1.36%	158 mmol	458 mL	41.5 g	0 %	540 min
4x2L 3.86% + 4x2L 0%	158 mmol	456 mL	33.8 g	-19%	510 min
5x2L 3.86% + 5x2L 0%	157 mmol	457 mL	32.3 g	-22%	475 min

Simulated 'bi-modal' regimes were each dwell is optimized for either UF (using 3.86% glucose) or small-solute transport (using 0% glucose) keeping the glucose absorption low. The IPV vs. time curves for the different scenarios are shown in Figure 7. Additional examples can be found in a Supplemental material.

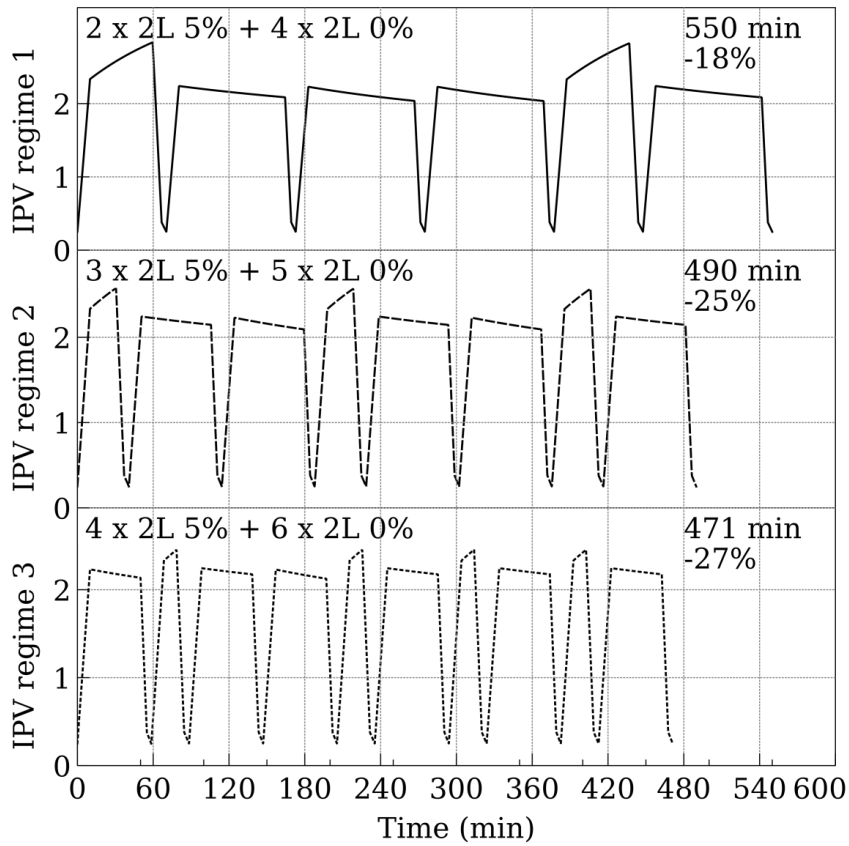

Simulated scenarios using a 5% glucose dialysis fluid. A reduction of up to 27% of the glucose absorption was obtained compared to the “standard prescription”.

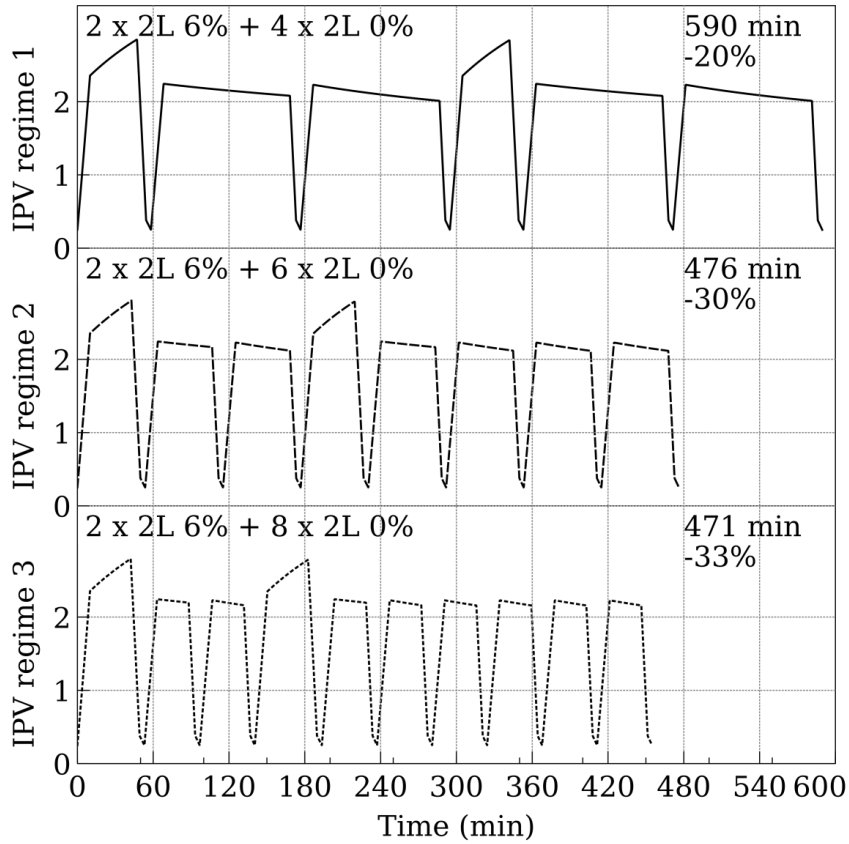

Simulated scenarios using a 6% glucose dialysis fluid. A reduction of up to 33% of the glucose absorption was obtained compared to the “standard prescription”.

Glossary

22 Symbols

A	effective surface area available for restricted diffusion (i.e. $A_0 \geq A$)
A_0	total cross-sectional (pore) area
A_L	effective large pore diffusion area
A_S	effective small pore diffusion area
Å	length unit (1Å= 10^{-10} m)
$\frac{A}{A_0}$	diffusive transport restriction coefficient (effective/total area ratio)
a_e	Molecular (Stokes-Einstein) radius (Å)
c	speed of light ($2.997925 \cdot 10^8$ m/s)
Δc_s	solute concentration gradient $\Delta c_s = c_s^o - c_s^i$
c_s^i	solute concentration in the "inner solution"
c_s^o	solute concentration in the "outer solution"
$c(x)$	concentration profile along the length of the pore (mol/mL)
$\bar{c}$	average radial solute concentration inside the pore
$\tilde{c}(\beta)$	radial solute concentration profile
C_0	see C_p
C_i	downstream (filtrate) concentration (mol/mL)
C_L	see C_i
C_p	plasma water concentration (mol/mL)
D	free diffusion coefficient (cm²/min)
D_i	Diffusion coefficient of solute i
D_2O	Heavy water
$E(x)$	Electric potential field
E_{cap}	Electric potential (voltage) in the capillary lumen
F	Faraday constant ($9.64846 \cdot 10^4$ C/mol)
f_L	fractional volume flux across the large-pore population (i.e. $J_{v,L}/Jv$)
f_S	fractional volume flux across the small-pore population (i.e. $J_{v,S}/Jv$)
G	Lag coefficient (cf. [24])
H	Diffusive hindrance factor, see $\frac{A}{A_0}$.
J_i	Phenomenological flows

J_s	total solute flux across the entire barrier (mol/min)
J_v	total volume flux across the entire barrier (mL/min)
$J_{v,i}$	volume flux across the i:th pore population in a heteroselective barrier (mL/min)
$J_{v,L}$	volume flux across the large-pore population (mL/min)
$J_{v,S}$	volume flux across the small-pore population (mL/min)
k	Boltzmann constant ($1.38066 \cdot 10^{-23}$ J/K)
K	Drag coefficient (the increased drag due to the presence of the pore walls)
K_c	Intra-pore convective hindrance
K_d	Intra-pore diffusive hindrance (K_dD is the average intra-pore diffusion coefficient)
K_e	Intra-pore electro-diffusive hindrance ($K_eD\frac{z_i e}{kT}$ is the average intra-pore electric mobility)
K_f	see LpS
L_{ik}	phenomenological coefficients relating the driving force to its effect on the flows
L_p	total hydraulic conductivity (mL min-1 mmHg-1 cm-2)
L_pS	filtration coefficient; total hydraulic conductance (mL min-1 mmHg-1)
$\dot{n}_s$	Solute flow
$\dot{n}_w$	Solvent (water) flow
N	Local solute flux
$N_i(t)$	molar amount of D_2O in the inner compartment
N_s^i	molar amount solute in the inner compartment
N_w^i	molar amount solvent (water) in the inner compartment
$\bar{N}$	Average solute flux over the pore section
N_A	Avogadro constant ($6.02205 \cdot 10^{23}\ mol^{-1}$)
P	permeability coefficient; $D/\Delta x$ (cm/min)
PA	see PS
PS	diffusion capacity (mL/min)
ΔP	Hydraulic pressure gradient (mmHg)
R	Gas constant ($kN_A = 8.31441$ J/K/mol)
r_S	Small pore radius (Å)
r_L	Large pore radius (Å)
S	Entropy
s	geometric pore standard deviation
s_L	geometric large-pore standard deviation
s_S	geometric small-pore standard deviation
T	temperature (°K) body-temperature = 310°K
u	geometric mean pore radius
u_L	geometric mean large-pore radius (Å)
u_S	geometric mean small-pore radius (Å)
U	Terminal velocity of the solute sphere (cm/min)
V	Water flux velocity inside the pore (cm/min)
$\bar{v}$	Average fluid velocity inside the pore (cm/min)
V_i	Volume of the inner compartment (inside the frog egg)
Δx	total barrier thickness (cm)
X_i	Phenomenological forces

23 Greek letters

α_i	fractional hydraulic conductance for the i:th pore population
α_L	fractional hydraulic conductance for the large-pore population (i.e. $K_{f,L}/K_f$)
α_S	fractional hydraulic conductance for the small-pore population (i.e. $K_{f,S}/K_f$)
β	fractional radial position ($\frac{r}{r_p}$) of the solute in relation to the pore radius r_p
γ	molar fraction
σ	Staverman (homoselective) reflection coefficient [91]
σ_d	solvent-drag reflection coefficient
σ_f	see σ_d
σ_o	osmotic reflection coefficient
σ_S	homoporous small-pore reflection coefficient
σ_L	homoporous small-pore reflection coefficient
η	viscosity of water (0.7 $mPa \cdot s$)
λ	solute to pore radius ratio (e.g. $\frac{a_e}{r_S}$)
μ	frictional coefficient
$\Delta\mu_s$	Solute chemical potential
$\Delta\mu_w$	Solvent (water) chemical potential
ν_s	partial molar volume of the solute
ν_w	partial molar volume of the solvent (water)
ξ_z	modified "reflection coefficient" for steady state ion transport
$\Delta\pi$	osmotic pressure gradient (mmHg)
Φ	Partition coefficient
Φ_d	Thermodynamic dissipation function
$\Psi(x)$	Potential energy of radial interaction (see also [64])

Printed by Media-Tryck, Lund University 2016
Nordic Ecolabel 3041 0903

Carl Mikael Öberg

DOCTORAL THESIS

Most of us go through life without giving much thought to the smallest blood vessels in the body - the capillaries. It is in these, extremely thin, only about 5-7 thousandths of a millimeter thick, blood vessels that the exchange of important nutrients and water occur between the blood circulation and the different tissues in the human body. Among the most important substances that are transported to the tissue are, for example, oxygen and glucose without which the cells in the body cannot survive for very long. Similarly, the end-products of the metabolic activity that occurs throughout the different tissues in the body, such as carbon dioxide and water, are transported away from the tissue. The aim of this thesis is to understand the basic mechanisms – the physiology - behind the transport of various substances that occur over the walls of capillaries - the smallest blood vessels in the body. In general terms, this is accomplished by constructing mathematical models which are then used to analyze experimental data from experimentally observed transport phenomena. The main focus will, in this thesis, be on the capillaries in the kidney and in the peritoneum - two very different kinds of blood vessels.

LUND UNIVERSITY
Faculty of Medicine

Department of Clinical Sciences, Lund

Lund University, Faculty of Medicine
Doctoral Dissertation Series 2016:145
ISBN 978-91-7619-372-3
ISSN 1652-8220